THE UNIVERSITY OF MANITOBA

LIMIT STATE STUDIES IN WINNIPEG CLAYS

by

MICHAEL L. NOONAN

A THESIS
SUBMITTED TO THE FACULTY OF GRADUATE STUDIES
IN PARTIAL FULFILLMENT OF THE REQUIREMENTS FOR THE DEGREE OF
MASTER OF SCIENCE

DEPARTMENT OF CIVIL ENGINEERING

WINNIPEG, MANITOBA

OCTOBER 1980

LIMIT STATE STUDIES IN WINNIPEG CLAYS

BY

MICHAEL LEONARD NOONAN

A thesis submitted to the Faculty of Graduate Studies of
the University of Manitoba in partial fulfillment of the requirements
of the degree of

MASTER OF SCIENCE

ABSTRACT

This study investigates the applicability of the limit state concept to the highly plastic, lacustrine clays of the Winnipeg area. The thesis begins with a literature review of the concepts of limit state and critical state, which is followed by discussion of YLIGHT, the most recent qualitative model for the behavior of natural clay.

Using the careful sampling and laboratory testing techniques outlined in this thesis, nine three-inch diameter, undisturbed triaxial samples were tested from depths of 8.2 m and 10.0 m in the Lake Agassiz clay from Winnipeg. Data was obtained on both drained and undrained triaxial behavior. Drained stress-controlled triaxial tests were used to establish limit state envelopes for both depths. Strain energy was used as a limit state criterion along various stress paths.

The undrained, strain-controlled triaxial tests examined the pore-water pressure generation characteristics, elastic moduli, and strain rate effects for this clay. Values of A_f between 0.45 and 1.34 were found depending on the consolidation stress levels. The relative stiffness, $(E_{50}/(\sigma_1-\sigma_3)/2)$, varied from 171 to 388. The strain rate parameter, $\rho_{0.1}$, was found to lie between 4.5 percent and 10.1 percent. An average effective, normally consolidated, Coulomb-Mohr rupture envelope for the Winnipeg clay at both depths was found using drained and undrained test results. The effective strength parameters, c' and ϕ', were 0 and 18°, respectively, in this range of stresses.

ACKNOWLEDGEMENTS

My sincere appreciation and gratitude is extended to Dr. J. Graham for his guidance and assistance in the preparation of this thesis and for his generous and unstinting support during all phases of this work.

I would also like to extend my thanks to Dr. L. Domaschuk and Prof. A. Baracos for reviewing this thesis and for their support during my degree program.

The help of the technical staff during the experimental investigation, especially Mr. N. Piamsalee, is gratefully acknowledged. I also wish to thank Mrs. Valerie Ring for doing a fine job with the typing of this thesis. Financial assistance, in the form of a National Research Council Post-graduate Scholarship, is also acknowledged.

A special thanks is extended to Ms. Carol Nielson for her patience and understanding during the course of my graduate studies.

TABLE OF CONTENTS

		PAGE
	ABSTRACT	i
	ACKNOWLEDGEMENTS	ii
	TABLE OF CONTENTS	iii
	LIST OF SYMBOLS	v
	LIST OF TABLES	viii
	LIST OF FIGURES	ix
CHAPTER		
1.	INTRODUCTION	
	1.1 General	1
	1.2 Historical Development	4
	1.3 Objective of Study	13
2.	A QUALITATIVE MODEL FOR THE BEHAVIOR OF NATURAL CLAYS	16
	2.1 The Concepts of Limit State and Critical State	16
	2.2 The YLIGHT Model	27
	2.3 The Implications of the Model	32
	2.4 The Application of Limit State and Critical State to Practice	36
3.	TEST RESULTS	
	3.1 Introduction	39
	3.2 Testing Program	44
	3.3 Triaxial Consolidation	49
	3.3.1 Reconsolidation to In-Situ Stresses	49
	3.3.2 Drained Compression Behavior	51
	3.3.2.1 Introduction	51
	3.3.2.2 Test Series: T201 to T204	53
	3.3.2.3 Test Series: T205 to T209	61

CHAPTER PAGE

3.4 UNDRAINED SHEARING
3.4.1 Introduction 66
3.4.2 Test Series: T201 to T204 67
3.4.3 Test Series: T205 to T209 71
3.5 One-Dimensional Consolidation 75

4. DISCUSSION OF TEST RESULTS
4.1 Introduction 78
4.2 Drained Compression Results 80
4.2.1 Defining Limit State 80
4.2.2 The Limit State Envelopes 84
4.2.3 Testing Techniques 91
4.2.4 Other Considerations 96
4.3 Undrained Shearing Results 98
4.3.1 Stress-Strain Behavior 98
4.3.2 Strain Rate Effect 101
4.3.3 The Normally Consolidated Strength Envelope .. 102

5. CONCLUSIONS AND SUGGESTIONS FOR FURTHER RESEARCH
5.1 Conclusions 104
5.2 Suggestions for Further Research 105

TABLES 108
FIGURES 118
BIBLIOGRAPHY 151
APPENDIX A LABORATORY TECHNIQUES FOR TRIAXIAL TESTING OF UNDISTURBED COHESIVE SOILS 155
APPENDIX B STRESS CONTROLLED DRAINED TEST RESULTS 185

LIST OF SYMBOLS

a	-	area of loading piston in the triaxial cell
A_o	-	initial sample area
$\bar{A}$,B	-	porewater pressure parameters (see Bishop and Henkel, 1962)
A_f	-	value of $\bar{A}$ at failure
c'	-	effective cohesion intercept
C_c	-	compression index
CAD	-	consolidated anisotropically, stress controlled drained compression test along a predetermined stress path
CAD($\bar{U}$)	-	strain-controlled, undrained compression test with porewater pressure measurements preceded by CAD test
CA$\bar{U}$	-	strain controlled, undrained compression test with porewater pressure measurements after reconsolidation to in-situ stresses
C.V.R.	-	critical voids ratio
e	-	voids ratio
e_o	-	initial voids ratio
E_{50}	-	elastic modulus
G.W.T.	-	groundwater table or phreatic surface
H_o	-	initial sample height
K_o	-	coefficient of earth pressure-at-rest
p'	-	mean principal stress; $= (\sigma_1' + \sigma_2' + \sigma_3')/3$
p_c'	-	effective preconsolidation pressure

$(p_c')_{iso}$ - effective preconsolidation pressure in an isotropic compression test

p_o' - effective vertical overburden stress

$(p_{vert}')_{max}$ - maximum effective vertical overburden pressure (approximately equal to p_c')

q - principal stress difference; = $(\sigma_1-\sigma_3)$

s_u - maximum deviator stress; = $(\sigma_1-\sigma_3)_{max}/2$

u - porewater pressure

V_o - initial sample volume

W - strain energy absorbed per unit volume

$\varepsilon_1, \varepsilon_3$ - major and minor principal strains (i.e. axial and radial strains in triaxial compression) calculated with respect to the original sample dimensions

$\varepsilon_{1c}, \varepsilon_{3c}$ - ε_1 and ε_3 at the end of triaxial consolidation to σ_{1c}', σ_{3c}'

ε_v - volumetric strain; = $\frac{\Delta V}{V_o}$

ε_{vc} - ε_v at the end of triaxial consolidation to $\sigma_{1c}', \sigma_{3c}'$

ε_ρ - average axial strain during relaxation test in CAD($\bar{U}$) and CA$\bar{U}$ tests

$\dot{\varepsilon}_1$ - axial strain rate

$\rho_{0.1}$ - strain rate effect parameter

σ_1', σ_3' - major and minor effective principal stresses

$\sigma_{1c}', \sigma_{3c}'$ - σ_1' and σ_3' at the end of triaxial consolidation

σ'_{dev} - effective deviator stress; = $(\sigma_1-\sigma_3)/2$

σ'_h - effective horizontal stress

σ'_n - effective normal stress

σ'_{oct} - effective octahedral normal stress; = $(\sigma'_1+\sigma'_2+\sigma'_3)/3$

σ'_{scalar} - effective scalar stress; = $\Sigma(\Delta p'^2+\Delta\sigma'^2_{dev})^{0.5}$

σ'_v - effective vertical stress

λ_f - shear strength at failure

ϕ' - effective angle of shearing resistance

LIST OF TABLES

TABLE		PAGE
3.1	Basic Soil Properties	109
3.2	Shear Test Results	110
3.3	One-Dimensional Consolidation Test Results	111
3.4	Triaxial Consolidation Results for Restressing to In-situ Stresses	112
3.5	Triaxial Consolidation Results to the End of Stress Controlled Testing	113
3.6	Yield Stresses from Different Criteria for Test Series T201 to T204	114
3.7	Yield Stresses from Different Criteria for Test Series T205 to T209	115
4.1	Strains at Limit State Stresses	116
4.2	Volume Change Measurements	117

LIST OF FIGURES

FIGURE		PAGE
2.1	Yield Surface and C.V.R. Line	119
2.2	Typical Critical State Line, Limit State Envelope, and Associated Parameters	120
2.3	The Effects of Time on a Normally Consolidated Clay	121
2.4	Typical Values of S_u/p'_o and p'_c/p'_o Observed in Normally Consolidated Late Glacial and Postglacial Clays	122
2.5	S_u/p' for Young and Aged Clays	122
2.6	The YLIGHT Model for the Behavior of Clays	123
3.1	Average Borehole Log Information, University of Manitoba Campus	124
3.2	Proposed Effective Stress Paths - Test Series: T201 to T204	125
3.3	Proposed Effective Stress Paths - Test Series: T205 to T209	126
3.4	Effective Stress Paths - Test Series: T201 to T204	127
3.5	Effective Stress Paths - Test Series: T205 to T209	128
3.6	The Relationship Between Effective Axial Stress and Axial Strain for Test Series: T201 to T204	129
3.7	The Relationship Between Principal Stress Difference and Axial Strain for Test Series: T201 to T204	130
3.8	The Relationship Between Effective Octahedral Normal Stress and Volumetric Strain for Test Series: T201 to T204	131

FIGURE		PAGE
3.9	The Relationship Between Effective Radial Stress and Radial Strain for Test Series: T201 to T204	132
3.10	The Relationship Between Strain Energy Absorbed Per Unit Volume and the Effective Scalar Stress for Test Series: T201 to T204	133
3.11	The Relationship Between Volume Change and Log Time for Different Stress Levels in Test T203	134
3.12	The Relationship Between Effective Axial Stress and Axial Strain for Test Series: T205 to T209	135
3.13	The Relationship Between Principal Stress Difference and Axial Strain for Test Series: T205 to T209	136
3.14	The Relationship Between Effective Octahedral Normal Stress and Volumetric Strain for Test Series: T205 to T209	137
3.15	The Relationship Between Effective Radial Stress and Radial Strain for Test Series: T205 to T209	138
3.16	The Relationship Between Strain Energy Absorbed Per Unit Volume and Effective Scalar Stress for Test Series: T205 to T209	139
3.17	Undrained Stress-Strain Results for Test Series: T201 to T204	140
3.18	Undrained Stress-Strain Results for Test Series: T205 to T209	141
3.19	One-Dimensional Consolidation Test Results	142
3.20	Average Limit State and Coulomb-Mohr Envelopes for Samples from 8.2 m to 10.0 m	143
3.21	Elastic Moduli Results for Undrained Tests	144
3.22	The Relationship Between Porewater Parameter and Consolidation Pressure	145

FIGURE		PAGE
3.23	Average Strain Rate Effect from Relaxation Tests for Test Series: T201 to T204	146
3.24	The Relationship Between Strain Rate and Plasticity Index	147
3.25	Average Strain Rate Effect from Relaxation Tests for Test Series: T205 to T209.....	148
4.1	Summary of Limit State and Oedometer Data	149
4.2	Yield Stresses by Different Yield Criteria - T206	150

CHAPTER 1

INTRODUCTION

1.1 GENERAL

All Civil engineering works apply loads to underlying strata. The response of the soil to the resulting stresses constitutes a major area of concern for geotechnical engineers. Quantitative predictions of this response require a behavioral model of the soil's mechanical properties. With man-made construction materials, such as steel or concrete, generally acceptable behavioral relationships can be developed to predict the stress-strain-time behavior. This enables the design of structures to withstand loads with an adequate safety factor against collapse and to limit displacements within acceptable bounds. In contrast with these controlled, man-made materials, soils are inherently particulate and multiphase. This produces complex constitutive stress-strain-time relations, which can involve both elastic and plastic strains, and strain-hardening or strain-softening. This complicated behavior distinguishes soil mechanics problems from most solid mechanics applications which use simpler constitutive relationships. Researchers have found it difficult to develop a comprehensive model of soils which accounts for stresses, strains, and time effects.

For this reason, the analysis of many practical problems in soils engineering is based on various stress-strain models which are often inconsistent, involve separate and frequently unrelated parameters, and are often restrictive in their assumptions (Kenney and Folkes, 1979).

Design procedures in soil problems usually consider stability and deformation separately. If the soil mass is found to be stable with respect to catastrophic failure, further analysis must then be undertaken to confine deformations within tolerable limits. Deformation calculations usually assume either linear, isotropic elasticity or strain-hardening, one-dimensional consolidation. Stability calculations, on the other hand, assume the soil to be rigid until failure is reached, and then to behave as if it possessed a constant angle of internal friction and constant cohesion. This is simply a statement of the Coulomb-Mohr failure criteria: $\tau_f = c' + \sigma_n \tan\phi'$.*

From full scale field studies it is known that the strength of clay soils depends on the nature of the stress changes producing failure. Nevertheless the influence of stress path is commonly ignored in stability analysis by assuming uniform shearing resistance along a slip surface. It should be noted that some work has been done using strengths which depend on the inclination of the failure surface (Ladd and Foott, 1974; Graham 1979), but this is not common practice. In most stability analysis the deformation of the soil preceding failure is ignored. After failure, deformation is assumed to be catastrophically large and non-quantifiable. The soil parameters used for stability and deformation calculations are measured from 'undisturbed' samples in standard laboratory tests such as the oedometer, direct shear and triaxial tests. These tests produce soil parameters which are only strictly applicable to the field conditions if the stress path defined by the test is closely similar to the stress path produced by the field loading.

---

* Symbols are defined in LIST OF SYMBOLS on page

In contrast with the assumptions used in analysis, the deformations preceding failure in most field problems are important and cannot be predicted on the basis of existing models of soil behavior. This is especially true of the many clay soils throughout the world which exhibit mechanical behavior which is both anisotropic and time-dependent. Thus an improved understanding of the constitutive relations governing the behavior of clay soils is most important in the development of more realistic testing, analysis, and design procedures in geotechnical engineering. Although these considerations apply equally to granular soils, this thesis will only examine a model for the stress-strain-time behavior of clay soils.

In the past, many elastic (Poulos and Davis, 1974), plastic (Chen, 1975), and elastic-plastic (Schofield and Wroth, 1968) mathematical models have been developed to simulate the behavior of natural clay soils. In most cases they have unfortunately been based on studies of remoulded soils (for example, Schofield and Wroth, 1968). For this reason, the models have failed to simulate the mechanical behavior of the majority of natural clay soils in which anisotropy and time are important factors (Bjerrum, 1973; Ladd et al., 1977). However, more recently several investigators (for example, Mitchell, 1970; Crooks and Graham, 1976; Tavenas and Leroueil, 1977) have examined the stress-strain behavior of natural clays through high quality laboratory testing of carefully handled samples. These efforts have culminated in recent studies by workers at Université Laval in Quebec. On the basis of their research a general model for the behavior of Champlain Sea clays has been

proposed which incorporates the concepts of limit state and critical state along with ideas on ageing and time effects.* Although quantitative analysis on the basis of this model is not possible at this stage it has proved useful in unifying the understanding of soil behavior along various stress paths. It provides a useful qualitative model on which the prediction of the behavior of natural clay soils can be made. This thesis examines the applicability of this model to the highly plastic, lacustrine, anisotropic clays of the Winnipeg area.

In the following section a brief historical review of the research leading to the development of this model for the behavior of natural clays is presented.

1.2 HISTORICAL DEVELOPMENT

Although many earlier researchers attempted to generate mathematical models of the mechanical behavior of soil which accounted for strains, the development in the 1950's at Cambridge, England, of a group of plasticity models was the first important step toward this goal. Over the past three decades, one of the primary aims of the research at Cambridge was the development of stress-strain theories for soils in terms of fundamental soil constants (Roscoe, 1970). In their research, they worked with soils in their simplest possible state, that is, with well-graded sands and saturated remoulded clays, so that their properties could be described by a minimum number of parameters. A convenient review of this work is given by Bolton (1979).

---

* These terms are used here in a technical sense and are defined carefully in Chapter 2.

Roscoe, Schofield, and Wroth (1958), while working with saturated remoulded samples of Weald clay and Supreme Kaolin, and testing under both drained and undrained triaxial compression, discovered that a normally consolidated, remoulded clay has a characteristic yield or limit state surface which contains a Critical Voids Ratio (C.V.R.) line, to which all stress paths converge at high strains. They proposed that the limit state surface and C.V.R. line, as they exist in a (p', e, q) space, that is, a three-dimensional plot of mean principal effective stress, $p' = (\sigma_1' + 2\sigma_3')/3$, void ratio, e, and principal stress difference, $q = (\sigma_1 - \sigma_3)$, is independent of drainage conditions. If the initial state of a soil sample and its drainage conditions during testing are known, the stress path for a triaxial test can be determined. The stress path, when reaching the yield surface, traverses this surface until the C.V.R. line is reached. Thereafter the soil continues to deform at constant stress and constant void ratio.

During the ten years following the publication of the work of Roscoe et al. (1958) the original theory for the behavior of normally consolidated, remoulded clays was extended and revised, particularly in the light of a new work equation proposed by Burland (1967). This culminated in the publication of Schofield and Wroth's 1967 book, "CRITICAL STATE SOIL MECHANICS", in which the authors set out the Cam-clay Model to describe the mechanical behavior of wet, that is, normally consolidated remoulded clay. The focus of the model is the behavior of clay soils which remain in a quasi-elastic state up to a limit state surface, after which they behave more plastically. It draws together the following: elastic and plastic compression due to all forms of stress increase;

settlements due to both shear and spherical pressure increments; and the increase in stiffness and strength due to consolidation of loose soils. Additionally, it incorporates three-dimensional stress conditions; a new yield or limit state locus which accounts for shear distortion occurring without plastic volume change for stress paths below the critical state line; and the Coulomb-Mohr failure criterion for the prediction of rupture. The reader is again referred to Chapter 2 for a more detailed explanation of the concepts of critical and limit state.

The 'Critical State' model proposed by Schofield and Wroth draws a comprehensive and unified picture of the concepts of compressibility, elasticity, yield, friction, and cohesion as they apply to soil (Bolton, 1979). It was shown by the authors that the use of the Cam-clay model, in conjunction with a model of plane dilatant rupture for a soil in a dense condition, can provide a strong framework by which field behavior of a soil may be qualitatively predicted. However, the model has proven somewhat lacking in terms of quantitative predictions (Burland, 1971; Parry and Amerasinghe, 1973). This is due in part to some of the assumptions inherent in the model. For example, rupture frequently interrupts a soil's progress towards its critical state, thereby destroying the uniformity of strains on which the model is based (Bolton, 1979). More important however, is the anisotropic and time-dependent nature of many natural clay soils. The remoulded clay, on which the Cam-clay model was based, behaved isotropically and produced a limit state surface which was centered on the isotropic stress axis in a plot of deviator stress, q, versus mean principal effective stress, p'. In natural clays, deposition and preconsolidation develop under anisotropic stress conditions

which lead to an anisotropic clay structure (Tavenas et al., 1977). Thus the stress conditions leading to volumetric yield in a natural clay are more logically referred to the K_o-condition (Ohta and Hata, 1971). However, in spite of its limitations, the Cam-clay model provides a strong framework on which succeeding researchers could base their studies of the behavior of natural clay soils.

One of the most important concepts inherent in the Cam-clay model was the supposition that a limit state surface exists in conjunction with the rupture envelope. This limit state surface represents a set of yield points in stress space. Stress states inside the limit state surface behave in a pseudo-elastic, stiff manner and are identified with small strains, strain rates, and porewater pressures. Stress states on the limit state surface behave in a more plastic fashion, leading to much larger strains, strain rates, and porewater pressures. This behavior is observed in oedometer tests as the characteristic pre-consolidation pressure, p'_c, and in undrained triaxial compression by the maximum deviator stress. In both cases the laboratory test imposes a formalized stress path on the soil. However in the field, soil elements may be subjected to many other stress paths and a complete definition of the limit state envelope requires examination of several stress paths. The quantitative identification of the limit state envelope for a natural clay soil allows the prediction of those stress states which do not cause failure of the soil mass, but lead to the occurrence of zones of plastic deformation, and large settlements or porewater pressures.

Much of the early work in identifying limit state envelopes for natural clays was focussed on sensitive Norwegian clays (Graham, 1969;

Brown, 1969) and cemented sensitive Champlain Sea clays in Eastern Canada (Mitchell, 1970; Sangrey, 1972). At a microscopic level, highly sensitive clay soils consist of plate-shaped particles in an edge-to-face flocculent structure. The sensitivity of quick clays may be due to leaching producing pore fluid changes, whereas cementation bonds the particle contacts in a cemented clay. The stress-strain behavior and the strength of these soils are intimately related to their grain structure; that is, to the physical arrangement of soil particles (Bjerrum and Kenney, 1967). Consequently, the concept of a limit state was recognized as resulting directly from the clay structure itself. Limit state represents the stresses at which the strength of the particle structure is mobilized and the point at which a significant number of localized failures at the points of particle contact occur. When the structure of a clay begins to yield in this way, its ability to resist deformation is reduced. This explains the change from small-strain to large-strain behavior. Although highly sensitive soils represent extreme examples of the effect of grain structure on soil behavior, most clay soils exhibit some effects of particle structure due to geologic or man-made loading, dessication, groundwater level changes, chemical changes, cementation, or delayed compression (Crooks and Graham, 1976). Therefore, the concept of limit state is not restricted to sensitive clays and may include all natural clays.

Due to the importance of grain structure on the mechanical properties of natural clays, considerable importance has been attached to avoiding disturbance of the in-situ particle arrangement and obtaining undisturbed samples (Crooks and Graham, 1976). The recognition and

development of careful sampling, trimming, and testing procedures proceeded simultaneously in the work of several investigators (Crooks, 1973; Crooks and Graham, 1976; Leroueil and Tavenas, 1977).

Independent of the work at Cambridge on remoulded clays, an understanding developed at the Norwegian Geotechnical Institute that the limit state concept could be applied to natural clays. Work by Graham (1969) and Brown (1969) on lean sensitive Norwegian clays confirmed the idea that many natural clays possess a critical stressing condition, or limit state, which is stress path dependent and lies somewhere below the Coulomb-Mohr rupture envelope.

Mitchell (1970), working with a natural cemented Champlain Sea clay from Eastern Canada, was able to identify a limit state envelope by a series of drained triaxial tests along predetermined stress paths in stress space. Additionally, he stated that the limit state envelope is associated with the destruction of cementation bonds and deviates from that expected for an isotropic material. Sangrey (1972) demonstrated similar envelopes for other cemented Canadian clays and speculated that the shape of the limit state envelope changes abruptly from horizontal to vertical in the vicinity of p'_c. On the basis of tests on lightly over-consolidated, remoulded kaolin specimens, Parry and Nadarajah (1973) found that the limit state envelope was asymmetric with the K_o-consolidation line. This conflicted with earlier work by Graham (1969), Ohta and Hata (1971) and Crooks (1973) which suggested that the limit state envelope was approximately symmetric with respect to the K_o-consolidation line. This latter view was confirmed further by Leroueil and Tavenas (1977) and is now commonly accepted.

Crooks and Graham (1976), working with the post-glacial organic silty clays of the Belfast area, determined limit state envelopes for two clays. Additionally, they pointed out the importance of laboratory reconsolidation to in-situ field stresses and related the energy supplied to a sample after reconsolidation to field stresses, to the limit state envelopes. Similarly, testing by Graham (1974) on sensitive Lyndhurst clay from Eastern Ontario, confirmed the relevance of limit state, and further proposed that a 'threshold' total strain energy might be used to define the limit state condition along generalized stress paths.

Although these earlier researchers were able to verify the existence of limit state envelopes for various natural clays, and were able to draw some conclusions about their nature, it was the workers at Laval University, led by Tavenas and La Rochelle, who were able to synthesize their observations and those of others in a systematic, coherent model. Leroueil and Tavenas (1977) examined the limit state envelopes of thirteen natural clays from various origins and they suggested that the general shape of the envelope could be characterized by three parameters: $(p'_{vert})_{max}$, which is close to the oedometer preconsolidation pressure; $(p'_c)_{iso}$, which is the limit state envelope's intersection with the isotropic stress line; and $(S_u)_{max}$, the maximum undrained strength. They also showed that the Cam-clay model cannot be applied to natural clays which have been deposited and consolidated under anisotropic conditions. This was based on a comparison of the shape of the limit state envelope for the isotropically consolidated clay of the Cam-clay model and its shape for several natural clays. The maximum possible ratio of $(p'_{vert})_{max}$ to $(p'_c)_{iso}$ from the Cam-clay model was 1.18, whereas the ratio ranged

between 1.4 and 1.8 for natural clays. Also, they suggested that the effects of ageing and strain rate on the preconsolidation pressure of natural clays proposed by Bjerrum (1967) apply to the entire limit state envelope.

Tavenas and Leroueil (1977), working with sensitive Champlain Sea clay, proposed a limit state model which in addition to dealing with the anisotropic nature of most natural clays, also includes the known effect of time on the preconsolidation pressure of natural clays. They suggested that the limit state envelope of a natural clay has an elliptical shape, is centered on the K_o-consolidation line of the normally-consolidated clay, and that the position of the envelope is governed by the preconsolidation pressure. Furthermore, they proposed that the limit state surface of a clay at any depth can be entirely determined from knowledge of its effective friction angle, ϕ', and preconsolidation pressure, p'_c. The qualitative model of clay behavior based on these proposals has become known as YLIGHT.

After proposing this model, the workers at Laval produced a succession of papers dealing with various aspects of the limit state concept (Tavenas et al., 1978a; Tavenas et al., 1978b; Leroueil et al., 1979). Tavenas et al. (1978a) examined the use of strain energy as a limit state and creep criterion in soft clay. They found that the strain energy could be used to define the limit state envelope because a clear discontinuity exists in the energy-stress relationship along all stress paths. However, their study did not find a distinct threshold energy at which all samples reached limit state, as was proposed by Graham (1974). They also showed that strain energy is a good indicator of the creep be-

havior of over-consolidated clays. In particular, the rate of dissipation of strain energy was shown to depend essentially on the relative position of the creep stresses to the limit state envelope.

Attempting to quantify the effects of time on the limit state envelope, Tavenas et al. (1978b) examined the relationship between the creep behavior of an over-consolidated clay and its proximity to the limit state envelope. They indicated that the creep deformations can best be described by referring the effective stresses under which these deformations develop to the limit state envelope of the clay. In addition, they proposed the existence of a general stress-strain-time function in terms of the limit state envelope.

Most recently, Leroueil et al. (1979) have investigated the effect of 'destructuration' due to consolidation on the limit state envelope and other mechanical properties of initially intact Champlain Sea clays. Intact clays have a grain structure due to the combined effects of depositional environment, ageing, consolidation, thixotropic hardening, and possibly cementation. It was concluded in their study that consolidation to stresses in excess of the original limit state envelope (i.e. destructuration) modifies the mechanical properties of the clay, even after unloading to a new over-consolidated state.

Whereas the most recent research by the Laval group represents movement towards further refining and quantifying the limit state concept, the YLIGHT model still stands as an elegant, though partly controversial, qualitative solution to the development of a conceptual model for the mechanical behavior of natural clay soils. It draws on the concepts first proposed by the Cambridge group on the mechanical behavior

of remoulded soils, and integrates this with research on the limit state concept in natural clays, and finally combines these with Bjerrum's ideas on the effect of time on the behavior of clay. The YLIGHT model involves several concepts which are not in common usage in customary soil mechanics applications. For this reason, and because it presents an easily understandable qualitative model of clay behavior, a more detailed presentation is given in Chapter 2 of this thesis.

As with any model, YLIGHT's validity must be reaffirmed with respect to both old and new investigations of soil behavior. Moreover, it must be noted that most of the studies at Laval University were performed on samples of Champlain Sea clay. Consequently, further investigations are required to confirm the applicability of the YLIGHT model to other natural clay soils. In this regard, work has begun at the University of Manitoba with the publication of preliminary results by Baracos et al. (1979) on the applicability of limit state to the highly plastic clays of the Winnipeg area. This thesis represents a continuation of that work. In particular, the present study investigates in more detail the limit state concept and makes a preliminary qualitative examination of the effect of time on the limit state envelope. At this stage, the introduction to the thesis will be concluded with a brief presentation of the objectives and scope of the testing program.

1.3 OBJECTIVE OF STUDY

This investigation is part of a larger inquiry into the geotechnical properties of the glacial Lake Agassiz clays which underly the Winnipeg area (Baracos et al., 1979). The larger inquiry was initiated

in an attempt to better understand the complex behavior of these non-homogeneous, anisotropic, highly plastic clays. Previous studies of their geotechnical properties have been done by several investigators, and are summarized by Baracos et al. (1979). However, recent studies on other post-glacial clays, for example by Crooks and Graham (1976), and by Tavenas and Leroueil (1977), have stressed that good quality research into the field behavior of soils requires that minimum disturbance occurs during sampling and laboratory preparation of samples. With this in mind, this study was conducted on samples taken with the block sampler devised by Domaschuk (1977) and used the careful trimming and testing procedures outlined in Appendix A.

As mentioned previously, the main purpose of this study was to investigate the concept of limit state as it applies to Winnipeg clays. Data was obtained on both drained and undrained triaxial behavior. Drained stress-controlled triaxial tests were used to examine the limit state condition along various stress paths. The results were examined with reference to the YLIGHT model proposed by Tavenas and Leroueil (1977) and with regard to the use of different components of the strain tensor to define the limit state condition. Samples which were not stressed to rupture during the drained portion of the triaxial test were tested to failure in undrained shear. The undrained part of the test allowed examination of the following characteristics: the influence of consolidation history on porewater pressure generation and elastic moduli; the normally consolidated Coulomb-Mohr rupture envelope; and the effect of the strain rate on the undrained shear strength.

The drained compression behavior along the K_o-consolidation line

was analysed through one-dimensional consolidation tests. In addition, standard geotechnical classification tests were performed on trimmings from all triaxial samples.

The laboratory testing program consisted of nine, large diameter (7.6 cm), triaxial compression tests, four oedometer tests, and standard classification tests. The samples of Winnipeg clay were obtained from two different depths in a borehole on the site of the proposed Physical Education Building at the University of Manitoba. Earlier studies by Baracos et al.(1979) used samples from this borehole and from others on the same site. A complete review of the testing program and the test results are presented in Chapter 3.

Before preceding to the testing program and its results, the thesis will present in Chapter 2 a more detailed discussion of the YLIGHT model proposed by Tavenas and Leroueil (1977).

CHAPTER 2

A QUALITATIVE MODEL FOR THE BEHAVIOR OF NATURAL CLAYS

2.1 THE CONCEPTS OF LIMIT STATE AND CRITICAL STATE

In the first chapter extensive use was made of the concepts of limit state and critical state to describe models of the stress-strain-time behavior of clay soils. These terms, although not new (Schofield and Wroth, 1968), are not commonly used in normal geotechnical engineering applications and are still the subject of some controversy. They originated primarily with the workers at Cambridge (Roscoe et al., 1958; Burland, 1967; Schofield and Wroth, 1968) and from their development of the Cam-clay model of clay behavior. Tavenas and Leroueil (1977) used these terms to describe the YLIGHT model for the mechanical behavior of Champlain Sea clays. Before presenting the details of this model, the concepts of limit state and critical state will be further reviewed.

Roscoe, Schofield, and Wroth (1958) first established the existence of 'yield' or 'state boundary' surfaces, and a Critical Voids Ratio (C.V.R.) line. Working with normally consolidated, saturated remoulded Weald clay, they found that the stress paths of triaxial samples in either drained or undrained shear follow a surface or three-dimensional boundary in (p', e, q) space. This is shown in Fig. 2.1 by the drained stress path DFKC and the undrained stress path DEB followed by tests on normally consolidated samples. This surface was called the yield surface and was a state boundary because it separated stress-voids ratio states which samples could achieve, from those which they could never achieve.

In the case of lightly overconsolidated clays, stress paths rise to the yield surface and then follow that surface to the end of the test. This is illustrated by stress path GHB in Figs. 2.1(a) and (b). They also proposed that the termination of these paths at high strains defined a unique set of points in (p', e, q) space which was called the Critical Voids Ratio Line. This line is represented by a single critical voids ratio point, B, in the constant e-plane shown in Fig. 2.1(b). Upon reaching this line, samples would deform at a constant stress and constant voids ratio. This steady-state condition became known as the critical state and the C.V.R. line became the critical state line (Schofield and Wroth, 1968). It was suggested that both the yield surface and the critical state line are characteristic of a clay and applicable under all drainage conditions. In addition, they showed that the critical state line is a unique function of voids ratio and that the stresses at critical state satisfy the Coulomb-Mohr rupture criterion.

Later work summarized by Atkinson and Bransby (1978) has suggested that the critical state concept could be applied to overconsolidated remoulded clays. In a drained test on an overconsolidated clay sample the deviator stress, q, first increases to a peak, and then begins to reduce as the sample dilates until the end of the test. The critical state, as defined earlier, is a steady-state condition at which large shear strains occur with constant shear stress and at constant volume. It is difficult to achieve this steady-state condition in overconsolidated clays because triaxial test data becomes unreliable at large strains. This is due to the reduction of shearing resistance at larger strains which tends to concentrate strains in weaker regions of the

specimen. The concentration of strain leads to the formation of thin zones of deformation with the specimen, thus bringing into question the accuracy of strains and stresses based on the assumption of uniform strains in the sample. However, the validity of the critical state concept for overconsolidated remoulded clays was confirmed by examining the direction, at failure, of the stress paths followed by these samples in (p', e, q) space. The examination indicated that overconsolidated samples were moving towards the critical state line at rates which are related to their distance from the critical state line. The stress path, followed by an overconsolidated sample, is illustrated by GHB in Figs. 2.1(a) and (b). On this basis, it was proposed that the critical state line in (p', e, q) space represented the steady state conditions, at which large strains can occur with no change in stresses or volume, for both normally consolidated and overconsolidated samples of a clay.

Initially, the concept of a critical state condition at which large shear strains can occur at constant volume and shear stress, may have seemed incompatible with the concept of residual strength. However, this was not the case. It was found that critical state conditions would seldom develop uniformly in a shearing soil sample. Strains seldom remain uniform throughout a sample because of the non-homogeneous nature of most clays, and because of stress rotation caused by horizontal shear stresses at the top and bottom of the sample. This leads to the formation of a thin slip zone over which a sample slides as two distinct blocks. As a sample fails in this manner it is found that the strength of the soil is reduced substantially below the critical state strength (Skempton,

1964). This strength reduction was attributed to the re-orientation and gradual parallel alignment of the clay particles after large displacements have occurred in the slip zone. In contrast, the critical state strength can be thought of as the final state which could be reached by homogeneous shearing of an element or clay sample in which the arrangement of the particles remained essentially random (Atkinson and Bransby, 1978). The two concepts were not, therefore, incompatible.

At this point it is useful to examine the relationship between the Coulomb-Mohr rupture criterion and the critical state condition. The Coulomb-Mohr rupture criterion, first proposed by Coulomb in 1776, is a commonly used expression for the shear strength of soils which describes the stress conditions causing failure of a soil element. The shear strength (τ_f) of a soil on a particular plane was expressed as a linear function of the effective normal stress (σ_n') on the same plane:

$$\tau_f = c' + \sigma_n' \tan \phi'$$

where c' and ϕ' are the effective shear strength parameters, now described as the cohesion intercept and the effective angle of shearing resistance, respectively. The application of this criterion to soft clays lead to a question as to whether the $(\sigma_1'/\sigma_3')_{max}$ or $(\sigma_1 - \sigma_3/2)_{max}$ criterion should be used to describe failure. Theoretically, the Coulomb-Mohr criterion is a limiting shear stress condition identical to $(\sigma_1'/\sigma_3')_{max}$. However, this condition usually occurs at large strains; whereas the maximum shearing resistance occurs at smaller strains. This is especially true when particular efforts are taken to preserve the in-situ particle arrangement of the clay. For this reason, the two criteria can lead to different shear strength parameters (Graham, 1974; Crooks and Graham, 1976).

Bjerrum and Kenney (1967) pointed out that the two failure criteria describe different aspects of soil behavior. They stated that the structure or mechanical skeleton of the clay is the key to this difference. The maximum shear strength criterion is associated with quasi-static yielding of the grain structure of the soil at small strains. On the other hand, the maximum stress ratio criterion represents the dynamic yielding of the clay structure at large strains once a statistically constant condition of sliding friction* between the particles has been obtained (Graham, 1974). Since the maximum stress ratio occurs at relatively large strains, it may be reasonably concluded that failure stress states represented by this criterion are in close proximity to those defined by the critical state condition.

It has been pointed out by Leroueil et al. (1979) that the determination of critical state conditions in overconsolidated natural clays is difficult. They specified several causes for the difficulty. Firstly, the critical state condition corresponds to a homogeneous state of stress in a clay, whereas shear tests, especially on intact samples, usually leads to the formation of a well-defined failure surface which governs its large-strain strength. Secondly, the stress-strain computations in a triaxial test are subject to significant error at strains greater than 5 percent. This is because the corrections commonly used to allow for cross-sectional area changes and membrane and filter stiffness, are not sophisticated enough. However, Leroueil et al. (1979) stated that there are some indications that the strength developed at large strains presents many of the characteristics of critical state.

It was proposed earlier that the maximum principal stress ratio

---

* This occurs when the number of bonds being formed between clay particles equals the number being broken in a given time.

criterion for failure described the ultimate frictional resistance between soil particles, and was only mobilized at high strains (Bjerrum and Kenney, 1967). On the basis of this, and the earlier statement about the strength developed at large strains representing many of the characteristics of critical state (Leroueil et al., 1979), it may be stated that the normally consolidated branch of the Coulomb-Mohr rupture envelope is close to the critical state line (Fig. 2.2). In the overconsolidated region, samples first reach a maximum deviator stress, which is a function of the in-situ grain structure of the soil, and which occurs at small strains. The maximum deviator stress, $(\sigma_1-\sigma_3)/2_{max}$, represents the structural strength of the soil's grain skeleton and is therefore a part of the 'yield' or 'limit state' surface. Further straining causes a reduction in strength until the maximum stress ratio, and therefore critical state,is reached at high strains. These ideas are illustrated in Fig. 2.2. The concept of the limit state surface is discussed further later on in this section.

In summary, it may be stated that the critical state line is an inherent characteristic of a clay, although at times it may be difficult to reach this condition with normal testing procedures. In addition, the critical state line in (p', q) stress space is closely similar to the normally consolidated Coulomb-Mohr strength envelope. In the model presented by Tavenas et al. (1977) the critical state replaced the normally consolidated branch of the Coulomb-Mohr strength envelope (Fig. 2.2).

Although the concept of critical state presented a useful conceptual model for failure, the limit state concept has proved more helpful

in understanding the behavior of natural clay soils. This idea was first mentioned by Roscoe et al. (1958) who discovered that for a given void ratio, e, an undrained test on a normally consolidated, remoulded clay follows an effective stress path, which defined a characteristic yield or state boundary line in the (p', q) stress space. This is shown by stress path DEB in Figs. 2.1(a) and (b). The yield line terminates at the point on the Critical Voids Ratio line corresponding to that void ratio. All of the points on the Critical Voids Ratio line represent critical state conditions. In addition, Roscoe et al. (1958) found that the stress paths followed by both drained and undrained triaxial tests traversed a three-dimensional yield surface in (p', e, q) space until reaching the critical state line (Fig. 2.1). States outside this surface in (p', e, q) space were not possible. It was noted that a truly isotropic, normally consolidated clay will not have a yield surface lying outside its consolidation state in (p', e, q) space. This was because the grain structure* of such a clay is randomly oriented and strictly a function of its consolidation stress level. The application of stresses higher than these consolidation stresses caused an immediate breakdown and readjustment of the grain structure or mechanical skeleton of the clay. This breakdown of the grain structure was known as yielding; hence the term 'yield surface'.

It is important to note the difference between a yield surface and a yield envelope. A yield envelope may only be defined in a constant voids ratio plane, such as the constant e-plane in Figs. 2.1(a) and (b).

---

* Grain structure may be defined as the physical arrangement of the soil particles of the clay.

The shape of the yield envelope at different voids ratios is similar, but the size of the envelope varies with e. For instance, in Fig. 2.1(c) the yield envelopes corresponding to the void ratios at points D, F, K, and C are shown. In an undrained test the void ratio is constant and therefore the stress path will follow the yield envelope for that voids ratio until the path reaches the critical state line. In contrast the voids ratio constantly changes in a drained test. This is shown in Figs. 2.1(a) and (c) by stress path DFKC. Consequently, a drained test on a normally consolidated clay follows a three-dimensional yield surface defined in (p', e, q) space. This surface is the aggregate of the yield envelopes found at each different voids ratio. As Fig. 2.1(c) shows, the stress path in a drained test on a normally consolidated clay is always on the yield envelope corresponding to its voids ratio at that point in the test.

The use of the term 'yield' to describe the behavior of soils has recently been the subject of some controversy. This term is most often used in applied mechanics to describe the change from elastic to plastic behavior. It is therefore somewhat misleading to use it in conjunction with clay soils where purely elastic or plastic behavior does not occur. As yet the terminology has not been standardized. However, for the remainder of this thesis the term 'limit state' will be used synonymously with the term 'yield'.

Later investigators (for example, Mitchell, 1970; Crooks and Graham, 1976; Tavenas and Leroueil, 1977) showed that yield envelopes could be defined in (p',q) stress space for natural clays. However, the yield envelopes for these natural clays were found to exist at stresses

higher than those corresponding to in-situ levels. The grain structure of a natural clay is affected by several factors including: depositional environment, ageing, thixotropic hardening, leaching, and in some cases cementation (Tavenas et al., 1979). It is known that most natural clays have developed a grain structure which is over-competent (Bjerrum, 1967; Graham, 1974; Crooks and Graham, 1976). That is, the clay can withstand stresses somewhat higher than its in-situ stress levels without an appreciable breakdown or 'yield' of its grain structure.

The causes for this over-competency are many. Overconsolidation due to off-loading, dessication, and groundwater level changes cause the clay structure to adjust to higher stress levels. When these stress levels are subsequently decreased the grain structure does not change by a corresponding amount. This leaves the clay with a reserve resistance, above the structural strength it would have had at lower stress level if it had remained normally consolidated. Bjerrum (1967) has shown that an over-competent structure has developed in Norwegian clays by a combination of the following: depositional environment and subsequent geochemical changes, and delayed compression or ageing. In addition, cementation has been shown to cause an over-competent structure in some Canadian clays (Samgrey, 1972).

In order to apply the yield envelope concept to natural clays it was necessary to define exactly what constituted yield for these clays. For the normally consolidated clays examined by Schofield et al. (1958), yielding or structural breakdown occurred immediately on the application of additional stresses above in-situ levels. However, natural clays have developed an over-competent grain structure which does not break down

immediately on the application of stresses larger than those in-situ.

A generally accepted definition for the limit state or yield envelope of a natural clay is the set of points in (p', q) stress space inside which strain, strain rates, and porewater pressures are low, and outside which all of these parameters are much higher (Baracos et al., 1979). States of stress inside this envelope produce a stiff and largely recoverable response associated with the static or small strain readjustment of the grain structure of the clay. States of stress outside the limit state envelope, in (p', q) space, but on the limit state surface in (p', e, q) space, produce a more compressible and irreversible response associated with the dynamic or large strain readjustment of the clay structure by a statistically constant condition of sliding friction between particles (Graham, 1974). This behavior is most easily observed in one-dimensional consolidation tests where it is manifested as the standard p_c' (i.e. preconsolidation pressure) break in the voids ratio-effective vertical pressure semi-logarthmic plot. Consequently, the introduction of the concept of limit state envelope in a clay is only a generalization of the overconsolidation effect measured in the oedometer test.

The difficulty of finding a method for determining the limit state envelope has been reviewed by Tavenas et al. (1978a). For some time the most accepted method of finding the envelope has been the incremental loading of drained triaxial samples along a series of stress paths representing various loading systems in the field. The limit state stresses are defined by examining various stress-strain relationships for a

bi-linearity which distinguishes pre-limit state from post-limit state behavior. However, no unique stress-strain criterion has been found that defines limit state along all stress paths. Baracos et al. (1979) pointed out that limit state in tests involving generally increasing shear stresses can be most easily defined by plotting σ_1' versus ε_1, whereas tests with increasing cell pressures required graphs of σ_3' versus ε_3, or σ_{oct}' versus ε_v. Additionally, following an earlier suggestion by Graham (1974), Tavenas et al. (1978a) have shown the scalar, 'strain energy absorbed per unit volume', plotted against octahedral normal stress can provide a useful limit state criterion, which is applicable to all stress paths. The problem of defining limit state is examined later in this thesis.

With regard to finding the limit state envelope for an undisturbed natural clay, an assumption inherent in all previous work is that the in-situ voids ratio of the clay does not change significantly prior to the clay reaching the limit state envelope corresponding to its in-situ voids ratio. If, however, voids ratio changes occur and are more significant along certain stress paths than others, the limit state envelope defined by drained stress probing would be skewed to the constant e-plane limit state envelope, shown in Fig. 2.1(a).

Prior to the work by Tavenas and his co-workers at Laval University (Leroueil and Tavenas, 1977; Tavenas and Leroueil, 1977) limit state (i.e. yield) envelopes for various clays had been found (for example, Mitchell, 1970; Crooks and Graham, 1976), but an overall picture of the nature of the limit state envelope for a clay and the factors affecting

it had not been drawn. The next section presents the model developed by the Laval workers and a discussion of the factors affecting limit state and critical state.

2.2 THE YLIGHT MODEL

On the basis of their own work and that of others, the workers at Laval University were able to come to several important conclusions about the nature and shape of the limit state envelope for natural clay soils (Leroueil et al., 1977). In addition, they have shown that the known effects of time (Bjerrum, 1967) can be accounted for in their model. This behavioral model, known as YLIGHT, was initially proposed for Champlain Sea clays (Tavenas and Leroueil, 1977). Its applicability to all natural clays appears promising and is presently being evaluated. This section presents a detailed examination of the model and the logic behind it.

The deposition and consolidation of natural clays has been shown to be anisotropic with a constant stress ratio (i.e. σ'_h/σ'_v), at least during the early stages of consolidation (Salah and Krizek, 1976). As a result of this stress anisotropy the structure of a natural clay was found to be anisotropically arranged. Therefore it was reasonable to accept that the limit state envelope of natural clays should be approximately centered on the K_o-consolidation line (Graham, 1969; Ohta and Hata, 1971) and not on the isotropic line, as the work on remoulded clays had indicated (Schofield and Wroth, 1968). In addition, it was known that the coefficient of earth pressure at rest, K_o, is a function of the normally consolidated friction angle, ϕ'. For example, Jaky's empirically

derived formula for K_o, as described by Tavenas et al. (1977), was:

$$K_o = [(1 + \frac{2}{3} \sin\phi')/(1 + \sin\phi')] (1 - \sin\phi').$$

Accounting for this and their own test results, Tavenas and Leroueil (1977) stated that the limit state envelope of a natural clay has an elliptical shape, centered on the K_o-consolidation line of the normally consolidated clay, and the position of the limit state locus along that line was governed by the preconsolidation pressure (Fig. 2.2). In fact, the intersection of the limit state envelope and the K_o line corresponded roughly to p'_c. They concluded that the limit state surface of a natural clay was completely determined by its effective angle of shearing resistance, ϕ', which governed the K_o stress condition during deposition, and by its preconsolidation state of stress with its corresponding voids ratio.

With regard to the shape of the limit state envelope, Tavenas et al. (1977) found that the general shape of the limit state envelope for a natural clay can be characterized by three important soil parameters: $(p'_{vert})_{max}$, which is the maximum vertical pressure to which the clay has been exposed and which is close to p'_c from the oedometer test; $(p'_c)_{iso}$, which is the limit state stress in isotropic compression; and $(s_u)_{max}$, which is the maximum undrained strength of the clay. These parameters, along with a typical limit state envelope and critical state envelope for a natural clay, are presented on the (p', q) stress space in Fig. 2.2.

Earlier in this section the magnitude of the preconsolidation pressure was shown to govern the position of the limit state envelope in stress space. Consequently Tavenas et al. (1977) concluded that all

factors affecting the preconsolidation pressure would also affect the entire limit state envelope. It was in this regard that the work of Bjerrum on the effects of time on preconsolidation pressure was introduced. Bjerrum (1967) pointed out that with increasing time, the voids ratio of a clay at constant effective stresses decreased due to secondary compression (Fig. 2.3). This caused a 'quasi-preconsolidation' pressure to develop over-and-above any preconsolidation due to usual overconsolidation phenomena, such as desiccation, unloading, or groundwater table movements. The 'young', normally consolidated clay at an effective vertical pressure of p_o' has a void ratio of e_o. With the passage of time, secondary or delayed compression occurs, due to time-dependent adjustments of the soil structure at constant effective stresses. The rate of decrease of the voids ratio was approximately proportional to the logarithm of time. This leads to a more stable arrangement of the soil particles with a greater strength and reduced compressibility. After a period of 10,000 years, corresponding approximately to the geologic age of many post-glacial deposits, the void ratio of the clay has decreased to e_1. The clay then is classified as an 'aged', normally consolidated clay and exhibits a quasi-preconsolidation pressure of p_c', as shown in Fig. 2.3. This same process of ageing occurs in overconsolidated clays where part of the preconsolidation pressure is due to

Bjerrum (1973) indicated that the value of p_c' for a given time of loading increased in proportion to the value of p_o'. He showed that since the (p_c'/p_o') ratio depends on the amount of secondary compression and since, for a given time, the amount of secondary compression increases

with plasticity index of the clay, then the ratio of (p'_c/p'_o) increases with plasticity index. In addition, he indicated that the ratio of (s_u/p'_o) increased with plasticity index for both young and aged clays. These two relationships are shown in Figs. 2.4(a) and (b).

Tavenas et al. (1977) combined the relationships given by Bjerrum (1973), as shown in Figs. 2.4(a) and (b), to produce the broken line shown in Fig. 2.5. This broken line describes the relationship between the ratio $(s_u/p'_c)_{aged}$ and the plasticity index. Its importance lies in the fact that it was nearly identical to the $(s_u/p'_o)_{young}$ line. Because of this, they stated that the increase in strength, due to ageing, is proportional to the increase in p'_c. More generally, they stated that ageing would cause not only an increase in p'_c, but also an homothetic (i.e. geometrically similar) displacement of the entire limit state envelope.

With respect to strain rate Tavenas et al. (1977) confirmed the effect of rate or duration of loading on the preconsolidation pressure and the limit state envelope. By means of oedometer tests, similar to those of Bjerrum (1967), they showed that the preconsolidation pressure of a clay is reduced if the duration of loading is increased. Similarly, undrained triaxial tests at different strain rates indicated a reduction in strength as strain rate decreases. The magnitude of the displacement of the limit state envelope indicated a relatively homothetic movement with time. On this basis Tavenas et al. (1977) showed that the known effects of ageing and strain rate on p'_c applied to the entire limit state envelope. This hypothesis that the time-dependent behavior of a clay is completely described by the time-dependent displacement of its limit surface was also confirmed by Tavenas et al. (1978b).

The YLIGHT model for the stress-strain-time behavior of a natural clay can be summarized by the following:

1) the limit state envelope has an elliptical shape centered on the K_o-consolidation line of the normally consolidated clay;

2) the position of the limit state envelope in stress space is governed by the magnitude of the preconsolidation pressure;

3) the limit state envelope of a natural clay can be qualitatively determined by its effective friction angle, ϕ', which governs the K_o stress condition of the normally consolidated clay, and by its preconsolidation state of stress;

4) the limit state envelope can be quantitatively situated in stress space with knowledge of the parameters $(s_u)_{max}$, $(p'_c)_{iso}$, and $(p'_{vert})_{max}$, and the K_o-consolidation line (see Fig. 2.2);

5) the limit state envelopes at different depths and thus different p'_c values are all homothetic; and finally

6) the critical state line, as used in this model, is identical to the large strain, normally consolidated Coulomb-Mohr strength envelope.

It should be noted that further testing is required to confirm the general validity of this model for all natural clays. In particular the elliptical shape of the limit state envelope needs further investigation.

In this section the YLIGHT model and some of the thinking behind it has been presented. In the following section the qualitative predictive value of the model is examined by means of an example.

2.3 THE IMPLICATIONS OF THE MODEL

The importance of the YLIGHT model and the clarity with which it allows a qualitative understanding of clay behavior is best presented in an illustration. The example following was first presented in the 1977 paper of Tavenas and Leroueil.

When a clay is first deposited, its effective angle of shearing resistance and e-log p' relationship depend on its mineralogy, and the physical and chemical conditions present during its deposition. A clay with an effective angle of shearing resistance, ϕ', and an e-log p' relationship is shown in Fig. 2.6. As deposition of the clay occurs, the clay is exposed to increasing vertical overburden stresses, p'_o, and corresponding horizontal stresses, $K_o\ p'_o$. That is, consolidation takes place under anisotropic stress conditions. At the end of the deposition process the clay has a void ratio, e_B, corresponding to its final effective vertical stress, p'_B, and is normally consolidated. Corresponding to these stresses the clay has a limit state envelope, Y_o, as indicated in Fig. 2.6. At this point the in-situ stresses, p'_B and $K_o\ p'_B$, correspond to the point of intersection of the limit state envelope and K_o-line. The in-situ stresses are located on the limit state envelope because the clay is normally consolidated and further stresses would lead to a yielding or breakdown of its present structure.

With the development of delayed compression over a period of 10,000 years, the void ratio of the clay reduces from e_B to e_A at a constant overburden stress of p'_B. As a result of this reduction of voids ratio the clay builds up a reserve resistance in its grain structure over and above that which it has as a normally consolidated clay

(i.e. the clay becomes over-consolidated). This causes a homothetic movement of the limit state envelope of the clay to Y_1, which passes through point C. Point C represents the apparent preconsolidation pressure, p'_c, due to the delayed compression. If, in addition to this, the clay is off-loaded, for example by erosion or groundwater table movements, its stress state is then described by point A in Fig. 2.6.

Both the limit state envelope and the preconsolidation pressure of a clay are time-dependent. The limit state envelope, Y_o, represents the limit state conditions of this clay when it is normally consolidated at an effective vertical pressure of p'_o and has a voids ratio of e_B along its virgin compression line. This envelope indicates the lowest locus of stresses at which limit state is reached because it is a function of the normally consolidated grain structure and voids ratio of the clay. Off-loading to stresses at point A does not change the position of the 'young' limit state envelope at Y_o. However, if time effects cause the apparent preconsolidation pressure of the clay to increase, the limit state envelope moves homothetically to the right to a point corresponding to the apparent preconsolidation pressure, p'_c. The value of p'_c is time-dependent and, as shown by Bjerrum (1967), decreases with time. Therefore, with time this 'aged' limit state envelope, Y_1, moves to the left and eventually approaches Y_o. The implications of this are discussed in the following paragraphs.

On the basis of Fig. 2.6, constructed with the principles of the YLIGHT model, the behavior of a clay which is presently at point A in stress space can be presented qualitatively for any future stress conditions.

If the clay were submitted to stresses to the left of α along Y_1, failure would occur immediately after reaching the limit state surface, Y_1. Failure would be preceded only by small strains since the limit state envelope and Coulomb-Mohr envelope coincide in this case. For stresses to the right of α, failure would occur on reaching the normally consolidated branch of the Coulomb-Mohr rupture envelope. It would be preceded by fairly large strains because the stress path followed would first have reached the limit state envelope Y_1, and would then have followed the limit state surface until reaching the rupture envelope (i.e. critical state line).

If stress conditions in zone II were applied, the soil would suffer large consolidation deformation. As the stress path reaches the limit state envelope the behavior of the soil would switch from small strain to large strain. On a stress path following the K_o-consolidation line, the change in behavior in zone II is represented by the preconsolidation pressure break in an oedometer test using 1 day loading intervals.

Applied stresses in zone III would not lead to failure of the clay because they are below the Coulomb-Mohr rupture line. In this region between the 'young' (Y_o) and 'old' (Y_1) limit state envelopes the clay will develop secondary deformations at a rate associated with the position of the applied stresses relative to the two limit state envelopes. Stresses in zone III close to Y_o would develop only small secondary volumetric deformations. The rate and magnitude at which these deformations occur is analogous to those produced by stresses below the preconsolidation pressure in an oedometer test. As the preconsolidation pressure is approached, the rate of time-dependent deformation increases.

This is completely analogous to the rate of volumetric deformation which occurs as the stresses approach the Y_1 limit state envelope.

A stress condition in zone IV would initially be stable because it lies below the short-term limit state envelope, Y_1. However, with the passage of time the limit state envelope will move from Y_1 to Y_o, passing through any stress level in zone IV and leading to failure of the clay by creep when its stress level is reached. The loss of strength with time in this region is exemplified by the reduction of undrained strength which occurs with a decreased strain rate.

Zone V represents stress conditions which would not cause failure and under which only small deformations would occur. The Y_o limit state envelope is the lower strength limit of the clay corresponding to its grain structure as a normally consolidated clay. At stresses inside the Y_o envelope the clay behaves in an over-consolidated manner with only limited deformations occurring.

This example provides insight into the usefulness of the YLIGHT model for predicting the behavior of a clay exposed to various loading conditions. It is the first model for the mechanical behavior of clay which allowed some evaluation of the time effects and of possible deformations. It was theorized that a separate set of homothetic (Y_o-Y_1) limit state envelopes exist at each depth for a homogeneous deposit of clay with a given value of ϕ' (Tavenas and Leroueil, 1977).

The next section will briefly examine the applications of the YLIGHT model and the concepts of limit state and critical state to practical geotechnical engineering.

2.4 THE APPLICATIONS OF LIMIT STATE AND CRITICAL STATE TO PRACTICE

At present the major application of these concepts is as a useful conceptual tool for the geotechnical engineer in understanding and unifying the behavior of clay soils. The YLIGHT model, in particular, represents the most comprehensive picture of the stress-strain-time behavior of natural clay soils produced to this time. The previous section (section 2.3) has shown that identification of the limit state envelope and critical state line for a clay gives the engineer a powerful means to qualitatively predict the consequences of stress changes in the soil along any stress path. An early version of these practical considerations was given by Crooks and Graham (1976). Although these concepts and the YLIGHT model are useful in a qualitative sense, numerical analysis using mathematical relationships based on them has still not been developed. There are still several problems to be solved before any form of quantitative analysis based on these principles can take place. Most importantly, research studies must be performed on other types of clay soil in order to confirm that the YLIGHT model applies to soils other than the Champlain Sea clays for which it was developed. This thesis represents one such investigation.

The influence of time on the behavior of clay soils has been the subject of a large amount of research (for example, Lo, 1961; Leonards et al., 1964; Bjerrum, 1967). The incorporation of the time dependence of the limit state surface is probably one of the most satisfying aspects of the YLIGHT model. However, in its original presentation, the YLIGHT model, and in particular its proposal of homothetic movement of the limit state locus with time, was most speculative. A recent study

by Tavenas et al. (1978b) on the creep behavior of an undisturbed lightly over-consolidated clay has shown that the limit state surface was indeed time-dependent for Champlain Sea clays. Further research is needed to quantify this time dependence.

Having recognized the limitations of these concepts in terms of quantitative engineering analysis, it should be noted that these concepts have provided qualitative insights into several present practices in geotechnical engineering. In particular, Tavenas et al. (1977) illustrated several examples of this usage of the YLIGHT model. With regard to the interpretation of laboratory and in-situ tests, they stated that the measured shear strength of an undisturbed clay was a function of the effective stress path followed in the test. As a consequence, the strength measured in any test was only applicable to a practical problem if the stress paths in the test and the problem were similar. In addition, they noted that the limit state concept has shed some light on the analysis of settlements under structures which did not follow the stress path of an oedometer test. For example, McRostie, Burn, and Mitchell (1972) showed how the shape of the limit state envelope for Ottawa clay could explain serious consolidation settlements due to induced moderate horizontal pressures in a tied-back wall.

The most important application of these concepts to date was in the understanding of the behavior of embankments on clay foundations. This was thoroughly presented by Tavenas (1979). In this paper he discussed the limitations of the present practices used in embankment design on soft clays. He then used available field observations to develop a new understanding of the behavior of clay foundations during

and after embankment construction. The main finding was that clay response during construction was not truly undrained and that a significant consolidation develops initially in an over-consolidated natural clay foundation. It was not until the effective stress path of the clay reached the limit state envelope that it behaved in an undrained manner. However, upon reaching the limit state envelope the clay became 'normally consolidated' (i.e. destructured), and was then characterized by the undrained stress-strain properties of the normally consolidated clay. Therefore, an undrained analysis based on the properties of the intact (i.e. structured) clay was not relevant. The importance of this paper was twofold. Firstly, it provided a better understanding of the behavior of embankments on clay foundations. Secondly, it confirmed that limit state and critical state did indeed model the true behavior of the natural clay foundation. Nevertheless it should be pointed out that although this work has been widely accepted in general principle, it is still considered somewhat controversial in some details.

In summary, the concepts of limit and critical state, unified in the YLIGHT model, present the first useful qualitative model of the stress-strain-time behavior of natural clays. Prior to its use as a geotechnical design tool further research is required to verify and quantify these concepts in various different natural clay soils.

The next chapter presents the testing program and test results of this thesis.

CHAPTER 3

TEST RESULTS

3.1 INTRODUCTION

This study is part of a larger investigation by the geotechnical group at the University of Manitoba of the geotechnical properties of the glacial Lake Agassiz clay which underlie the Winnipeg area (Baracos et al., 1979; Pietrzak, 1979). Specifically the applicability of the limit state concept to these clays is examined. The testing program and test results are presented in this chapter.

The investigation was carried out on undisturbed block samples from the site of the proposed Physical Education Building at the University of Manitoba (Pietrzak, 1979). In accordance with the importance of minimizing soil disturbance during sampling, good quality samples from depth were obtained using the block sampler designed by Domaschuk (1977) at the University of Manitoba. After the block samples were removed from the ground, they were carefully transported to the laboratory where they were sealed with saran wrap, cheesecloth, and wax. Subsequently, they were placed in a moisture controlled storage room prior to testing. This storage room was not temperature controlled and some temperature fluctuations were noted during the storage period.

The samples used in the present study were taken in October, 1977 from borehole number three on the site. An average log for the boreholes on the site was presented by Baracos et al. (1979) and is included in this thesis as Fig. 3.1. Typically, the soil profile in the Winnipeg

area consists of a brown silty clay layer 1 m to 2 m thick, an irregular layer of tan-coloured silt usually less than 1 m thick, followed by a 3 m thick layer of brown clay, and a layer of blue clay 8 m to 10 m thick. These strata are underlain by tills and Ordovician dolomitic limestone. Although this is a typical profile, all layers may not be present at any given site.

All of the samples used in the present study were taken from block samples in the blue clay layer. The blue clay is medium to highly plastic, has medium stiff to stiff consistency, has no visible fissures, and contains numerous pockets, or inclusions, of grey silt and some pebbles. The standard classification data and mineralogy of the blue clay have been described previously by Baracos et al. (1979).

Although the deposits in the Winnipeg area have not been subject to any known geologic off-loading, they have been found to have over-consolidation ratios varying from 5 at the top of the blue clay to approximately 2 or 3 deeper in the deposit (Baracos et al.,1979). This is probably due to a combination of groundwater fluctuations; suction pressures associated with drying and freezing mechanisms; delayed compression or creep; and possibly cementation bonding formed at interparticle contacts by upward flowing groundwater with a high salt content (Render, 1970).

In order to investigate the applicability of the limit state concept to the blue clay, it was necessary to examine the strains resulting from applied stress increments up to and beyond the limit state envelope for the clay at a particular depth. To accomplish this, a series of nine, 76 mm diameter, drained stress controlled compression tests were

performed on specimens carefully trimmed from two block samples from two different depths in the blue clay. The trimming was done using equipment designed and constructed at the University of Manitoba and based on earlier equipment proposed by Landva (1964). Appendix A presents a detailed outline of the sample preparation and testing techniques used in the triaxial compression portion of this investigation. They are similar to those used by Crooks (1973), but have been carefully rewritten to conform with practice currently in use at the University of Manitoba. Since all samples at each depth were taken from the same block sample, the scatter in the data due to the natural variability of the clay was minimized.

The first phase of the triaxial compression tests was reconsolidation of the samples to their approximate in-situ stress levels. The importance of this with respect to preserving the field structure of the clay has been emphasized by Crooks and Graham (1976). They showed that laboratory reconsolidation strongly influences the stress-strain behavior and porewater pressure generation during subsequent shearing of a sample. In order to simulate as closely as possible the in-situ behavior of the clay, careful anisotropic reconsolidation to in-situ stresses is mandatory.

In this regard, there is some difficulty associated with estimating the in-situ effective vertical stresses for the block samples in this study because the groundwater table fluctuates with time. Baracos et al. (1979) stated that the general pattern of overall equilibrium of groundwater levels in the Winnipeg area is strongly influenced by seasonal changes and by recurring floods in areas not protected by the

Winnipeg floodway. The phreatic surface may vary from ground level during extremely wet years, to 6 m or deeper (Baracos et al., 1979) in periods of severe drought. For this reason, the value of p'_o is difficult to determine and an average value between these extremes was used in this study. The effective vertical stress for each block sample was calculated assuming the phreatic surface at a depth of 3 m and an average saturated unit weight of 17.5 kN/m^3 both above and below the phreatic surface.

The difficulties associated with identifying the in-situ horizontal effective stresses and the value of horizontal stress to use during reconsolidation have been addressed generally by Graham (1974). More specifically for Winnipeg clays, Baracos et al. (1979) found that at stresses below p'_o the stress ratio required to keep sample areas constant was approximately 0.65. This value was adopted during the reconsolidation phase of the present study.

Once the triaxial samples were reconsolidated to approximate in-situ stresses, the shape of the limit state envelope in (p', q) stress space was explored. To accomplish this, a series of stress paths were chosen such that they would define limit state stresses in various regions of stress space. Along each stress path the stresses were applied in stages,which were usually maintained for a period of 24 hours to ensure drainage. During each loading stage the axial and volumetric deformations were recorded at time intervals similar to the standard oedometer test (i.e. 1 min, 2 min, 4 min, etc.). The stress increments along each stress path were constant and based on accommodating a reasonable number of increments between the in-situ stress level and the limit

state stress level predicted on the basis of the preliminary limit state envelope determined by Baracos et al. (1979) (see Fig. 3.2). The samples were stressed well past the previously identified limit state envelope. In most cases, if a sample had not failed in drained compression, it was stressed four increments past the previously defined envelope. At that point the drainage was closed, and the sample was sheared to undrained failure.

During the undrained shear portion of a test, pore pressure and cell pressure were monitored with pressure transducers, reading to 0.1 kPa, mounted on the cell base. Axial displacements were measured to 0.01 mm with a dial gauge, while a proving ring was used to measure axial load. Initially, the sample was compressed 1 or 2 percent axial strain past its maximum shearing resistance, $(\sigma_1-\sigma_3/2)_{max}$. At that point the compression machine was switched off and readings of axial load and displacements were taken with time. This so-called relaxation test allows the relationship between shearing resistance and strain rate to be examined. After this overnight delay, the sample was sheared to large axial strains. Subsequently, the failed samples were removed from the triaxial cell and cut longitudinally. One-half of the sample was stored in a moist condition for electron microscope examination of its failure planes for another study. The other half was used to determine the final moisture content of the sample.

The nine triaxial compression tests on 76 mm diameter samples were designated T201 to T209. Tests T201 to T204 were performed on samples taken from block sample 4 at a nominal depth of 8.2 m, and tests T205 to T209 utilized samples from block sample 6 at a nominal depth of 10.0 m.

In addition to the triaxial compression tests two oedometer tests were carried out for each block sample. They were designated as C1 to C4. Tests C1 and C2 were taken from block sample 4. The sample for test C1 was prepared in the standard manner so that the compressibility in the direction of the in-situ vertical effective stress was measured. This procedure was also followed for tests C3 and C4 from block sample 6. In contrast, the sample for test C2 was prepared so that the compressibility in the direction of the in-situ horizontal affective stresses was found.

Standard classification tests (hydrometer, grain size analysis, Atterberg limits, and moisture content) were performed from the trimmings taken from each triaxial compression sample. Furthermore, two specific gravity tests were done from each block sample. The results of these tests are presented in Table 3.1 and are in general agreement with the classification results for the blue clay from Baracos et al. (1979).

The following sections present a more detailed review of the testing program and a detailed quantitative presentation of the test results. A discussion of the results is presented in Chapter 4.

3.2 TESTING PROGRAM

The drained triaxial testing comprised the largest and most important part of the investigation. It was essentially divided into two parts. Part one was basically a pilot series and consisted of tests T201 to T204. These samples were taken from block sample 4 of borehole number 3 at the site and were from a recorded depth between 7.9 and 8.4 m. In order to define the limit state envelope at this depth in (p', q) stress space, a set of four stress paths, lying below the Coulomb-Mohr envelope

previously defined by Baracos et al. (1979), were arbitrarily chosen (Fig. 3.2). Fig. 3.3 shows the proposed stress paths for the second test series, T205 to T209. Figs. 3.4 and 3.5 respectively, show the stress paths which were actually followed in the two test series. In Fig. 3.6 to 3.10 the stress-strain and strain energy plots for samples T201 to T204 are shown. These will be discussed in section 3.3.2.2.

The triaxial samples were first anisotropically restressed to approximate in-situ stress levels in three increments. Previous preliminary work by Baracos et al. (1979) had defined an average limit state envelope in the blue clay from tests on samples from depths ranging from 6.3 m to 12.3 m. The intersection of the proposed stress paths of Fig. 3.2 with this average limit state envelope established an expected limit state stress level along each path. The incremental stress levels along each stress path were determined by allowing six equal increments between in-situ stresses and the stresses at this expected limit state stress level. The samples were to be stressed along their respective stress paths until limit state stresses had been clearly established. Each stress level was to be maintained for 24 hours at which time it was expected that excess porewater pressures due to loading would have completely dissipated. Axial and volumetric deformations were recorded with time at each stress level. At the completion of the drained stress controlled portion of the test, the samples were transferred to a strain-controlled compression machine for undrained shearing.

During tests T201 and T202 of the pilot series some anxiety developed as to whether complete dissipation of excess porewater pressures (i.e. consolidation) was occurring in the 24-hour period following the

application of each new load increment. The plots of volume change versus the logarithm of time for each stress level of tests T201 and T202 indicated that at higher stress levels the volume change had not begun to decrease with log time after 24 hours. This is contrary to the traditional 'S' shape curve which is predicted by Terzaghi consolidation theory when a sample has consolidated fully under a load increment. Subsequently it was decided that the load duration of each stress level in tests T203 and T204 would be determined by the time required for the 'volume change-log time' plot to flatten, and thereby indicate complete consolidation. The relationship between volume change and time for each stress level past p_o' in test T203 is presented in Fig. 3.11. It was noted from these plots that as the stress level increased, the tendency for the volume change-log time plot to flatten off with log time decreased. The load increment ratios in test T203, in terms of σ'_{oct}, varied from 1.4 for stress level 4 to 1.1 for stress level 16. It was speculated by the author, with reference to earlier work on the effects of load duration and load increment ratio in one-dimensional consolidation (Lo, 1961; Leonards et al., 1964), that pore pressure generation and dissipation would not follow standard Terzaghi consolidation theory in these tests because of the small load increment ratios applied. As a consequence the volume change-log time plot would not give any indication of the end of the consolidation period, and there was no way of differentiating between the end of consolidation period and the beginning of creep.

To the knowledge of the author, the effect of load duration and load increment ratio on the determination of yield stresses has not been investigated by previous researchers. It has been shown by Tavenas et

al. (1977) in the YLIGHT model that time, and therefore load duration, has the effect of shrinking the yield envelope homothetically. However, previous investigators (for example, Graham (1974) and Tavenas et al., (1978)) have used the standard 24-hour load duration successfully in defining yield envelopes. The assumption inherent in their work is that the majority of the strains occurring the first 24 hours are due to creep (not consolidation) and that the majority of the movements occur during this period. These assumptions depend on the size of the sample and the load increment ratio. The verification of these assumptions would require an independent study of its own and is outside the scope of the present study. Due to this, and because previous investigators have apparently felt these considerations (that is, load duration and load increment ratio) to be of only secondary influence on the yield envelope determination, it was decided that the standard 24-hour load duration would be adopted in the further tests. These considerations will be discussed further in Chapter 4.

Test T204 was started with load durations greater than 24 hours. However, during its testing the author decided to abandon these longer load durations in favour of the 24-hour period because of the considerations discussed earlier. Therefore, the drained portion of this test was terminated prior to identifying yield and the sample put in undrained shear. This completed the pilot test series.

The complete stress-strain results for the drained portion of this series are presented in Appendix B, Tables B.1 to B.4, and in Fig. 3.6 to Fig. 3.11 of this chapter. The axial strains, ε_1, and volumetric strains, ε_v, for the drained portion of the tests were calculated using the original sample dimensions, and the recorded drainage burette and

dial gauge readings.

Based on the results of the pilot test series, it was decided that the second series of tests would follow the standard methodology used by Baracos et al. (1979) and others, (for example, Graham (1974), Crooks and Graham (1974), Tavenas et al. (1978a)). Each stress level was applied for a period of 24 hours. The stress increments along any given stress path were kept equal and chosen so that a minimum of three to four increments occurred between in-situ stresses and the estimated limit state envelope. The proposed stress paths for the second series, T205 to T209, are shown in Fig. 3.3. Three increments were used to reach in-situ stresses. The stress increments along each stress path were established by assuming four increments between in-situ stresses and the preliminary limit state envelope (except test T208 which had five increments). Test T209 was reconsolidated to in-situ stresses and then put directly into undrained shear in order to obtain information on the undrained behavior of the clay in-situ. The complete stress-strain results for the drained portions of these tests are found in Appendix B, Tables B.5 to B.9, and in Figs. 3.12 to 3.16.

The undrained stress-strain results for test series T201 to T204 and series T205 to T209 are found in Figs. 3.17 and 3.18 respectively. They are summarized in Table 3.2.

The two oedometer tests associated with each triaxial test series, were performed using standard one-dimensional consolidation techniques (Bowles, 1978). A Wykeham Farrance front loading consolidometer was used and the load increment ratio was 1.6. An initial vertical load of approximately 3/4 of p_o' was used to minimize swelling and perhaps enable a

more accurate determination of the preconsolidation pressure. The results of these tests are summarized in Table 3.3 and illustrated in Fig. 3.19. The following section reports the results of the drained, stress controlled, triaxial consolidation portion of the triaxial testing.

3.3 TRIAXIAL CONSOLIDATION

3.3.1 Reconsolidation to In-Situ Stresses

The limit state envelope of a clay is controlled by the in-situ grain structure of the soil. In order to examine the field behavior of a soil it is important to minimize the disturbance of the in-situ structure of the soil by careful sampling and laboratory preparation of samples. Although careful sampling and laboratory techniques minimize disturbance, changes in effective stresses in the soil samples due to these procedures are inevitable. Therefore, it is required that the samples be restressed to their in-situ effective stress levels. The problem of determining the in-situ effective stresses of clays in the Winnipeg area was discussed in section 3.1. The effective in-situ vertical stress for the samples of the pilot series, T201 to T204, was estimated to be 91.0 kPa. For the second series, T205 to T209, it was 106.2 kPa. On the basis of the previous test program (Baracos et al., 1979), the ratio of horizontal to vertical effective stress during restressing was taken as 0.65. The estimated in-situ stresses were applied in three equal increments, with at least 24 hours between each increment.

Table 3.4 compiles the results of reconsolidating the samples to the estimated in-situ stresses. In the pilot series, T201 to T204, the

strains on restressing were generally low with the maximum lateral strain at in-situ stresses being 0.33 percent. The axial strains at in-situ stress levels were all less than 2.33 percent. In test T203 the small volumetric strain (0.08 percent) and subsequent negative lateral strain (-0.78 percent) came as a result of an apparently large volume increase during the first stress increment. The volume decrease in the subsequent two increments was only slightly larger than the initial volume increase. It is suspected that the initial volume increase could represent a burette zeroing problem at the start of this test.

The strains on restressing to in-situ stress levels were somewhat larger in the second series of tests, T205 to T209. The axial strains to in-situ stresses were quite consistent for all five samples and were close to 2 percent. The lateral strains to in-situ stresses were also fairly uniform and varied from 0.61 to 0.89 percent.

The amount of straining which occurs during restressing is in part a measure of the amount of sample disturbance. Crooks (1973) states that axial strains below 2 percent at p_o' result when a small degree of disturbance occurs during sample preparation. With regard to this statement the axial strains in these tests of about 2 percent to p_o' are not very good. However, it should be noted that these axial strains to p_o' are also a reflection of the stress ratios used during restressing and also changes in the clay during storage. These considerations will be discussed in Chapter 4.

3.3.2 DRAINED COMPRESSION BEHAVIOR

3.3.2.1 Introduction

The proposed effective stress paths to be followed by the samples in both test series are shown in Figs. 3.2 and 3.3. Figs. 3.4 and 3.5 show the actual effective stress paths and stress levels of the samples in both series. The development of stresses and strains during the drained portion of each test is summarized in tabular form in Appendix B.

The purpose of the drained portion of the triaxial tests was to examine the development of strains as the samples were stressed along different stress paths. In previous studies (Graham, 1974; Crooks and Graham, 1976; Tavenas et al.,1977; Baracos et al.,1979),yield or limit state stresses were identified by stress-strain criteria which depended on the stress path of the test. For drained tests in which the shear stress was generally increasing (for example, T201, T202, T207 and T208) a plot of $(\sigma_1-\sigma_3)$ or σ_1' versus ε_1 could be used to identify yield stresses for the test. When the shear stress was nearly constant and only the octahedral stress was increasing (for example, tests T204 and T205), a plot of σ'_{oct} versus ε_v or σ_3' versus ε_3 was found best for identifying the yield stresses. In the case of a stress path between these extremes (for example, T203 and T206), no single criterion was best for defining the yield stresses.

In the earlier work, the limit state envelope was defined by the stresses at which the behavior of the soil changes from a stiff, largely recoverable response to a more compressible, irreversible response. This can be manifested in the stress-strain behavior by a bilinear relationship. The intersection of the projection of the linear sections is

identified as yield or limit state.

In addition to using various stress-strain plots to identify limit state, a plot of the scalar 'strain energy absorbed per unit volume', W, against σ'_{scalar} has been shown (Graham, 1974; Tavenas et al., 1978a) to be a useful limit state criterion. The incremental strain energy absorbed per unit volume between two stress levels, A and B, assuming a linear stress-strain relationship, is given by:

$$\Delta W = ((\sigma'_{1A} + \sigma'_{1B}/2)(\varepsilon_{1B} - \varepsilon_{1A}) + 2((\sigma'_{3A} + \sigma'_{3B}/2)(\varepsilon_{3B} - \varepsilon_{3A}) \ .$$

The total strain energy absorbed per unit volume at any particular stress level is calculated by summing the incremental strain energy absorbed per unit volume from each preceding stress level. The effective scalar stress $\sigma'_{scalar}{}^{*}$ is found by summing the changes in σ'_{scalar} between successive stress levels. The value of σ'_{scalar} at any stress level is the length of the stress path on a plot of (q/2) versus p'. The change in the effective scalar stress between two stress levels is given by:

$$\Delta\sigma'_{scalar} = (\Delta p'^{2} + (q/2)^{2})^{0.5}.$$

The new stress term was introduced, instead of using σ'_{oct} (as suggested by Tavenas et al. (1978a)), because there are some stress paths in which σ'_{oct} is constant. Along these paths a plot of W versus σ'_{oct} would not provide a useful limit state criterion. It should be noted that the strain energy absorbed to the in-situ stress level is approximately constant for each test series. For this reason it is shown in each test series (Figs. 3.10 and 3.16) as one data point.

---

* A more fundamental stress term, identified very late in this investigation, is: $\sigma'_{scalar} = ((\Delta\sigma'_1)^2 + (\Delta\sigma'_2)^2 + (\Delta\sigma'_3)^2)^{0.5}$. It is noted that the σ'_{scalar} term is not a true 'scalar' quantity. The term is used in this thesis to identify a empirical parameter which has proved useful in defining limit state.

In the following subsections of Chapter 3, the stress-strain data for each test is examined to determine, if, in fact, there is an identifiable limit state stress at which the behavior of the sample changes. The pertinent stress-strain plots and the W versus σ'_{scalar} plot will be presented in turn for each test.

3.3.2.2 Test Series: T201 to T204

The proposed and actual stress paths for this test series are presented in Figs. 3.2 and 3.4 respectively, and the complete stress-strain data is found in Appendix B, Tables B.1 to B.4. In addition, the triaxial consolidation results at the end of the drained portion of the test are summarized in Table 3.5. As was explained earlier (section 3.2), the standard 24-hour load duration for each stress level was not used in tests T203 and T204, and for the last three stress levels of test T202. In spite of this variation of load duration in tests T202 and T203, yield or limit state stresses were identified along those stress paths (see Fig. 3.4). However, the drained portion of test T204 was was terminated prematurely and yield was not identified along this stress path. This section will illustrate the procedures by which the drained stress-strain data was used to define a yield or limit state envelope.

As shown in Fig. 3.4, test T201 followed a stress path with generally increasing principal stress difference. Its stress path lay below the previously defined Coloumb-Mohr envelope and was parallel to its normally consolidated branch (Fig. 3.2). The stress levels past the estimated p'_o were determined such that there were six equal increments between the in-situ stress level and the previously defined limit state envelope.

Table B.1 lists the complete stress-strain results from this test. The sample was stressed for fifteen equal increments past p'_o. During the fifteenth increment (at stress level 18) it failed in 'drained shear' overnight, after the 8 hour-reading. As indicated in Table B.1 of Appendix B, the load duration for each stress level was approximately 24 hours during this test.

To determine the limit state point along this stress path, all of the various available yield criteria were examined. In the case of a stress path with generally increasing principal stress difference it is expected that plots of $(\sigma_1-\sigma_3)$ or σ'_1 versus ε_1 would be the most useful. Figure 3.6 shows the relationship between σ'_1 and ε_1 for T201. An initial linear relationship is well-defined and includes stress levels 3 to 13. A second linear section is more difficult to define because the last stress level (18) represents the stress-strain state of the sample just as it moves off towards rupture. However, a second tentative linear section is shown drawn through stress levels 16 and 17. This allows a yield or limit state stress point to be defined as indicated prior to rupture. Figure 3.7 shows the relationship between $(\sigma_1-\sigma_3)$ and ε_1. An initial linear relationship is quite evident through stress levels 3 through 13. However, a second linear section is again difficult to determine because the lack of data points between the first linear section and rupture at stress level 18. In spite of this, a tentative second linear section is proposed allowing a yield stress point to be defined as indicated.

Figure 3.8 shows the relationship between σ'_{oct} and ε_v for this test. A bilinear behavior is again noted. However, there is significant scatter associated with the initial linear section and the second section

is defined by only three data points. For these reasons the intersection of the two lines was not considered a valid determination of limit state in this test. It should be noted that on stress paths with generally increasing shear stresses the component of volumetric strain can be small, and for that reason not useful in defining limit state.

Along some stress paths a plot of σ_3' versus ε_3 has been found useful in defining limit state (Baracos et al.,1979). However, for this test the plot does not reveal a distinct change in behavior of the sample (see Fig. 3.9). Because ε_3 is calculated from measured volumetric and axial strains and contains the experimental error of both, this plot was found to exhibit significant scattering in almost all tests in this program.

Figure 3.10 shows the relationship between strain energy absorbed per unit volume, W, and the effective scalar stress, σ'_{scalar}, along the stress paths. For test T201 the plot of W versus σ'_{scalar} shows a clearly definable bilinear behavior.

The yield points defined by the different stress-strain relationships and by the energy criterion are summarized in Table 3.6. By interpolating along the stress path of the test the yield points defined by the different criteria have been resolved to a common stress component, σ'_{oct}. For test T201, the three useful criteria predict limit state stresses in terms of σ'_{oct} which are within 4 kPa. The range of limit state stresses along this stress path are shown in Fig. 3.4.

In test T201 the sample 'ran away' to failure between 8 and 24 hours after the final stress level was applied. The average axial strain rate over the first 8 hours of this stress application was 0.56 percent

per hour. This strain rate is from 0.5 to 2.0 times the strain rates used in the undrained portion of the other tests in this series. For this reason the stress calculated after 8 hours for the last stress level have been taken as the critical state stress for this test, and no strain rate correction has been applied.

The stress path for test T202 is shown in Fig. 3.4 and Table B.2 contains the complete stress strain data from the drained portion of the test. The plots of the various stress-strain data are found in Figs. 3.6 to 3.10. The sample was stressed by seventeen equal increments past p'_o. The load duration for each stress level was approximately 24 hours except for the last three stress levels, which were applied for 117, 145, and 264 hours respectively. The load duration was increased for these stress levels because the previously mentioned concern about the effect of load duration was to be investigated. The sample did not fail during the drained portion of this test.

In the plot of σ'_1 versus ε_1 shown in Fig. 3.6, a distinct bilinear behavior is observed. An initial linear section is well-defined with very little scatter. A second linear section with a flatter slope is also apparent using stress levels 15, 16 and 17. The intersection of these two lines marks a distinct change in behavior which is noted as yield. It is of interest to note that a line parallel to the second linear section may be drawn through the final three stress levels which had longer duration loading. The significance of this will be discussed in Chapter 4. The plot of $(\sigma_1-\sigma_3)$ versus ε_1 for T202 (see Fig. 3.7) produces an identifiable bilinear behavior and yield point also. However, the construction of a parallel line through the final three stress levels

is much more tentative. Plots of σ'_{oct} versus ε_v and σ'_3 versus ε_3, as shown in Figs. 3.8 and 3.9 respectively, do not produce any identifiable bilinear behavior; the behavior is multilinear and complex. The relationship between W and σ'_{scalar} for test T202 is shown in Fig. 3.10. This relationship shows a clear discontinuity in behavior which may be interpretted as two linear sections. It is noted that there is a set of transition stress levels (10 to 14) between the two linear sections. Also, a line parallel to the second linear section may again be drawn through the last three stress levels with longer load duration.

The yield points defined by the different stress criteria are listed in Table 3.6 in terms of σ'_{oct} along the stress path for this test. The values of limit state produced by the σ'_1 versus ε_1 and $(\sigma_1 - \sigma_3)$ versus ε_1 criteria are almost the same. This is expected because the two criteria are smaller. The yield stress predicted from the energy criterion is somewhat smaller but still within 6 percent of the average yield stress predicted by the other two criteria.

The stress path for test T203 is shown in Fig. 3.4 and the complete stress-strain results for the drained portion of the test are found in Table B.3. As noted earlier, questions about the effect of load duration on the limit state envelope led to this test being conducted with load durations greater than one day. The length of the load duration for each stress level is listed in Table B.3.

Figures 3.6 and 3.7 show the plots of σ'_1 and $(\sigma_1 - \sigma_3)$ against ε_1 for this test. The relationship between σ'_1 and ε_1 seems to indicate a strain hardening bilinear behavior with the change in behavior occurring at stress level 8. This same interpretation is made from the plot of

($\sigma_1 - \sigma_3$) versus ε_1 in Fig. 3.7. This type of behavior has been noted by Baracos et al. (1979) in their stress controlled drained tests on Winnipeg clays. The low principal stress difference along the stress path of the test makes these two stress-strain plots of little value for defining limit state stresses.

The relationship between σ'_{oct} and ε_v is more helpful in defining limit state stresses along this stress path. An initial linear behavior is well-defined and includes stress levels 3 through 11. After stress level 11 there is an abrupt change in behavior and an increased volumetric straining per incremental loading. Figure 3.11 shows the relationship between volume change and log time for each stress level past p'_o. The very large volume changes recorded for stress levels 12 and 13 are possibly in error. The error may be due to the generation of gas in the sample, or to incorrect readings. It is noted that the 'σ'_{oct} versus ε_v' data points for the final three stress levels (14, 15 and 16) can be joined to form a straight line with a flatter slope than the initial linear portion through levels 3 to 11. It may be speculated that stress levels 12 and 13 would have been on that same line had the correct volume changes been recorded. The credibility of the explanation is strengthened when it is noted that the total volume changes recorded for this test were larger than the volume change calculated from the change in moisture content during the test. This point is discussed further in the next chapter.

In Fig. 3.11 it is noted that for stress levels below the limit state (stress level 11) a large proportion of the volumetric straining occurs in the first 24 hours and the rate of volumetric strain seems to decrease with log time. In contrast at stress levels past limit state a

substantial portion of the volumetric strain occurs after the first 24 hours and the volumetric strain rate of the sample in log time seems to approach a constant value.

Figure 3.9 shows the relationship between σ_3' and ε_3 for test T203. Since ε_3 is calculated from the measured volumetric and axial strains, it also shows a marked discontinuity at stress level 11. This tends to confirm this stress level as limit state. However, as mentioned earlier, the scatter associated with the 'σ_3' versus ε_3' plots makes their use as a limit state criterion difficult.

The plot of W versus σ'_{scalar} for this test is shown in Fig. 3.10. In this case the data does not produce well-defined bilinear behavior. However, there is a clear discontinuity in the relationship occurring at stress level 11. This discontinuity can reasonably be taken as the limit-state stress level. The different length of load durations for each stress level probably contributed to the scatter associated with the plot. In addition, the questionable volume change readings associated with stress levels 12 and 13 has produced uncertainty in these energy calculations.

The yield points associated with the various stress-strain criteria are shown in Table 3.6 in terms of σ'_{oct} along the stress path for T203. In this case only the 'σ'_{oct} versus ε_v' and the 'W versus σ'_{scalar}' plots are useful and they both indicate yield at stress level 11.

The stress path followed by test T204 is shown in Fig. 3.4 and Table B.4 lists all of the stress-strain data associated with the drained portion of the test. This test was only carried to stress level 6 along its proposed stress path. The test was originally begun with the intention of allowing the sample to consolidate at each stress level until the

volume changes began to level off on a plot of ΔV versus log time. However, as discussed earlier in section 3.2, test T203 showed that this methodology was only adding ambiguity to the results. For this reason it was decided to terminate the drained portion of T204 and the pilot test series at stress level 6,and go on to the next series of tests. The plots of the various stress-strain criteria (Fig. 3.6 to 3.10) all show a linear relationship for this test up to stress level 6. It is assumed, therefore, that limit state stress along this stress path had not been reached when the sample was put into undrained shear.

On the basis of the limit state stresses identified during these tests a tentative yield envelope for the blue clay at 8.2 m depth has been drawn on Fig. 3.4. Because of the limited amount of data the shape of the envelope could not be determined accurately. The exact shape has been drawn similar to the previously defined envelope of Baracos et al. (1979) and is subjective. No attempt was made to draw the envelope through the yield point identified in test T203. The reason for this will be discussed in Chapter 4 and is related to the load durations used during this test. The branch of the limit state envelope in the overconsolidated region is defined by one test only and is therefore rather speculative.

The drained results of the second test series, T205 to T209 are presented in the next section. The drained portion of the tests in this series were performed using a standard '24-hour' load duration period throughout.

3.2.2.3 Test Series: T205 to T209

The proposed effective stress paths for this series of tests are shown in Fig. 3.3. Test T209 was consolidated to in-situ stresses only and therefore did not provide any information on the drained stress-strain behavior of the soil. In the other tests in this series the size of the load increment was based on having four equal increments between in-situ stresses and the previously defined limit state envelope. In the case of T208 five increments were used between in-situ stresses and the previously defined envelope. The load duration used in all of these tests was 24 hours.

The actual effective stress paths followed in the tests is shown in Fig. 3.5 and the complete stress-strain data for the drained portion of the tests is given in Appendix B, Tables B.5 to B.9. Figures 3.12 to 3.16 show the relationships between the various stress-strain parameters for each test. The triaxial consolidation results at the end of the drained portion of the tests are summarized in Table 3.5.

Test T205 follows a stress path of almost constant principal stress difference (see Fig. 3.5). For this reason the plot of $(\sigma_1-\sigma_3)$ against ε_1 for this test (Fig. 3.13) is linear and provides no information about limit state. Similarly the relationship between σ_1' and ε_1 shown in Fig. 3.12 is linear and does not indicate any change in behavior of the sample as it is stressed along its stress path. However, the relationship between σ'_{oct} and ε_v for this test, shown in Fig. 3.14, is revealing. A distinct bilinear behavior can be identified, with the second section having a flatter slope than the first (i.e. there is greater volumetric strain per unit of octahedral stress). The yield

stress has been indicated on the figure.

The plot of σ_3' against ε_3 for this test (Fig. 3.15) can be interpretted in a bilinear manner. However, the scatter of the data points makes a range of interpretations possible and for this reason a yield stress was not identified using this stress-strain behavior. In contrast, the relationship between strain energy absorbed per unit volume and the effective scalar stress (Fig. 3.16) shows a clear discontinuity which can be identified as the yield stress. The yield points defined by this criterion and by the other stress-strain criteria are summarized in Table 3.7. There is good agreement between the yield stress defined by 'σ_{oct}' versus ε_v' and 'W versus σ'_{scalar}'. The range of possible yield stresses along the stress path is illustrated on Fig. 3.5.

The stress path followed by sample T206 is shown in Fig. 3.5 and the stress-strain results of the drained portion of this test are found in Appendix B, Table B.6. The stress path of this test has both principal stress difference and effective octahedral stress increasing, and lies below the previously defined normally consolidated Coulomb-Mohr envelope. The relationship between σ_1' and ε_1 indicates a distinct bilinear behavior. The two linear sections are well-defined and intersect at the yield point shown in Fig. 3.12. Similarly the plot of $(\sigma_1-\sigma_3)$ versus ε_1 for this test in Fig. 3.13 indicates a distinct bilinearity separated by the yield point shown. In the graph of σ'_{oct} versus ε_v two linear sections are definable. Although the interpretation of the linear sections is subjective, there is no doubt that the behavior does change along the stress path. The yield point interpreted from the plot is shown on Fig. 3.14. As in earlier tests, the plot of σ_3' versus ε_3 shown in Fig. 3.15 exhibits too much scatter to be of any use in locating the

yield point. The strain energy absorbed per unit volume against the effective scalar stress is shown in Fig. 3.16. There is an obvious change in behavior shown, but defining the stress at which it takes place is subjective due to scatter in the data. In spite of this, a yield point has been defined from the data and is shown in the figure.

Table 3.7 summarizes the yield points defined by various criterion for this test. There is some scatter but on the whole the values found show good agreement. The range of yield stresses for the stress path is shown on Fig. 3.5.

The stress path of test T207 had octahedral stress and principal stress difference increasing at about the same rate. The sample was assumed to have failed at stress level 12 after 26 hours. Continuous axial deformation was occurring at that point. Figure 3.5 illustrates the stress path for the test and Table B.7 of Appendix B contains the complete stress-strain results. It should be noted that there was a loss of cell pressure for a short period of time during stress level 5 of this test. Therefore, the stress-strain results at this stress level exhibits some scatter.

As with test T201, there is some difficulty in identifying yield along this stress path because rupture follows yielding within two or three stress levels. For that reason it is difficult to identify a second linear behavior prior to rupture. However, there is a definiite change in behavior of the sample prior to rupture. Figure 3.12 shows the relationship between σ_1' and ε_1 for this sample. An initial linear section up to stress level 9 is well-defined, afterwhich the amount of straining per increment of stress increases markedly. A second linear

section has been shown through stress levels 10 and 11. The interpretation of this is subjective, but nevertheless it would not change the identified yield point significantly. The plot of $(\sigma_1-\sigma_3)$ versus ε_1 in Fig. 3.13 has been interpreted in a similar manner, and the yield point found is shown on the figure. The relationship between effective octahedral stress and volumetric strain is shown in Fig. 3.14 and is linear for the entire range of stresses. The plot of radial stress versus radial strain for this test shows an abrupt discontinuity between stress level 9 and 10. This is illustrated in Fig. 3.15 and can be interpreted as a yield point. For T207 the W versus σ'_{scalar} plot does not reveal a distinct yield point. The relationship is shown in Fig. 3.16 and can only be interpreted as curvilinear without any distinct changes in behavior.

The yield points identified by the different criterion for T207 are summarized in Table 3.7 and are in good agreement. They are shown on the stress path in Fig. 3.5.

Sample T207 failed in drained shear during the twelfth stress level. The average axial strain rate over the 26-hour load duration was 0.23 percent per hour. This average strain rate is within a factor of 4 of the initial strain rates of the undrained portions of the other tests in this series. For this reason the stresses calculated at 26 hours and shown in Fig. 3.5 are taken as the critical state stress for this test. No correction for strain rate has been applied.

The final drained test in this series, T208, followed a steep stress path in (p',q) stress space. This is shown in Fig. 3.5, while the stress-strain results are tabulated in Table B.8 of Appendix B. The

sample failed abruptly approximately 90 minutes after the application of the thirteenth stress level. The plots of σ_1' against ε_1 and $(\sigma_1-\sigma_3)$ versus ε_1 shown in Figs. 3.12 and 3.13 respectively, may be interpreted as linear prior to the sample moving to failure at stress level 11. There is no yield or limit state prior to rupture. The graphs of σ'_{oct} versus ε_v and σ_3' versus ε_3, shown in Figs. 3.14 and 3.15, also reveal linear behavior up to rupture. The energy criterion, W versus σ'_{scalar}, shown in Fig. 3.15, was interpreted as curvilinear and does not indicate a limit state stress prior to rupture. On the basis of the various yield criterion for this test it is concluded that the sample does not yield prior to failure. The failure stresses are taken as those just prior to the sample running away after 90 minutes. It is noted that the average axial strain during this final stress level was 0.56 percent per hour.

On the basis of the limit state stresses defined in Table 3.7 for this test series, it was possible to propose a limit state envelope for the blue clay at the 10.0 m depth. This is shown in Fig. 3.5 and is better defined than the one from 8.2 m depth. The interpretation of the shape of the envelope is less speculative because of the increased amount of data.

The limit state stresses from both the 8.2 m and 10.0 m tests have been plotted together in Fig. 3.20. An average limit state envelope can be reasonably drawn through this data and is shown on the figure. It is noted that this envelope is much larger than the limit state envelope defined by Baracos et al. (1979) on the basis of samples of the blue clay

from depths of 6.3 to 12.3 metres. Also, the orientation of the limit state envelope, as interpreted by the author from the present data, is somewhat different. These results will be discussed in Chapter 4. The next section presents the results of the undrained portion of the triaxial tests.

3.4 UNDRAINED SHEARING

3.4.1 Introduction

Samples which had not failed during the drained, stress controlled portion of their test, were then transferred to a strain controlled compression frame for undrained shearing to rupture. The testing procedures associated with the undrained portion of this study are outlined in Appendix A, sections D and E. These tests provided information on several aspects of the soil's behavior during shearing under undrained conditions. In particular, the stress-strain and porewater pressure generation characteristics of each sample were examined. This included examination of the porewater pressure parameter, A_f, the strain rate parameter, $\rho_{0.1}$, and the elastic modulus, E_{50}, for each test. In addition, the failure stresses found in the test permitted an evaluation of the normally consolidated Coulomb-Mohr envelope for the clay at both depths. The failure stresses from the undrained tests on overconsolidated samples (T204 and T209) were used, in conjunction with the drained stress controlled data, to identify the limit state envelope in the overconsolidated region. The normally consolidated Coulomb-Mohr envelope and the limit state envelope for the 8.2 and 10.0 m depths have been illustrated in Figs. 3.4 and 3.5 respectively. The average envelopes from the samples

at both depths is shown in Fig. 3.20.

The results of the undrained shear tests, as well as those tests which failed in drained shear, have been summarized in Table 3.2. The next section will present the undrained results for each test series in more detail. A detailed discussion of the results is found in Chapter 4.

3.4.2 Test Series: T201 to T204

All of the tests of this series, except test T201 which failed in drained shear, were put into undrained shear at the end of the drained consolidation phase of the testing. The stress-strain conditions for each sample prior to undrained shearing are summarized in Table 3.5. The undrained stress paths to maximum deviator stresses are shown in Fig. 3.4 for each test and the complete shear test results are summarized in Table 3.2.

The normalised undrained stress-strain behavior for each test is presented in Fig. 3.17. Samples T202 and T203 were consolidated well past limit state stresses prior to undrained shearing. Therefore the in-situ grain structure of the sample had been completely modified and the reserve resistance associated with overconsolidation had been destroyed. The stress-strain curves for these tests indicate typical normally consolidated behavior. The normalised deviator stress-axial strain plot shows the deviator stress rising quickly to a peak deviator stress, then gradually decreasing with increasing axial strain. Sample T202 reaches maximum deviator stress at 0.58 percent, whereas the maximum principal stress ratio occurs at an axial strain of 2.3 percent. On the other hand, sample T203 reached maximum deviator stress at 2.05 percent axial

strain, and the maximum principal stress ratio does not occur until axial strains of 10.1 percent. It should be noted that the maximum principal stress ratio in this test was reached after the relaxation test, after the initial strain rate that has been approximately doubled.

The elastic modulus values, E_{50}*, were 54.1 MPa and 42.9 MPa for tests T202 and T203 respectively. The value of another useful parameter, the relative stiffness, $(E_{50}/(\sigma_1-\sigma_3)/2)_{max}$, was almost identical in the two tests (see Table 3.2).

Curves of porewater pressure increase, $\Delta u/\sigma'_{1c}$, versus ε_1 for these two tests are similar (Fig. 3.17). They rise fairly rapidly up to maximum deviator stresses, at which point they increase less rapidly and become substantially constant at large strains. It is noted that the value of $\Delta u/\sigma'_{1c}$ for sample T203 with the flatter stress path (i.e. closer to isotropic consolidation) is about twice that of sample T202 which underwent more anisotropic consolidation.

It should be noted that both of these samples were allowed to remain at their final consolidation stresses for a considerable period of time prior to undrained shearing. Samples T202 and T203 remained at their final stresses for 11 and 5 days respectively. In theory, this period of delayed compression may have allowed the samples to gain some degree of reserve resistance at their final consolidation stresses. The stress-strain behavior does not seem to indicate any degree of over-consolidation, however there is no way of analysing the effect of this delay period.

---

* E_{50} is the secant modulus obtained by measuring the slope of the $(\sigma_1-\sigma_3)$ versus ε_1 plot from the beginning of shear to 50 percent of maximum deviator stress.

As indicated in Fig. 3.4, sample T204 was only stressed three increments past in-situ stresses in drained shear. The drained consolidation results indicated that the sample had not reached limit state stresses prior to undrained shearing (see section 3.3.2.2). Therefore, the sample was overconsolidated ($p'_c/\sigma'_{1c} = 1.72$) and still had some of the reserve resistance associated with its in-situ grain structure. The stress-strain behavior of this sample, illustrated in Fig. 3.17, is more brittle than that of the normally consolidated samples (T202 and T203). The maximum deviator stress and the maximum principal stress ratio occur concurrently at an axial stress of 2.62 percent. Thereafter, the deviator stress falls off abruptly to a much lower value at which it remains essentially constant.

The elastic moduli, E_{50}, and the relative stiffness $E_{50}/(\sigma_1-\sigma_3)/2_{max}$ for this test are significantly lower than tests T202 and T203 (see Table 3.2). This is contrary to what might have been expected. Crooks (1973) suggested that overconsolidated samples might have a lower relative stiffness because their field grain structure may have been disturbed to some extent during sample and laboratory preparation. On the other hand, samples with a new normally consolidated laboratory-formed grain structure have not been disturbed since formation, and have a relative stiffness which is strictly a function of their consolidation stress, σ'_{1c}. Figure 3.21 shows a plot of relative stiffness versus (σ_c^{-1}) for all of undrained tests.

The porewater pressure generation during this test is shown in Fig. 3.17. It rises quickly to a peak at maximum deviator stress, then drops off abruptly. After this, it decreases only slightly during the remainder of the test.

As in test T202 and T203, it should be noted that sample T204 was allowed to consolidate at its final stress level for an extended period of 9 days prior to undrained shearing. The overconsolidated behavior of the sample may then be due to a combination of two effects. Firstly, the sample had not been stressed past its limit state envelope and therefore retained a portion of its reserve resistance* due to its in-situ grain structure. Secondly, the extended period of time at the last stress level would have allowed the sample to gain some reserve resistance due to delayed compression or creep.

On the basis of the maximum deviator stresses found in these undrained tests and the drained tests discussed earlier, the limit state envelope and the normally consolidated Coulomb-Mohr envelope for the clay at this depth have been found and are shown in Fig. 3.4. Due to the small amount of data the envelopes established are admittedly tentative.

The values of the porewater pressure parameter, A_f, for each test have been tabulated in Table 3.2. Previous work has shown that this parameter is related to consolidation history, and it is usually plotted against overconsolidation ratio, p'_c/p'_o (Baracos et al., 1979). However, previous work on Winnipeg clays by Baracos et al. (1979) plotted A_f values against $(1/\sigma'_{1c})$ because of uncertainty about their oedometer results. The values from this test series are shown on the plot in Fig. 3.22. They exhibit some scatter about the line for 76 mm samples proposed by Baracos et al. (1979).

In order to investigate the effect of strain rate on the undrained strength of the soil a relaxation test was performed on each sample after

---

* See definition of over-competent structure on page 24.

approximately one or two percent strain past the maximum deviator stress. This relaxation test, first developed by Kenney (1966), is described in Appendix A and involves stopping the motor drive at a given strain and taking readings of stress and strain with time. When the motor is stopped the sample continues to strain at a decreasing rate due to stored energy in the proving ring. The strain rate effect is represented by the parameter $\rho_{0.1}$, which gives the percent increase in undrained strength due to a tenfold increase in strain rate, as related to the strength at a strain rate of 0.1 percent per hour. The values of this parameter along with the average axial strain during the relaxation period, ε_ρ, are given in Table 3.2. The average undrained strength versus the axial strain rate, from the relaxation test data, is shown in Fig. 3.23. Previous work summarized by Graham (1979) has suggested that the $\rho_{0.1}$ parameter is related to the plasticity index of a clay. The values of $\rho_{0.1}$ versus plasticity index for these tests has been plotted along with other data from Graham (1979) and is shown in Fig. 3.24. This data only confirms the general scatter associated with the plot.

The next section reviews the undrained tests results from the second test series.

3.4.3 Test Series: T205 to T209

In this series, only samples T205, T206 and T209 were tested in undrained shear. The other two samples failed in drained shear. The undrained effective stress paths to maximum deviator stress are shown in Fig. 3.5. The stress-strain conditions for each sample prior to undrained shearing are presented in Table 3.5 and the complete shear test results

are found in Table 3.2.

Figure 3.18 shows the normalized undrained stress-strain behavior for each sample. Samples T205 and T206 were stressed well past limit state during the drained stress controlled portion of their tests. These samples were allowed to remain at their final stress for only a short period (approximately 1 day during back pressuring) prior to undrained shearing. Consequently no significant amount of delayed compression could occur and their grain structure was normally consolidated and strictly a function of the consolidation stresses. In both tests the deviator stress rises gradually to a maximum value at which point it remains relatively constant for the rest of the test. Sample T205 reached maximum deviator stress at an axial strain of 5.5 percent. The maximum principal stress ratio was reached at 10.3 percent axial strain after the initial strain rate had been approximately doubled. Sample T206 reached maximum deviator stress at an axial strain of 2.3 percent and maximum principal stress ratio at a slight larger axial strain of 4.6 percent. The axial strain rate in this test had been doubled after the relaxation test and prior to reaching the maximum principal stress ratio.

The elastic moduli for samples T205 and T206 were similar and had values of 28.2 MPa and 30.0 MPa respectively. The relative stiffness* measured in the two tests are also quite close and were calculated as 273 and 262 for samples T205 and T206 respectively.

The curves of normalized porewater increase, $\Delta u/\sigma'_{ic}$, versus ε_1 for these two tests, shown in Fig. 3.18, are of the same general shape with a gradual increase up to maximum deviator stress afterwhich the porewater

---

* Defined on page 69.

pressure increases only slightly. As noted in the pilot test series, the magnitude of the porewater pressure increase during shear seems to be a function of the consolidation history. Sample T205 was consolidated under essentially constant deviator stress while the stress path of sample T206 had an increasing component of deviator stress (see Fig. 3.5). Figure 3.18 shows that the normalized porewater pressure increase in sample T205, which has a more isotropic stress path, is significantly higher than sample T206 with more anisotropic consolidation.

As indicated in Fig. 3.5, sample T209 was consolidated only to its estimated in-situ stresses and then put into undrained shear. Reconsolidation to in-situ stresses preserves the grain structure of the soil in the field and allows its in-situ undrained behavior to be examined. The undrained stress-strain behavior of the sample during this test is shown in Fig. 3.18 and summarized in Table 3.2. The maximum deviator stress and maximum principal stress ratio occur together at an axial strain of approximately 2.1 percent. After reaching this peak the deviator stress decreases abruptly and eventually levels off at high strains. The porewater pressure behavior is similar showing a peak value at an axial strain of 1.6 percent, followed by an abrupt decrease and eventually a constant value. This behavior is characteristic of a lightly overconsolidated sample. The average overconsolidation ratio, p'_c/σ'_{1c}, from the oedometer testing presented in the next section, is 2.57. The elastic modulus and relative stiffness for this test are 8.5 MPa and 171 MPa respectively.

The values of the porewater pressure parmater, A_f, for the undrained tests of this series have been plotted on Fig. 3.22 with those

of the pilot series. As previously observed, the results from these tests do not fit the relationship proposed by Baracos et al. (1979) very well. However, it is noted that the results of T205 and T206 could reasonably lie on the projection of the proposed line for 76 mm samples.

The values of relative stiffness versus $(\sigma_c'^{-1})$ for the tests of this series are shown plotted on Fig. 3.21. As with the results of the pilot series, the values are not in good agreement with the line by Baracos et al. (1979).

A relaxation test was carried out for each undrained test of this series and the results are shown in Fig. 3.25. It is of interest to note that the strain rate effect for the two normally consolidated samples, T205 and T206, are closely similar. The values of the strain rate parameter, $\rho_{0.1}$, are listed in Table 3.2. They are plotted against plasticity index on Fig. 3.24 along with the tests of the earlier series. These values seem to indicate that a good correlation do not exist between $\rho_{0.1}$ and plasticity index.

Using the shear strengths obtained from these undrained tests and the previous information from the drained tests, the limit state envelope and normally consolidated Coulomb-Mohr envelope for the clay at a depth of 10.0 m have been tentatively identified in Fig. 3.5.

Figure 3.20 shows the limit state stresses and undrained strengths identified in both series of tests. On the basis of all tests in this study it is reasonable to form an average limit state envelope for samples from both the 8.2 and 10.0 metre depths. This is shown on Fig. 3.20. In addition an average normally consolidated Coulomb-Mohr envelope for both depths has been drawn. The effective angle of shearing resis-

tance determined from this line is 18° and the effective cohesion intercept is zero. This compares with a ϕ' value of approximately 20° and an effective cohesion intercept of 2 kPa for the 76 mm samples in the recent study by Baracos et al. (1979).

The final section of this chapter presents the results of the one-dimensional consolidation tests.

3.5 ONE-DIMENSIONAL CONSOLIDATION

Four oedometer tests were performed on 63.5 mm diameter samples which were trimmed from the same block samples used in the triaxial compression portion of this study. Standard one-dimensional consolidation testing techniques (see Bowles, 1978) were used in all tests, except that an initial vertical load of 3/4 of p_o' was adopted to minimize swelling and the load increment ratio was set at 1.6. The results of these tests are summarized in Table 3.3 and the e-log σ_v' curves are shown in Fig. 3.19.

Tests C1 and C2 were performed on samples taken from a nominal depth of 8.2 m. Sample C1 was trimmed such that the compressibility of the clay in the direction of the in-situ effective vertical stress was measured. In contrast, sample C2 was prepared such that the compressibility in the direction of the in-situ effective horizontal stress was measured. The preconsolidation pressure, p_c', and the compression index, C_c, for these two tests were determined from the e-log σ_v' curves in Fig. 3.19 and are listed in Table 3.3. The values of p_c' for tests C1 and C2 are both 270 kPa and were determined using the Casagrande construction. Due to the rounded nature of the curves and the slight concave upward

curvature of the virgin consolidation lines of these curves, the p_c' values are difficult to estimate. A distinct p_c' break is common for sensitive clays and a more rounded curve from these clays is usually an indication of poor sampling and/or trimming techniques. It is not clear whether this is the case for the tests shown in Fig. 3.19. It also is possible that the age of the samples and poor temperature control, during storage could have contributed to the lack of a distinct p_c' break in these e-log σ_v' curves.

Based on the estimated in-situ effective vertical stress and the p_c' value from test C1, the overconsolidation ratio of the blue clay at the 8.2 m depth is 3.0. Using this value of overconsolidation ratio and an average plasticity index of approximately 50 (see Table 3.1), the coefficient of earth pressure at rest, K_o, should be about 1.05 (Brooker and Ireland, 1965). It is of interest to note that the ratio of the maximum horizontal to maximum vertical effective stress determined from the p_c' values of tests C1 and C2 has a comparable value of 1.0.

The values of the compression index, C_c, from tests C1 and C2 are 0.90 and 0.86 respectively. The value of C_c from test C1 agrees with the earlier values of C_c in the blue clay which varied from 0.63 to 1.07 (Pietrzak, 1979).

Samples C3 and C4 were taken from a nominal depth of 10.0 m and were both oriented such that the compressibility in the direction of the in-situ effective vertical stresses was being measured. The e-log σ_v' curves are shown in Fig. 3.19 and the results are tabulated in Table 3.3. The curves are closely similar and exhibit the roundness and concave upward curvature found in tests C1 and C2. The p_c' values were 280

kPa and 265 kPa for tests C3 and C4 respectively. The compression indexes were 0.73 and 0.65 respectively.

The average value of p_c' from both depths, using tests C1, C3, and C4, is 272 kPa. The relationship between this value and the average limit state envelope shown in Fig. 3.20 will be discussed in Chapter 4.

This concludes the presentation of the test results. The next chapter will discuss these results and their possible interpretation.

CHAPTER 4

DISCUSSION OF TEST RESULTS

4.1 INTRODUCTION

The main object of this research was to examine the applicability of the limit state concept to the plastic, anisotropic, Lake Agassiz clay of the Winnipeg area.

As described in an earlier chapter, the hypothesis on which this concept is based, proposes that the stress-strain-time behavior of a natural clay in the field is to large extent controlled by its particle (or grain) structure. The particle structure of a natural clay is a function of its depositional environment and adapts to sustain the maximum stresses applied during and after its deposition. For most natural clays, this leads to an anisotropic particle structure. At some point during the history of a deposit, apparent overconsolidation can occur by one or a combination of the following factors: off-loading, groundwater level movements, delayed compression, the formation of cementation bonds, or desiccation. This overconsolidation leaves the clay with a reserve resistance over and above the particle structure strength corresponding to its in-situ stress level. When soil elements are stressed above their field overburden stresses, the soil initially behaves in a rather elastic manner with only small strains occurring. This is due to the overcompetent particle structure of the soil. However, at some limiting stress level (defined as limit state), the particle structure begins to yield or breakdown, with accompanying higher strain rates and porewater pressures.

Therefore, the particle structure can be seen to play an important role in the initial stress-strain behavior of a soil subjected to changing stresses from civil engineering works.

The limit state envelope is a function of the particle structure of a soil. It is the locus of stress states in (p', q) space at which the soil changes from essentially small strain, pseudo-elastic behavior to a larger strain, more plastic behavior. At limit state stresses, the maximum small strain resistance of the particle structure is mobilized and a significant number of localized failures at the points of the particle contact begin to occur.

Limit state envelopes have been established for a number of natural clays. However, with the exception of the work on Belfast estuarine clays (Crooks and Graham, 1976), the clays in these studies have been either sensitive or cemented (Mitchell, 1970; Graham, 1974; Tavenas and Leroueil, 1977) and represent extreme examples of the effect of particle structure. On the other hand, Winnipeg clays are generally accepted to be of low sensitivity and have not been identified as being cemented. The extension of the limit state concept to include Winnipeg clays is a significant step towards verifying its applicability to all natural clays. The work described in this thesis suggests that Winnipeg clays do have an in-situ particle structure which governs its initial stress-strain response to varying stress conditions.

The 1979 paper by Baracos et al. described, for the first time, a limit state envelope for Winnipeg clay. In that study, an average limit state envelope was drawn through data from undisturbed clay samples taken from depths between 6.3 m and 12.3 m (see Fig. 4.1). The envelope was

well-defined for stress paths with increasing shear stress but was poorly defined for those with increasing octahedral stresses.

The present study has extended the initial study by defining limit state envelopes for the Winnipeg clay at depths of 8.2 m and 10.0 m at the same site (Fig. 4.1). In addition, the drained test results showed that strain energy provides a useful limit state criterion along any generalized stress path.

The following sections discuss the results of the test program in detail.

4.2 DRAINED COMPRESSION RESULTS

4.2.1 Defining Limit State

A major problem in determining the limit state envelope of a clay is establishing a criterion by which limit state stresses are identified. Originally limit state stress condition was determined by observing the development of volumetric strains, ε_v, in drained stress controlled tests (Tavenas et al., 1978a). Limit state was the stress condition at which the effective octahedral stress-volumetric strain relationship changed from an initially linear, small strain behavior to more plastic behavior. This stress condition was identified on the stress-strain plot as the intersection of the two linear sections which defined the initial elastic and subsequent more plastic behavior. However, along certain effective stress paths volumetric strains can be zero, and along others it may exhibit only unilinear behavior. For this reason, the criterion could not be used to define limit state along all stress paths.

In test series T201 to T204, the σ'_{oct} versus ε_v plots, shown in Fig. 3.8, only produced an identifiable limit state stress in test T203. The stress path for test T203 is fairly flat in (p', q) stress space and has an increasing component of effective octahedral normal stress (Fig. 3.4).

In test series T205 to T209, the relationship between effective octahedral normal stress and volumetric strain was useful in defining limit state for test T205 and T206 (Fig. 3.14). Both of these tests follow stress paths with a generally increasing component of effective octahedral normal stress (Fig. 3.5). Therefore, it is seen that along stress paths with σ'_{oct} increasing significantly, the 'σ'_{oct} versus ε_v' plot is a good limit state criteria.

It was suggested by Crooks and Graham (1976) that another component of the stress tensor be used to determine limit state along stress paths in which the 'σ'_{oct} versus ε_v' plot was not helpful. Figures 3.6, 3.7 and 3.8 showed plots of 'σ'_1 versus ε_1', '$(\sigma_1-\sigma_3)$ versus ε_1', and 'σ'_3 versus ε_3' respectively, for test series T201 to T204. Along stress paths T201 and T202, which have generally increasing shear stress, the plots of σ'_1 or $(\sigma_1-\sigma_3)$ versus ε_1 provided identifiable limit state stresses. However, in test T203 limit state could not be identified from these plots. In fact, a strain hardening type of behavior was found at stress level 8 in this test. The plots of σ'_3 versus ε_3 for all of the tests in this series exhibited a fair amount of scatter and were not useful in identifying yield.

Figures 3.12,3.13, and 3.15 show plots of 'σ'_1 versus ε_1','$(\sigma_1-\sigma_3)$ versus ε_1', and 'σ'_3 versus ε_3' respectively, for test series T205 to T209. Again it was along the stress paths of generally increasing shear stress, T206 and T207

(see Fig. 3.5), that the plots of σ_1' or $(\sigma_1-\sigma_3)$ versus ε_1 produced an identifiable limit state stress. The plots of σ_3' versus ε_3 for this test series were not useful in identifying limit state except in the test T207. On this basis, it is seen that plots of $(\sigma_1-\sigma_3)$ or σ_1' versus ε_1 provide a good limit state criterion for stress paths in which deviator stress is generally increasing.

The limit state stresses determined from various stress-strain criteria are summarized in tables 3.6 and 3.7 for test series T201 to T204 and T205 to T209 respectively. It was observed that the limit state condition predicted by the different criteria were fairly close but not identical. Tavenas et al. (1978a) have suggested that the limit state stresses defined by the various strain components are frequently not identical. On the basis of tables 3.6 and 3.7, this point can be neither confirmed nor refuted. However it is certain that no one strain component can be used to define limit state stress along all stress paths.

It is for this reason that Tavenas et al. (1978a), following a suggestion by Graham (1974), proposed using strain energy as a limit state criterion. By plotting the strain energy absorbed per unit volume, W, against effective octahedral normal stress, all the components of the strain tensor were combined into a single limit state criterion. This criterion has been modified by the author with the substitution of a more fundamental stress, σ'_{scalar}, for the previously used σ'_{oct}. This renders the criterion useful for all stress paths, even those with a constant effective octahedral normal stress.

The plots of W versus σ'_{scalar} for test series T201 to T204 and T205 to T209 were shown in Figs. 3.10 and 3.16 respecitvely. In test series

T201 to T204, strain energy provided a useful limit state criterion along all stress paths. For stress paths T201 and T202, clear discontinuities occurred in the plots, and limit state stresses were defined by imposing two linear sections on the data. In test T203 it was not reasonable to impose a bilinear function on the data. However, a clear break in the plot did occur at stress level 11, and this was taken as limit state. In test T204, the plot was linear, indicating limit state had not been reached.

In the second test series, strain energy was again found to be a useful limit state criterion. In tests T205 and T206, clear discontinuities in the 'W versus σ'_{scalar}' plot indicated limit state. The plot of W versus σ'_{scalar} for test T207 did not reveal a distinct change in behavior which could be interpretted as limit state. The behavior was interpretted as curvilinear. The lack of a distinct limit state stress in this plot may have been due to the position of this stress path in (p', q) space (see Fig. 3.5). The path was almost parallel to the normally consolidated Coulomb-Mohr envelope; this made it difficult to distinguish between limit state and rupture in the test. In test T208, the strain energy plot was linear up to rupture stresses, and thus indicated no limit state behavior prior to failure.

Figure 4.2 shows the plots of the various limit state criteria for test T206. Because of the intermediate position of the stress path for the test (Fig. 3.5), four of the five criteria define limit state stresses. Although there is some variation in the limit state stresses found by the different criteria, they are in fact rather similar. Tables 3.6 and 3.7 revealed that in all tests where limit state was reached at least two of

the limit state criteria were useful. The strain energy plot produced identifiable limit state stresses in every test but T207. These findings confirm the suggestion by Tavenas et al. (1978a) that strain energy is indeed a good indicator of limit state along any stress path. Furthermore, because it includes the entire strain tensor, this criterion is the most justifiable means of demonstrating the fundamental change in stress-strain behavior which occurs at limit state. The use of a more general stress component, such as σ'_{scalar}, is also recommended.* This extends the applicability of the original criterion, W versus σ'_{oct}, to include stress paths in which σ'_{oct} is constant. It is noted that other scalar stress terms which incorporates the major principal stresses, could be used for σ'_{scalar}. Further work as to an appropriate scalar stress term is required.

4.2.2 The Limit State Envelopes

In Chapter 3, limit state envelopes were defined for the Winnipeg clay at depths of 8.2 m and 10.0 m (Figs. 3.4 and 3.5). The limit state envelope established in the pilot test series for the 8.2 m depth is rather speculative. In defining limit state stresses along the stress path of each test, no preference was given to any one limit state criterion. The range of limit state stresses established by the different criteria were shown on the stress path for each test. In the case of test T203, only two limit state criteria were useful in identifying limit state and both criteria indicated the same stress. Therefore for this test, only a single limit state stress is shown in Fig. 3.4. Test T204 was put into undrained shear prior to reaching limit state in drained compression. Consequently, limit state stresses were not established along a stress

* See page 52.

path of approximately constant shear stress.

The limit state envelope for 8.2 m was drawn such that it passed through the middle of the range of limit state stresses defined for tests T201 and T202. The section of the envelope below stress path T202 was drawn similar to the shape predicted by the YLIGHT model. It is therefore rather speculative. No attempt was made to draw the envelope through the limit state stresses for test T203. As explained in Chapter 3, the load duration in tests T203 and T204 was not constant, and was extended to periods of up to 9 days in an attempt to examine the effect of load duration. In spite of the variation of load duration at each stress level (see table B.3), limit state stresses were still identified in test T203. However, the author believes that the increased load durations used in this test have caused the limit state stress along this stress path to decrease. Tavenas et al. (1977) state that a reduction in the rate of loading or an increase in the duration of load application should result in a reduction of the limit state stress. On this basis, the limit state stress corresponding to 24 hour load durations for test T203 was presumed to be at a higher stress level. Therefore, the lower part of the limit state envelope shown in Fig. 4.1 for the 8.2 m depth was conjectural.

In the overconsolidated region, limit state and rupture coincide. Limit state has been defined as the stresses at which the maximum strength of the particle structure is mobilized and a significant number of localized failures at the points of particle contact begin to occur. In drained, stress controlled compression, this is evident by the change from elastic, small strain to more plastic, large strain behavior.

Bjerrum and Kenney (1967) state that the maximum shear strength rupture criterion for undrained shear is associated with the quasi-static yielding of the grain structure of a soil at small strains; whereas the maximum stress ratio rupture criterion for undrained shear represents the dynamic yielding of the clay structure at large strains once a statistically constant condition of sliding friction between soil particles has been obtained (Graham, 1974). Consequently, in undrained shear the maximum shear stress reached at small strains by an overconsolidated sample is a function of its particle structure and represents a limit state condition. The limit state envelope for test series T201 to T204 was thus extended to include the stresses defined by the maximum shear stress criterion for sample T204. This sample was not stressed to limit state in drained shear and for this reason, was overconsolidated prior to undrained shearing.

The limit state envelope for a 10.0 m depth from tests T205 to T209, is shown in Fig. 3.5. The envelope defined for this depth is less speculative than the one at 8.2 m. The three limit state stresses established during drained, stress controlled compression along stress paths T205, T206 and T207 allowed an accurate determination of the envelope in the region below the normally consolidated Coulomb-Mohr line. In the overconsolidated range, the envelope was well defined by tests T208 and T209.

Figure 4.1 shows the limit state envelopes established in this study. The nature of the envelopes may be compared with the details of the YLIGHT model explained in Chapter 2. The YLIGHT model proposes that the limit state envelope has an elliptical shape centered on the K_o-consolidation for the normally consolidated clay. Based on a normally

consolidated, effective angle of shearing resistance, ϕ', of 18°, and Jaky's formula for K_o (see section 2.2), a K_o-consolidation line has been shown in Fig. 4.1. The limit state envelopes shown for the two depths are roughly, but not precisely, symmetrical about this line.

The YLIGHT model also states that the limit state envelopes at different depths are all homothetic (i.e. geometrically similar). This is the case for the limit state envelopes in this study. However, the author concedes that limited amount of data allowed some freedom in the interpretation of exact shape and orientation of the limit state envelopes drawn.

Although the general shapes of the envelopes are faithful to the data, more extensive stress probing along other stress paths is necessary to more accurately define the shape and orientation of limit state envelopes in Winnipeg clay.

An important consideration in the YLIGHT model and the concept of limit state is that the position of the limit state envelope is governed by the magnitude of the preconsolidation pressure. Consequently, the limit state envelopes of a clay deposit at different depths are geometrically similar and positioned in stress space according to their preconsolidation pressure, p'_c. If the p'_c values at two different depths in a deposit are constants, they would share a common limit state envelope.

The YLIGHT model links the limit state envelope defined by drained, triaxial stress probing, to the preconsolidation pressure defined in the oedometer tests. The one-dimensional consolidation test occurs under K_o-consolidation conditions. However, the precise value of the effective horizontal stress during the test is unknown. In (p', q) stress space, a

line representing all of the possible states of stress of the oedometer sample at its preconsolidation pressure may be drawn by considering the extreme values of σ_h' which are possible. According to the YLIGHT model this line, known as the p_c' line, should intersect the K_o-consolidation line for a clay at the limit state envelope for the clay at that depth (see Fig. 2.2). The p_c' lines, based on the oedometer tests for this study, are shown in Fig. 4.1. The average values of p_c' for 8.2 m and 10.0 m were 270 kPa and 272.5 kPa respectively (Fig. 3.19). The p_c' lines for these values of p_c' intersect the K_o-line well inside the limit state envelopes defined for the two depths.

A possible explanation for these discrepancies is the quality of the standard trimming techniques used in the oedometer testing. These techniques did not preserve the particle structure as well as the more careful trimming techniques used in the triaxial testing program (see Appendix A). The rounded nature of the e-log σ_v' curves in this study are a general indication of the disturbance of these samples (Fig. 3.19). Furthermore, it is noted that the volume of soil in the triaxial samples is approximately twelve times the oedometer. For this reason, the triaxial sample will produce stress-strain data which is more representative of the soil's true behavior.

More recently, during the writing of this thesis, additional oedometer testing has been completed on samples from 8.2 m and 10.0 m by graduate students at the University of Manitoba. In these tests, preconsolidation pressures of 320 kPa and 365 kPa were found for samples from 10.0 m and 8.2 m respectively (Trainor, 1980). These values are in better agreement with the limit state envelopes defined in this study. For in-

stance, because the limit state envelope for 8.2 m lies outside of the envelope for 10.0 m, a higher value of p_c' would be expected in the oedometer tests at 8.2 m. This was the case in the oedometer results by Trainor (1980), but not in the oedometer tests of this study where p_c' for both depths was almost identical.

If the preconsolidation pressure for both depths was indeed constant, it would be reasonable to define one limit state envelope for both depths, as was done by Baracos et al. (1979). In view of the uncertainty associated with the p_c' values, an average limit state envelope has been shown between the envelopes defined for 8.2 m and 10.0 m (Fig. 4.1). This average envelope was drawn homothetically to the other two, and represents an average of the two envelopes shown.

Figure 4.1 shows the limit state envelope proposed by Baracos et al. (1979). Their envelope was drawn on the basis of limit state data from depths between 6.3 m and 12.3 m. The original limit state data points for that study were shown in Fig. 3.20. The limit state envelope defined by Baracos et al. (1979) lies well inside the envelopes defined in this study. They stated that their envelope was well-defined when shear stresses were increasing, but poorly defined along stress paths with increasing octahedral normal stress and nearly constant shear stress. The same statement is true of the results of this study. Limit state stresses were established in only one test with octahedral normal stress increasing and shear stresses remaining constant (i.e. test T205). The sections of the limit state envelopes drawn in this area of stress space were based solely on the data from test T205. It is of interest to note that the limit state stresses defined in T205 are quite close to those

defined for two tests in the work by Baracos et al. (1979) (see Fig. 3.20).

There is no obvious explanation for the discrepancy between the limit state envelope by Baracos et al. (1979) and those defined in this study. The shape of the envelopes shown for this study are only preliminary because of the small amount of data. However, there is no doubt that the limit state envelopes of this study lie significantly outside the one defined by Baracos et al. (1979). The block samples used in both studies were taken from the same site, and an examination of the classification data and moisture contents of the samples in both studies indicated no significant differences. The samples in this study were, however, stored for an extended period of time (about one year) prior to the testing. This may have led to thixotropic hardening*, although there is no previous evidence of this in Winnipeg clays. The storage room, although moisture controlled, was not temperature controlled, and some temperature fluctuations were noted during the summer months. These temperature fluctuations over the extended storage period could have affected the stress-strain properties of the samples in a way which cannot be explained on the basis of the present work. It is recommended that steps be taken to improve the storage conditions in the geotechnical laboratories at the University of Manitoba.

Another possible explanation for the large discrepancy in the limit state envelopes defined is the difference in load increment ratio between the two studies. This is discussed further in the next section.

---

* Thixotropic hardening is an increase in strength with time at constant composition.

4.2.3 Testing Techniques

During the pilot series, uncertainty developed about the effect of load duration and load increment ratio on the drained triaxial test results. This led to an extension of the load duration used in tests T203 and T204. However, this preliminary investigation of the effect of load duration was not systematic (i.e. load duration was varied from increment to increment in an attempt to achieve 'complete' consolidation) and did not significantly elucidate the problem. Because of the scope of this study, the second series of tests, T205 to T209, was conducted using a standard 24 hour load duration, and no further attention was given to the effect of load duration or load increment ratio on the test results. Subsequent to the completion of the testing program, the importance of these two testing parameters on the test results has become more apparent.

It is now generally accepted that the strength and deformation behavior of most natural clays is time-dependent (Campanella and Vaid, 1974; Tavenas et al.,1978b). Early investigators into the effects of time on the stress-strain behavior of natural clay followed the classical pattern of separating problems of stability, investigated by means of strength tests, from deformation problems investigated by oedometer tests.

Using the standard load increment ratio of 1*, Crawford (1964) showed that in oedometer tests, the value of p_c' decreased with the length of load duration. In addition, he stated that the rate of compression, which may be varied by the size of the load increment, also affects the preconsolidation pressure. He also stated that the division of consolidation into primary and secondary components was an arbitrary separation

---

* Load increment equals previous total load.

of a continuous compression process, and the relative contribution of each depends on the method of loading (see also Bjerrum, 1967).

Leonards et al. (1964) discussed the effect of load increment ratio on the results of one-dimensional consolidation tests. They stated that for small load increment ratios, the Terzaghi theory cannot predict, even approximately, the rate of pore pressure dissipation, and that measured pore pressures generally dissipate more rapidly than predicted by the Terzaghi model. They showed that as load increment ratio decreased, the compressibility decreased and the time required for pore pressure dissipation decreased.

With regard to drained triaxial consolidation tests, early investigators into limit state envelopes for natural clays did not specifically deal with the effect of time on the determination of limit state envelopes. Mitchell (1970) stated that major time effects occur only within the range of pressures in excess of the preconsolidation pressure, and that very slow rate of loading tests give rise to a void ratio-pressure curve essentially the same as the curve obtained from slow incremental loading tests. On this basis, he suggested that a limit state envelope can be established provided excess pore pressures are allowed to dissipate.

With regard to load increment ratio, Crooks and Graham (1976) stated that the load increment ratio is important only for sample tests along stress paths which intersect the Coulomb-Mohr envelope. They found larger load increments generate large porewater pressures which can lead to the Coulomb-Mohr rupture criterion being exceeded. In addition, they found that along two of their stress paths yielding and rupture could be distinguished only when a smaller load increment ratio was used.

Leroueil and Tavenas (1977) were the first to recognize that strain rate effects need be considered in the experimental determination of the limit state envelope of a natural clay. They suggested in the YLIGHT model that the effects of ageing and strain rates on the preconsolidation pressure of natural clays proposed by Bjerrum (1967), apply in fact to the entire limit state envelope. Moreover, they stated that it is mandatory to ensure the uniformity of rates of all tests used to determine the limit state envelope of a given clay, and to evaluate the rate dependency of this envelope if it is to be used in the analysis of practical problems.

Tavenas and Leroueil (1977) theorized that a reduction of the rate of loading or an increase in the duration of load will lead to a reduction of not only the oedometer p'_c value, but of the entire limit state envelope. Data from strain controlled tests on Champlain Sea clay showed that the limit state envelope in the overconsolidation region was indeed strain rate dependent. In addition, the reduction of the oedometer p'_c value with lengths of loading was shown using nine oedometer tests step loaded in one increment to their final vertical load. However, no attempt was made to unify the results of the strain controlled triaxial tests and stress controlled tests (both oedometer and drained triaxial) in terms of the various strain rates used. The time dependency of the limit state envelope was implied with reference to three tests. The decrease in strength from two CID tests taking 0.5 days and 8 days was plotted. The decrease in p'_c resulting from load durations between 0.7 days and 70 days was shown. Additionally, the decrease in limit state stresses when the load duration in isotropic, drained compression was varied from 1 day to

5 days was shown. These tests indicated a general reduction in limit state stresses as load duration increased, or rate of loading decreased.

A significant consideration in the stress controlled, drained triaxial testing of all previous studies is that the rate of loading is not constant. The rate of loading for samples loaded incremently varies greatly during a test and is dependent on both the load increment and the load duration. For this reason, the strain rate dependency of the limit state envelope cannot be fully defined in these stress controlled drained tests.

In this study, the incremental stress levels along each stress path were chosen such that an arbitrary number of stress levels occurred between the in-situ stresses and the previously defined limit state envelope by Baracos et al. (1979). In test series T201 to T204 and T205 to T209, there were six and four stress levels respectively. It is noted that in the previous study the load increments (and therefore load increment ratios) were generally smaller than those used in this study. This smaller load increment ratio represents a decreased rate of loading, and thus should cause an overall decrease in the limit state envelope. It is possible that the generally larger size of the load increment ratios used in this study could be partially responsible for the larger limit state envelope. However, there is no way of quantifying this affect in this thesis.

In this study some useful evidence of the effect of load duration was found in test T202. A load duration of 24 hours was used until the final three stress levels, which were continued for periods of 117h, 145h, and 264h respectively (table B.2). The stress-strain plots for this

test are shown in Figs. 3.6 through 3.10. From the plots of σ_1' and $(\sigma_1-\sigma_3)$ versus ε_1 in Figs. 3.6 and 3.7, a linear section, parallel to the initial post-limit state behavior, was defined through these last three stress levels. If the downward movement of this stress-strain data due to the longer load durations were assumed applicable to all the data for this test, it can be seen that the limit state stresses defined would be smaller. There is also evidence of a parallel shift in the post-limit state behavior in the plot of W versus σ'_{scalar} in Fig. 3.10. However, this evidence is admittedly insufficient to draw any conclusions.

It is noted that test T203 was conducted with longer load durations (see table B.3). However, the lengths of the load durations in this test were not constant and varied at each stress level. A comparable test with 24 hour loadings would be required to verify that the limit state stresses were reduced by longer load durations. A further more systematic study is required to verify the effect of load duration on the limit state envelope.

Since the stress-strain properties of most natural clays are time dependent, the limit state envelope (as suggested in YLIGHT) will also be time dependent. This time-dependency is simply evaluated in strain controlled testing where the rate of loading is easily varied. However, in stress controlled testing the rate of loading is not constant and is a function of both the load duration and load increment ratio. It is suggested by the author that the load duration and load increment ratio are important variables in a testing program for the determination of the limit state envelope of a natural clay. Further research is required to examine the effect of these parameters on the results of drained, stress

controlled, triaxial tests. Furthermore, some means of evaluating the rate dependency of the limit state envelope is required if it is to be used in practical analysis.

4.2.4 Other Considerations

Several additional aspects of the results of the drained, stress controlled portion of the triaxial tests are worth further discussion. With regard to the reconsolidation of the samples to in-situ stresses, the strains on restressing were tabulated in table 3.4. The maximum axial strain on restressing was 2.33 percent, while in most tests it was around 2 percent. Crooks (1973) stated that axial strains less than 2 percent to p'_o were considered an indication of minimal disturbance during sampling and preparation. With this in mind, it may be stated that the careful sampling and trimming techniques used in this study were helpful in minimizing disturbance in these samples. It is also noted that the amount of axial strain on reconsolidation was affected by the uncertainty associated with the actual in-situ stress levels, and by the stress ratio used during reconsolidation.

Table 4.1 summarizes the axial and volumetric strains at limit state stresses for the drained, stress controlled tests in this study. The strains at limit state are quite large and are approximately double those found in the tests by Baracos et al., (1979). These values of strain are somewhat disconcerting in that the limit state condition is thought to be associated with small strain behavior, whereas the strains in table 4.1 are quite large. However, the higher values of the limit state for Winnipeg clay may be a function of their less sensitive yet more active nature.

Table 4.2 lists the total volume change as measured in the drained portion of each test, and the total volume change as determined by the change in moisture content of the samples during testing. It is noted that in every case the volume change measured in the burette readings is significantly larger than that determined from the moisture content changes. One possible explanation for this discrepancy is leakage through the membranes into the sample. If this were the case, it would quite likely be of a nearly constant nature and therefore, should have effected the limit state determination. It is also possible that the samples in this study were gasing. That is, organic material in the samples was producing gas during the test, and this gas was causing erroneous volume change readings. The samples were flushed regularly during testing to remove any trapped air bubbles, and in many cases significant amounts of air were expelled. However, since this flushing was not performed on a regular and systematic basis, the volume of air expelled could not be discounted from the volume change readings. Fortunately, it appears that this problem has not affected the stress-strain results adversely. It may, however, account for the scatter associated with radial strain plots, which are calculated on the basis of ε_1 and ε_v. It is recommended that future testing incorporate daily flushing, and that the volume of air expelled be recorded and subtracted from volume change readings. Furthermore, it would be useful to determine the organic content of the samples prior to testing.

A third possible reason for the discrepancy in volume change measurements are poor building-out procedures which may have allowed the samples to take on water after stress removal.

The next section of this chapter discusses the results of the undrained tests.

4.3 UNDRAINED SHEARING RESULTS

4.3.1 Stress-Strain Behavior

Section 3.4 presented the results of the undrained portion of this study. Samples which had not failed during the drained, stress controlled portion of the testing program were put into undrained shear. The undrained effective stress paths of these samples are shown in Figs.3344 and 3.5.

The normalized undrained stress-strain behavior of the samples is shown in Figs. 3.17 and 3.18. In all cases except T204 and T209, the samples had been stressed well past their limit state envelopes prior to undrained shearing. This implies that their in-situ particle structure had been changed and the samples had a new particle structure which was normally consolidated and strictly a function of its consolidation stresses. Samples T204 and T209, which were not stressed to limit state, retained their original particle structure and were overconsolidated.

In tests T202, T203, T205 and T206, the stress-strain results are typical of a normally consolidated clay. The deviator stress and pore-water pressure both rise gradually to a maximum at which point they level off and remain essentially constant.

It is of interest to note that samples T202 and T203, which were allowed to remain at their final consolidation stresses for 11 and 5 days respectively, behave in a normally consolidated manner. Theoretically, the period of delayed compression at the end of consolidation should have

allowed the particle structure of samples to develop a reserve resistance, or overcompetency. This was not reflected in the stress-strain data.

With regard to porewater generation, it was noted that the samples which were normally consolidated with more isotropic stresses (i.e. T203 and T205), produced a higher normalized pore pressure increase, $\Delta u/\sigma'_{1c}$. The observation was made with respect to samples T202 and T206 which had higher components of deviator stress at their final consolidation stress level. This seems to indicate that a more isotropic consolidation stresses produce higher normalized porewater pressures during undrained shearing.

Samples T204 and T209, which were overconsolidated, behaved in a typical overconsolidated fashion. In both tests, the samples' stress-strain behavior was brittle. The deviator stress and porewater pressure reached a peak at relatively low strains, after which they both fell off abruptly to a lower value. As mentioned earlier, the limit state envelope and the rupture envelope are essentially the same in the overconsolidated region. Bjerrum and Kenney (1967) stated the maximum deviator stress criterion for rupture is associated with the quasi-static yielding of the particle structure of a soil at small strains. On the other hand, the maximum stress ratio criterion for rupture represents the dynamic yielding of the clay structure at large strains once a statistically constant condition of sliding friction between particles has been obtained. In the case of an overconsolidated sample, the quasi-static yielding of the particle structure at small strains (i.e. limit state) was followed immediately by dynamic yielding of the structure (i.e. rupture). In both T204 and T209, these criteria occurred simultaneously at low strains.

Young's modulus, E_{50}, was determined for each test and is listed in table 3.2. This modulus represents the slope of the plot of principal stress difference, $(\sigma_1-\sigma_3)$, versus axial strain, ε_1, from 0 to 50 percent of the maximum deviator stress increase. It finds application in finite element analysis. Another elastic parameter, the relative stiffness, $(E_{50}/(\sigma_1-\sigma_3)/2)$, was calculated and is shown in table 3.2. The values of the relative stiffness against $1/\sigma'_{1c}$ are plotted in Fig. 3.21. The tests in this study indicate a trend towards higher relative stiffness for the normally consolidated samples. This differs from the line proposed by Baracos et al. (1979) shown in Fig. 3.21. It does, however, agree with work of Crooks (1973) who proposed that the higher values for the normally consolidated samples were due to the fact that their laboratory formed particle structure was undisturbed. The field structure of the overconsolidated samples, on the other hand, had been disturbed somewhat by sampling and trimming.

The porewater pressure parameter, A_f, has been determined for each undrained test and is shown plotted against $1/\sigma'_{1c}$ in Fig. 3.22. This parameter is a function of consolidation history and is usually plotted against the overconsolidation ratio of the sample, p'_c/σ'_{1c}. However, in this case,$(1/\sigma'_{1c})$ was used because of the uncertainty associated with the one-dimensional consolidation test results. The results showed the same general trend as the work by Baracos et al. (1979). The value of A_f generally decreases with the degree of overconsolidation. However, there is some scatter about the line for 76 mm samples proposed by Baracos et al. (1979). The values of A_f above 1 for samples T205 and T206 are quite unusual; other values of A_f in the literature seldom exceed 1.

4.3.2 Strain Rate Effect

The importance of time on the stress-strain properties of natural clays is well known (for example, Bjerrum, 1967; Vaid and Campanella, 1974; Tavenas et al., 1978a). A method for measuring the effect of strain rate on the undrained strength of a soil is the relaxation test. This method, first proposed by Kenney (see Crooks (1973)), involves stopping the motor drive of the compression machine at a given strain and taking readings of stress and strain with time. After the motor drive is stopped, the sample continues to strain at a decreasing rate due to the stored energy in the proving ring. From this test, a plot of undrained resistance, S_u*, versus strain rate is formed, and the strain rate parameter, $\rho_{0.1}$, calculated. The parameter, $\rho_{0.1}$, gives the percentage increase in undrained strength as the strain rate is increased by a factor of 10. The parameter is related to the undrained strength at a strain rate of 0.1 percent/h.

The results of the relaxation tests are shown in Figs. 3.23 and 3.25. The $\rho_{0.1}$ results varied from 4.5 to 10.1 percent. It was noted that the two overconsolidated samples, T204 and T209, had lower values of $\rho_{0.1}$, 4.5 and 5.8 percent respectively. Whereas the normally consolidated samples (T202, T203, T205 and T206) had $\rho_{0.1}$ values ranging from 8.6 to 10.1 percent.

Graham (1979) has proposed, on the basis of data from several natural clays that $\rho_{0.1}$ increases with increasing plasticity index. This is shown in Fig. 3.24 along with the results of the present study. The few results do not confirm the proposed relationship by Graham (1979), and suggest that $\rho_{0.1}$ is independent of plasticity index. Highly struc-

---

* These are values of shearing resistance, $(\sigma_1-\sigma_3)$, measured after the maximum deviator stress, $(\sigma_1-\sigma_3)/2_{max}$, has been reached.

tured or sensitive clays have shown much higher $\rho_{0.1}$ values.

The author acknowledges the criticism that the relaxation test results are affected to some extent by the properties of the proving ring used. For this reason, it is suggested that undrained tests at variable strain rates be performed to confirm the strain rate effects reported herein.

4.3.3 Normally Consolidated Strength Envelope

On the basis of the drained and undrained tests to failure, the Coulomb-Mohr strength envelope in the normally consolidated region was defined separately for both depths, 8.2 m and 10.0 m. These envelopes were shown in Figs. 3.4 and 3.5. An average normally consolidated Coulomb-Mohr envelope for both depths is shown in Fig. 3.20. From this envelope, the effective strength parameters, c' and ϕ', were found to be 0 and 18°.

The previous study by Baracos et al.(1979) had found a c' of 5 kPa and ϕ' of 20° in the normally consolidated range with 76 mm samples. The extended storage period and the temperature fluctuations during storage are possible explanations for the lower strength parameters found in this study.

In Chapters 1 and 2, the concept of critical state was introduced. Critical state was defined as the steady state condition at which a clay would deform continuously with no further changes in stress or voids ratio. Furthermore, the stresses at critical state were said to satisfy the Coulomb-Mohr failure envelope.

The Coulomb-Mohr failure envelope describes the stress conditions at which failure occurs in a soil. These stress conditions are usually referred to the limiting shear stress condition, $(\sigma_1'/\sigma_3)_{max}$. This condition describes the stresses at which dynamic yielding of the particle structure is taking

place, and a statistically constant condition of sliding friction between particles has been obtained (Graham, 1974). Bjerrum and Kenney (1967) proposed that the maximum principal stress ratio for failure described the ultimate frictional resistance between particles, and was only mobilized at high strains. Leroueil et al. (1979) stated that there are some indications that the strength developed at large strains presents many of the characteristics of critical state. On this basis, the author proposed that critical state envelope and the Coulomb-Mohr envelope, defined by the $(\sigma_1'/\sigma_3')_{max}$ condition, were closely similar in the normally consolidated ranges.

During this study, relaxation tests were performed when the axial strains were about 1 to 2 percent past maximum deviator stress. This was done to avoid significant reductions in the strength which occur as strains increase. Upon completion of the relaxation test, the strain rate was increased and the sample sheared to large strains. The stress ratios, (σ_1'/σ_3'), increased significantly after the relaxation test. This may have been as a result of the larger strain rates, or possibly as a result of porewater equalization during relaxation. Because of the discontinuity in stress ratios after relaxation, the maximum stress ratio stresses could not be determined in the undrained tests. Therefore, the normally consolidated envelope for this study was based on the maximum deviator stress criterion and may not truly represent critical state conditions for the clay. The author suggests that the use of the critical state concept exclusively to define failure at $(\sigma_1'/\sigma_3')_{max}$ on (p', q) stress space is useful. It eliminates the uncertainty associated with which rupture criterion, $(\sigma_1'/\sigma_3')_{max}$ or $(\sigma_1-\sigma_3)/2_{max}$, is used to define failure. The critical state line would be clearly associated with large strain failure of the clay.

CHAPTER 5

CONCLUSIONS AND SUGGESTIONS FOR FURTHER RESEARCH

5.1 CONCLUSIONS

The results of this series of tests cannot be considered definitive because of the limited number of samples tested. However, several preliminary conclusions are possible on the basis of the results. These are presented below.

1) The existence of limit state envelopes which describe stress conditions at which the in-situ particle structure begins to yield or break down, was demonstrated for Winnipeg clay from the University of Manitoba campus at depths of 8.2 m and 10.0 m. The stress-strain data along various stress paths confirmed that there are stress levels, defining limit state conditions, at which marked changes occur in the stress strain behaviour.

2) Strain energy provides a limit state criterion which is not stress path dependent and which includes all components of the strain tensor. Furthermore, strain energy should be plotted against a scalar stress* component in order to generalize its applicability to any stress path.

3) The limit state concept is recognized to be a consequence of the in-situ particle structure of a soil. Careful sampling, sample preparation, and reconsolidation to in-situ stresses are required to preserve this in-situ structure.

4) The limit state envelopes in this study were at significantly higher stresses than those defined by Baracos et al. (1979).

---

* This is not a true scalar; it is a pragmatic, empirical quantity.

5) The effective stress, normally consolidated, Coulomb-Mohr strength parameters from this study were c' equals 0 and ϕ' equals 18°.

6) Verification of the applicability of the YLIGHT model to Winnipeg clays requires further testing. Because the shape and orientation of the limit state envelopes defined in this study are tentative, the details of the model cannot be confirmed. No useful work has yet been done on the time-dependent aspects of the YLIGHT model.

5.2 SUGGESTION FOR FURTHER RESEARCH

Due to its limited scope, this study has perhaps raised more questions than it has answered. As a consequence, the following suggestions are made with regard to further studies on the stress-strain-time properties of Winnipeg clay.

1) Conclusive definition of the shape and orientation of limit state envelopes in Winnipeg clay requires a larger number of tests. It is suggested that at least six drained, stress controlled triaxial tests be performed on samples from one depth. The effective stress paths followed by these tests should equally partition (p', q) stress space below the normally consolidated Coulomb-Mohr strength envelope and should include an isotropic, effective stress path.

2) In future studies, it is suggested that the storage time of samples prior to testing be minimized. The samples used in this study had been stored for over a year during which time properties of the clay may have been altered significantly. However, because of a lack of funds and the winter season, it was not possible to obtain new samples for this study.

3) With regard to sample storage, it is suggested that some form of temperature control be included in the geotechnical storage facilities at the University of Manitoba. Temperature fluctuations were observed during the storage period and may have had an adverse effect on the properties of the samples.

4) Standard research classification testing should be expanded to include geochemical analysis and organics testing. This information is noticeably lacking for Winnipeg clay and may provide insight into their behavior. The addition of fall cone testing to provide information of the sensitivity of Winnipeg clays would also be useful.

5) The effect of load duration and load increment ratio on the stress-strain time results requires further investigation. With regard to load increment ratio, a preliminary investigation could be conducted with two samples stressed along the same stress path using one-day load durations. In one test, the sample would be stressed in four increments to a certain stress level; whereas in the second test, twelve increments might be used to reach that same stress level. Similarly the effect of load duration could be investigated by stressing two samples along the same stress path with the same load increment ratio, but different load durations (for example, 1 day and 5 days).

6) Further oedometer testing is required to clarify the uncertainty associated with the preconsolidation pressure results. Improved sample preparation techniques in the oedometer testing may prove helpful in this regard.

7) The effects of time on the p'_c could be confirmed by means of special oedometer tests similar to those performed by Tavenas et al. (1977).

The procedure would involve step-loading oedometer samples in one increment to predetermined stress levels. The oedometer samples would then be allowed for a long period of time while strains were monitored. This would allow the construction of the e versus σ_v' curve for the clay at various times. From these curves, a quantitative indication of the effect of time on p_c' could be gained.

8) The effect of time on the overconsolidated branch of the limit state envelope could be investigated by conducting tests on triaxial samples, reconsolidated to in-situ stresses, at various strain rates. This would provide another means of verifying the strain rate effects from the relaxation test.

TABLES

TABLE 3.1 BASIC SOIL PROPERTIES

Test Number	T201	T202	T203	T204	T205	T206	T207	T208	T209
Test Hole Number	3	3	3	3	3	3	3	3	3
Block Sample Number	4	4	4	4	6	6	6	6	6
Test Type	CAD	CAD($\bar{U}$)	CAD($\bar{U}$)	CAD($\bar{U}$)	CAD($\bar{U}$)	CAD($\bar{U}$)	CAD	CAD	CA$\bar{U}$
Depth (m)	7.9-8.4	7.9-8.4	7.9-8.4	7.9-8.4	9.8-10.2	9.8-10.2	9.8-10.2	9.8-10.2	9.8-10.2
Initial Water Content (%)	55.9	56.5	56.6	56.5	58.3	53.8	57.5	58.3	49.3
Final Water Content (%)	-	47.5	50.3	-	47.8	46.2	49.8	57.1	52.7
Liquid Limit (%)	85	84	86	83	67	73	67	64	70
Plastic Limit (%)	31	30	29	30	28	28	31	34	28
Plasticity Index (%)	54	54	57	53	39	45	36	30	42
Clay Content (%)	73	73	-	-	78	75	-	-	-
Specific Gravity	2.74	2.74	-	-	2.70	2.74	-	-	-
Unit Weight (kN/m^3)	16.8	16.7	16.5	16.7	16.5	16.7	16.7	16.6	16.9

- Not obtained for this test.

TABLE 3.2 SHEAR TEST RESULTS

	Test Number	T201	T202	T203	T204	T205	T206	T207	T208	T209
	Test Hole Number	3	3	3	3	3	3	3	3	3
	Block Sample Number	4	4	4	4	6	6	6	6	6
	Nominal Depth (m)	8.2	8.2	8.2	8.2	10.0	10.0	10.0	10.0	10.0
Drained Shearing	$(\sigma_1-\sigma_3)/2_{max}$ (kPa)	95.1	-	-	-	-	-	89.5	65.3	-
	σ'_{oct} at $(\sigma_1-\sigma_3)/2_{max}$ (kPa)	285.1	-	-	-	-	-	258.0	126.9	-
	ε_1 at $(\sigma_1-\sigma_3)/2_{max}$ (%)	15.35	-	-	-	-	-	15.63	6.80	-
Undrained Shearing	σ'_{1c} (kPa)	-	571.9	474.4	156.9	471.2	412.0	-	-	106.1
	$\sigma'_{3c}/\sigma'_{1c}$	-	0.63	0.78	0.81	0.92	0.70	-	-	0.65
	p'_c/σ'_{1c}	-	0.47	0.57	1.72	0.58	0.52	-	-	2.57
	$(\sigma_1-\sigma_3)/2_{max}$ (kPa)	-	139.5	114.6	73.0	103.3	114.7	-	-	49.5
	σ'_{oct} at $(\sigma_1-\sigma_3)/2_{max}$ (kPa)	-	415.6	342.5	124.0	301.7	347.2	-	-	81.6
	$(\sigma_1-\sigma_3)/2\sigma'_{1c}$	-	0.24	0.24	0.47	0.22	0.28	-	-	0.47
	ε_1 at $(\sigma_1-\sigma_3)/2_{max}$ (%)	-	0.58	2.05	2.62	5.45	2.33	-	-	2.07
	E_{50} (MPa)	-	54.1	42.9	16.1	28.2	30.0	-	-	8.5
	$E_{50}/(\sigma_1-\sigma_3)/2_{max}$	-	388	374	221	273	262	-	-	171
	A_f	-	0.62	0.83	0.45	1.09	1.34	-	-	0.35
	$\rho_{0.1}$ at ε_ρ (%)	-	8.6	9.3	4.5	10.1	9.6	-	-	5.8
	ε_ρ	-	1.31	2.05	3.49	5.84	3.37	-	-	2.97
	Initial Strain Rate, $\dot{\varepsilon}_1$ (%/h)	-	0.46	0.43	0.92	0.96	1.01	-	-	0.91

TABLE 3.3 ONE-DIMENSIONAL CONSOLIDATION TEST RESULTS

Test Number	C1	C2	C3	C4
Test Hole Number	3	3	3	3
Block Sample Number	4	4	6	6
Depth (m)	7.9-8.4	7.9-8.4	9.8-10.2	9.8-10.2
Sample Orientation	Horizontal	Vertical	Horizontal	Horizontal
p'_c (kPa)	270	270	280	265
*P'_o (kPa)	91	59**	106	106
p'_c / p'_o	3.0	-	2.6	2.5
C_c	0.90	0.86	0.73	0.65

* Based on G.W.T. at 3 m and $\gamma_{sat} = 17.5$ kN/m^3

** Based on in-situ effective horizontal stress, $\sigma'_h = 0.65\ p'_o$

TABLE 3.4 TRIAXIAL CONSOLIDATION RESULTS FOR RESTRESSING TO IN-SITU STRESSES

Test Number	T201	T202	T203	T204	T205	T206	T207	T208	T209
p'_o* (kPa)	91.0	91.0	91.0	91.0	106.2	106.2	106.2	106.2	106.2
σ'_{1c} (kPa)	91.3	91.0	90.9	89.5	106.0	106.1	106.6	106.7	106.1
σ'_{3c} (kPa)	59.2	59.2	59.7	59.1	68.3	68.5	69.2	69.2	68.7
p'_c** (kPa)	270	270	270	270	272.5	272.5	272.5	272.5	272.5
σ'_{1c}/p'_o	1.00	1.00	1.00	0.98	1.00	1.00	1.00	1.00	1.00
p'_c/σ'_{1c}	2.96	2.97	2.97	3.02	2.57	2.57	2.56	2.55	2.57
$\sigma'_{3c}/\sigma'_{1c}$	0.65	0.65	0.66	0.66	0.65	0.65	0.65	0.65	0.65
ε_{1c} (%)	1.37	1.25	1.64	2.33	2.03	2.09	1.86	1.88	2.04
ε_{3c} (%)	0.13	0.33	-0.78	0.20	0.68	0.79	0.61	0.71	0.89
ε_{vc} (%)	1.63	1.91	0.08	2.72	3.38	3.68	3.08	3.30	3.82

* Based on G.W.T. at 3 metres and γ_{sat} = 17.5 kN/m^3

** From one-dimensional consolidation tests (see Table 3.3)

TABLE 3.5 TRIAXIAL CONSOLIDATION RESULTS TO THE END OF STRESS CONTROLLED TESTING

Test Number	T201#	T202	T203	T204	T205	T206	T207#	T208#	T209†
p'_o* (kPa)	91.0	91.0	91.0	91.0	106.2	106.2	106.2	106.2	106.2
σ'_1 (kPa)	411.9	571.9	474.4	156.9	471.2	522.2	375.9	214.0	106.1
σ'_3 (kPa)	221.7	360.2	372.3	127.8	433.6	362.8	199.0	83.4	68.7
p'_c** (kPa)	270	270	270	270	272.5	272.5	272.5	272.5	272.5
p'_c/σ'_{1c}	0.66	0.47	0.57	1.72	0.58	0.52	0.72	1.27	2.57
σ'_{1c}/p'_o	4.53	6.28	5.21	1.72	4.45	4.92	3.54	2.02	1.00
$\sigma'_{3c}/\sigma'_{1c}$	0.54	0.63	0.78	0.81	0.92	0.70	0.53	0.39	0.65
ε_{1c} (%)	15.35	14.88	7.37	3.40	7.20	12.09	15.63	6.80	2.04
ε_{3c} (%)	-1.32	0.03	5.15	0.93	3.97	1.82	1.56	0.95	0.89
ε_{vc} (%)	9.83	14.94	17.66	5.26	15.13	12.09	18.76	8.69	3.82

† Sample consolidated to in-situ stresses only

* Based on G.W.T. at 3 m and $\gamma_{sat} = 17.5$ kN/m^3

** From one-dimensional consolidation test results (See table 3.3)

Sample failed in drained shear at the values shown

TABLE 3.6 YIELD STRESSES FROM DIFFERENT CRITERIA FOR TEST SERIES T201 TO T204

	TEST NUMBER	T201	T202	T203	T204
Yield Criterion	σ'_1 vs ε_1	249	313	-	-
	$(\sigma_1-\sigma_3)$ vs ε_1	252	316	-	-
	σ'_{oct} vs ε_v	-	-	277	-
	σ'_3 vs ε_3	-	-	-	-
	W vs σ'_{scalar}	248	296	277	-

Note: The yield (or limit state) stresses presented in this table have been put in terms of σ'_{oct} along the stress path for the test.

TABLE 3.7 YIELD STRESSES FROM DIFFERENT CRITERIA FOR TEST SERIES T205 TO T209

	Test Number	T205	T206	T207	T208
Yield Criterion	σ_1' vs ε_1	-	266	215	-
	$(\sigma_1-\sigma_3)$ vs ε_1	-	274	215	-
	σ'_{oct} vs ε_v	266	285	-	-
	σ_3' vs ε_3	-	-	209	-
	W vs σ'_{scalar}	255	267	-	-

Note: The yield (or limit state) stresses presented in this table have been put in terms of σ'_{oct} along the stress path for the test.

TABLE 4.1 STRAINS AT LIMIT STATE STRESSES

TEST NUMBER	T201	T202	T203	T205	T206	T207
ε_1 (%)	7.5	6.7	5.4	4.5	6.5	7.4
ε_v (%)	7.2	8.3	5.2	8.7	9.5	12.3

TABLE 4.2 VOLUME CHANGE MEASUREMENTS

TEST NUMBER	T201	T202	T203	T204	T205	T206	T207	T208	T209
Total Measured Volume Change* (cm^3)	61.9	92.5	109.1	32.6	93.0	97.1	111.4	53.0	23.6
Total Calculated Volume Change** (cm^3)	-	59.1	41.7	-	68.8	51.9	49.7	8.4	-24.0

* From burette readings

** From sample moisture contents before and after testing

\- Moisture content not taken at the end of test

F I G U R E S

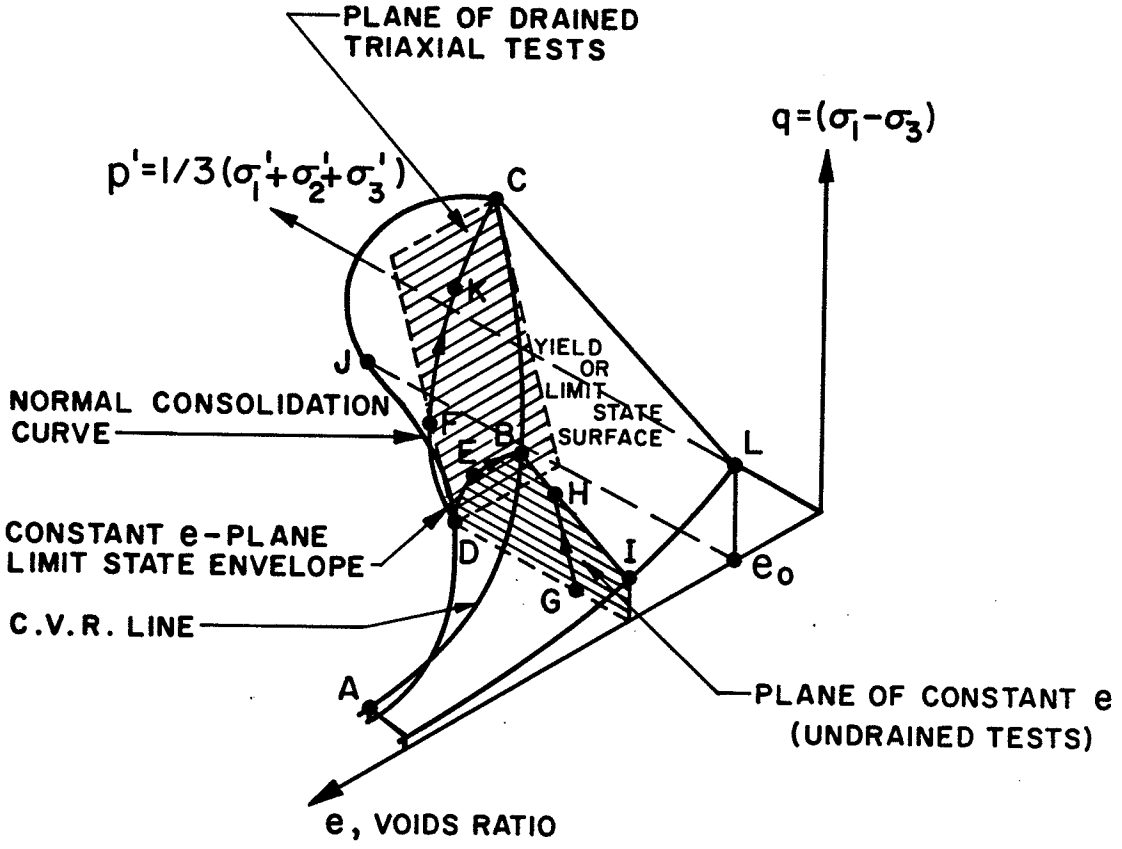

(a). Isometric view of Yield Surface

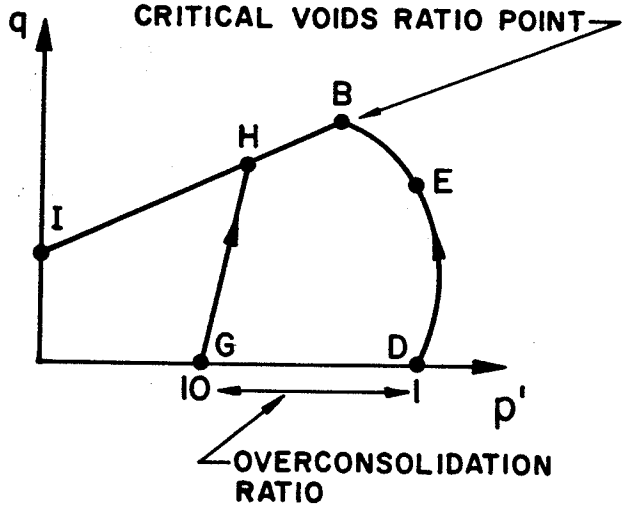

(b). Constant e-Plane

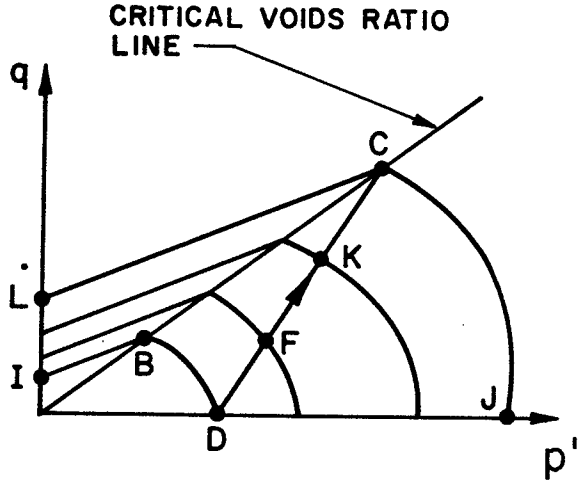

(c). Drained Plane in (p',q) Space

Fig. 2.1. Yield Surface and C.V.R. Line

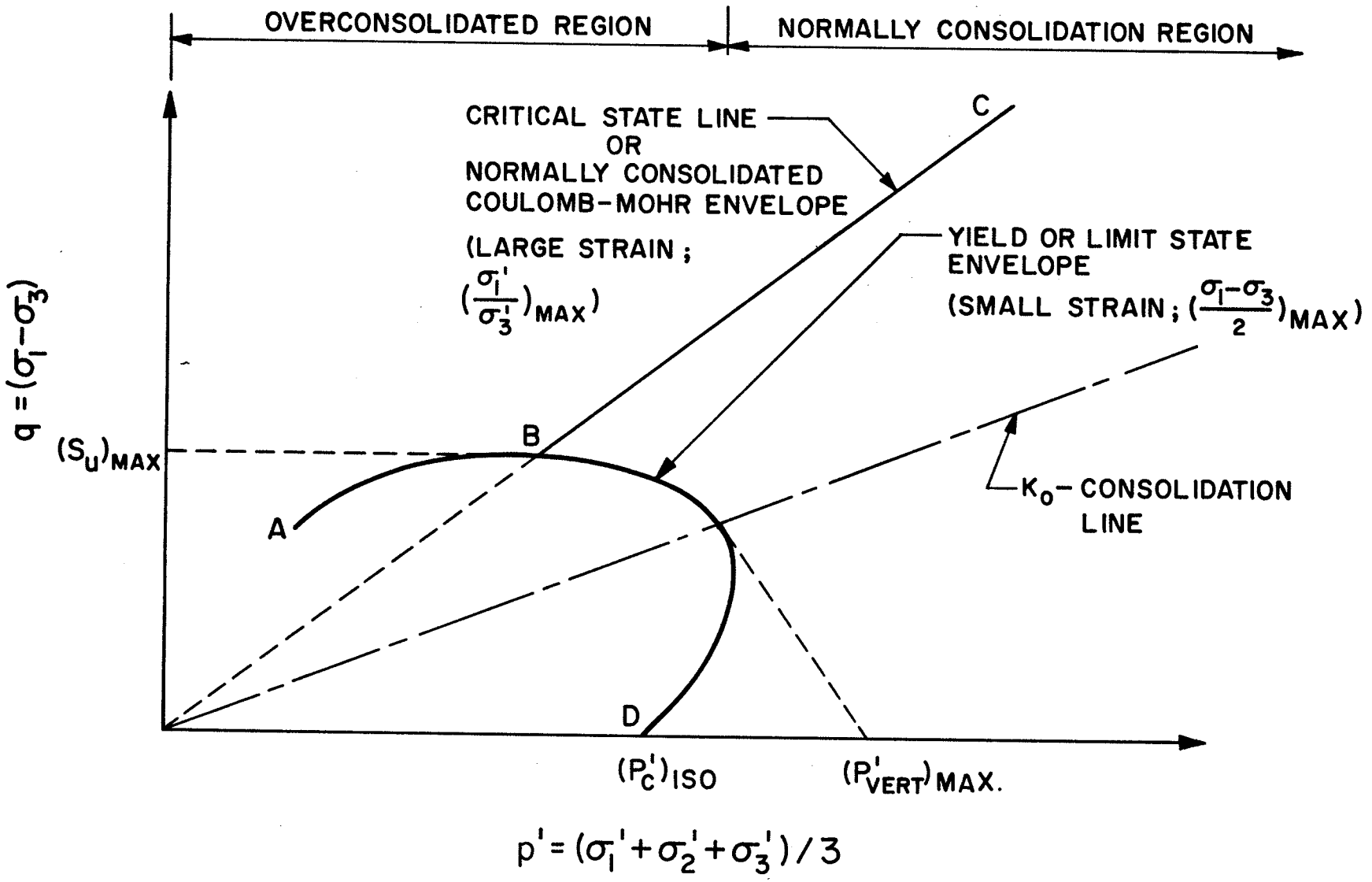

Fig. 2.2. Typical Critical State Line , Limit State Envelope , and Associated Parameters

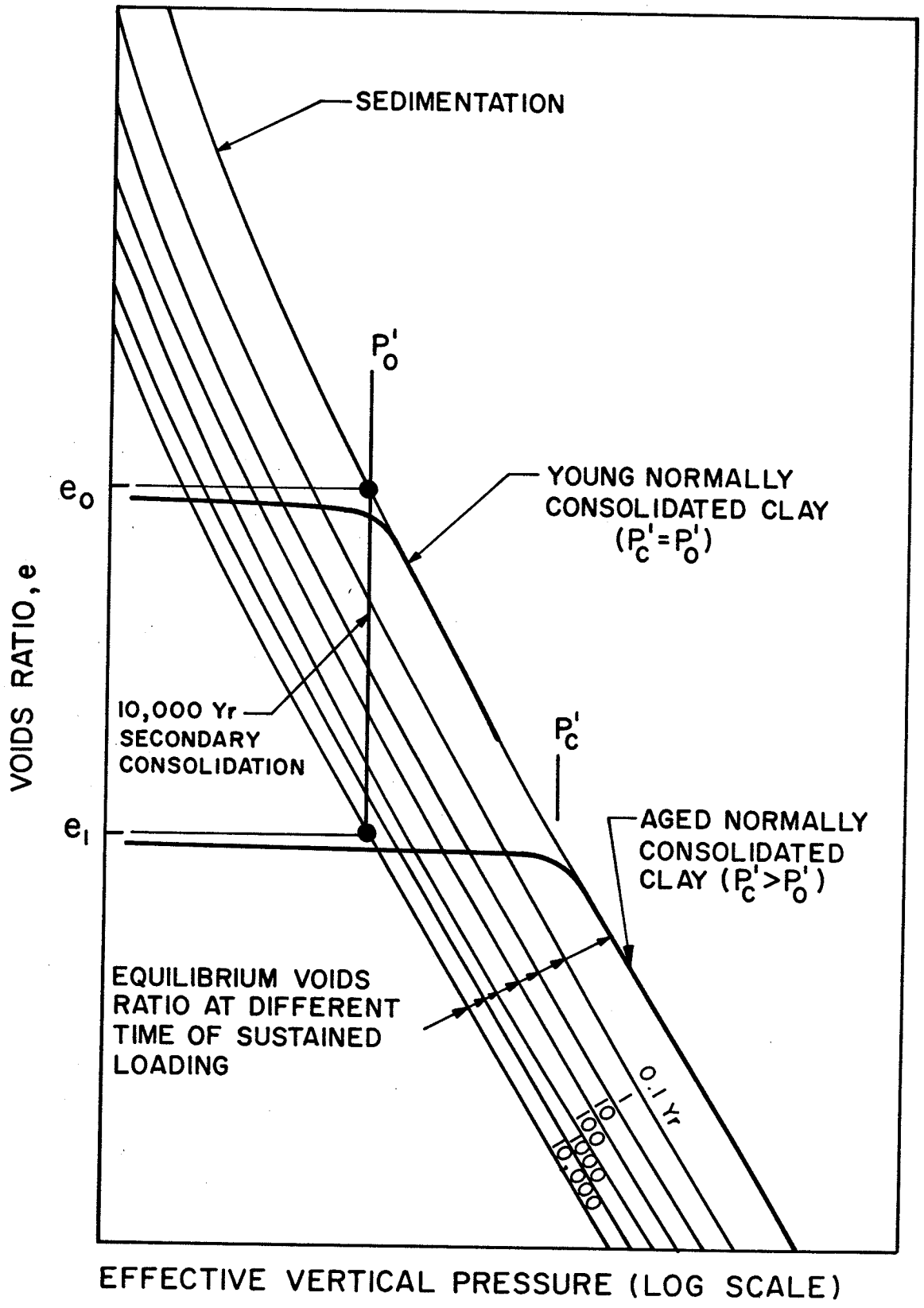

Fig. 2.3. The Effects of Time on a Normally Consolidated Clay (After Bjerrum, 1967)

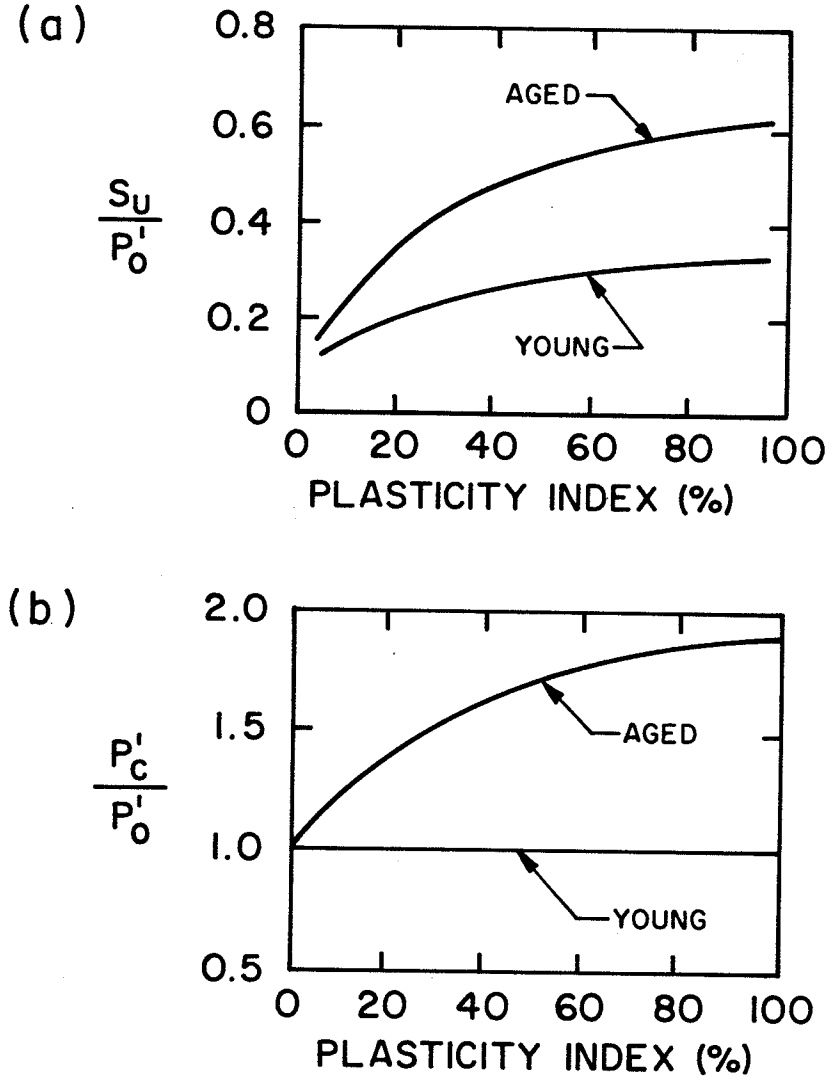

Fig.2.4. Typical Values of S_u/P_o' and P_c'/P_o' Observed in Normally Consolidated Late Glacial and Postglacial Clays. (After Bjerrum, 1973)

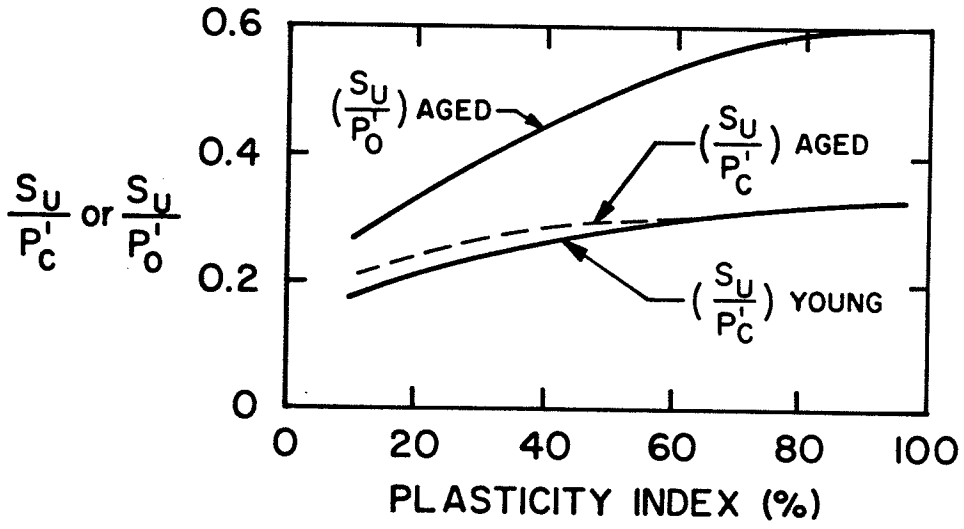

Fig. 2.5. S_u/P' for Young and Aged Clays. (From Tavenas and Leroueil, 1977)

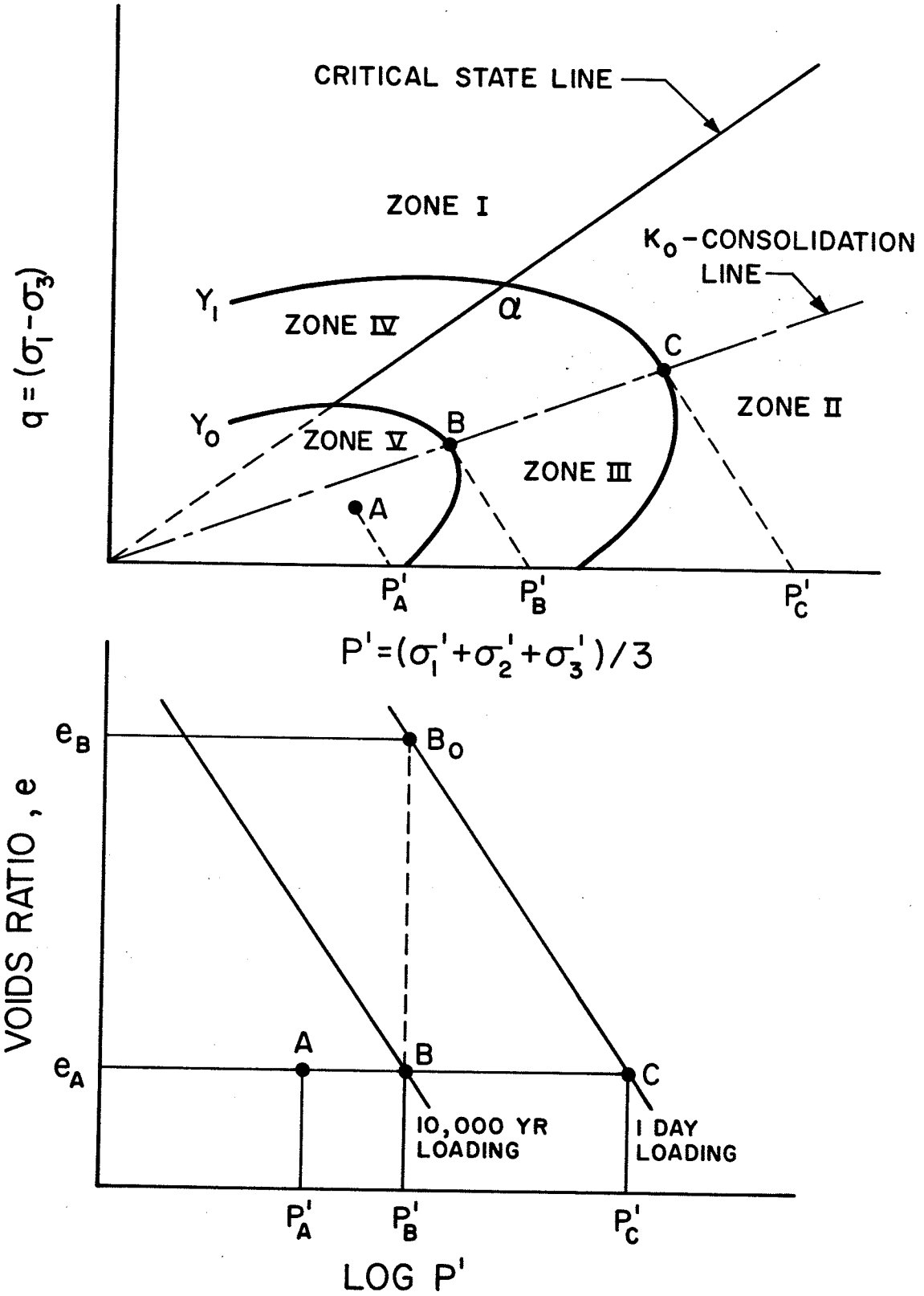

Fig. 2.6. The YLIGHT Model for the Behavior of Clays (After Tavenas and Leroueil, 1977)

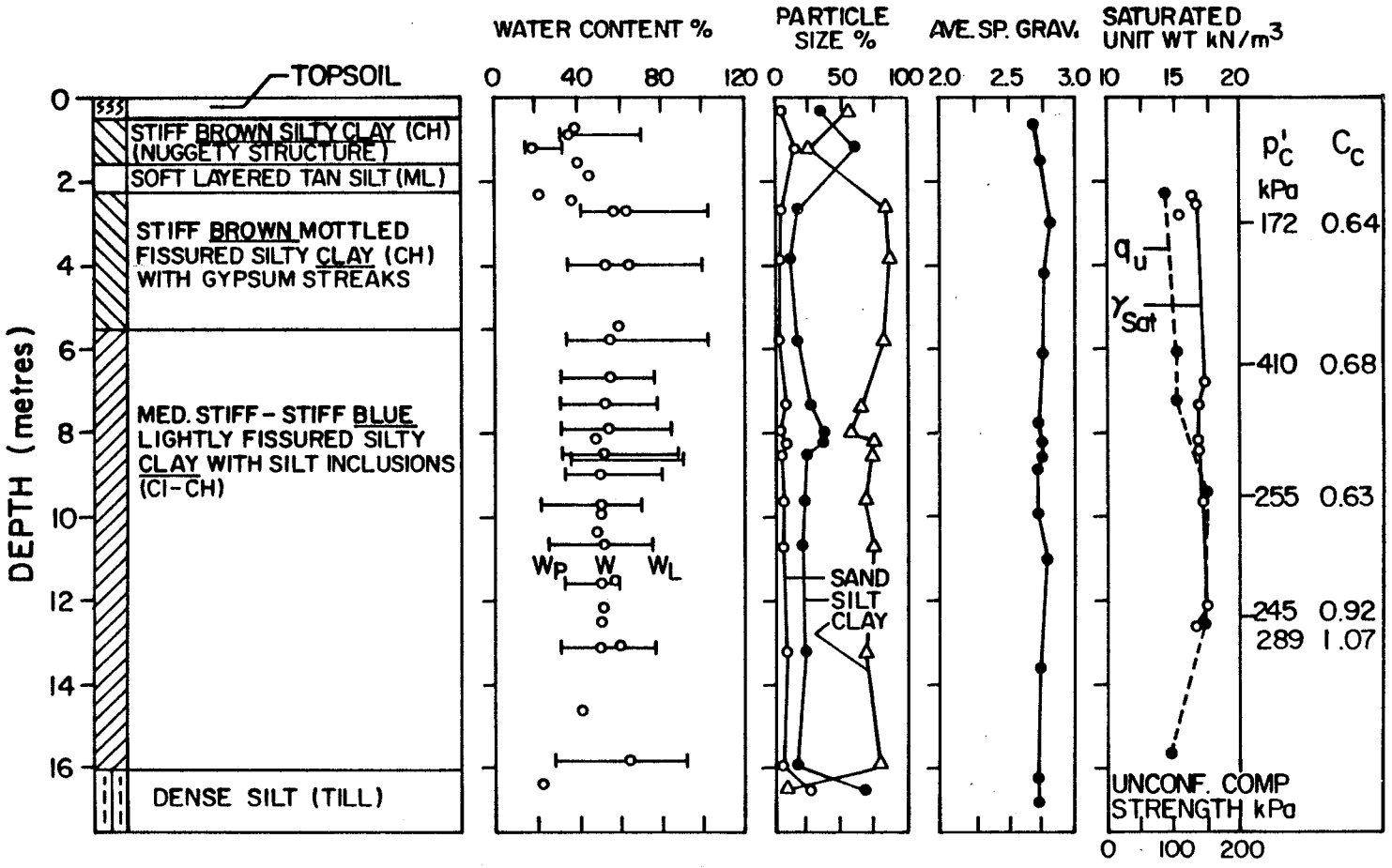

FIG. 3.1. AVERAGE BOREHOLE LOG INFORMATION, UNIVERSITY OF MANITOBA CAMPUS (FROM BARACOS et al., 1979)

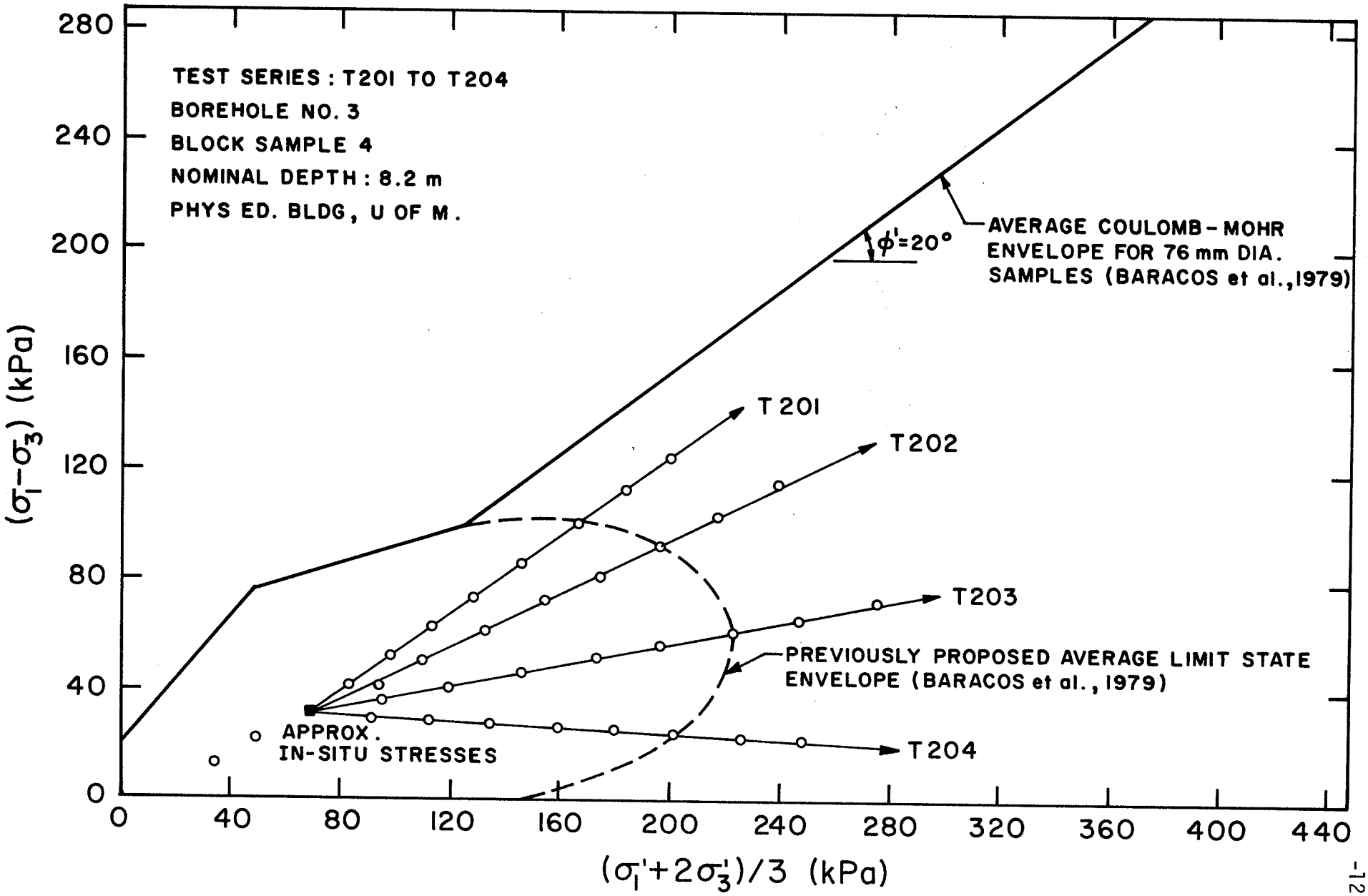

Fig. 3.2. Proposed Effective Stress Paths-Test Series : T201 TO T204

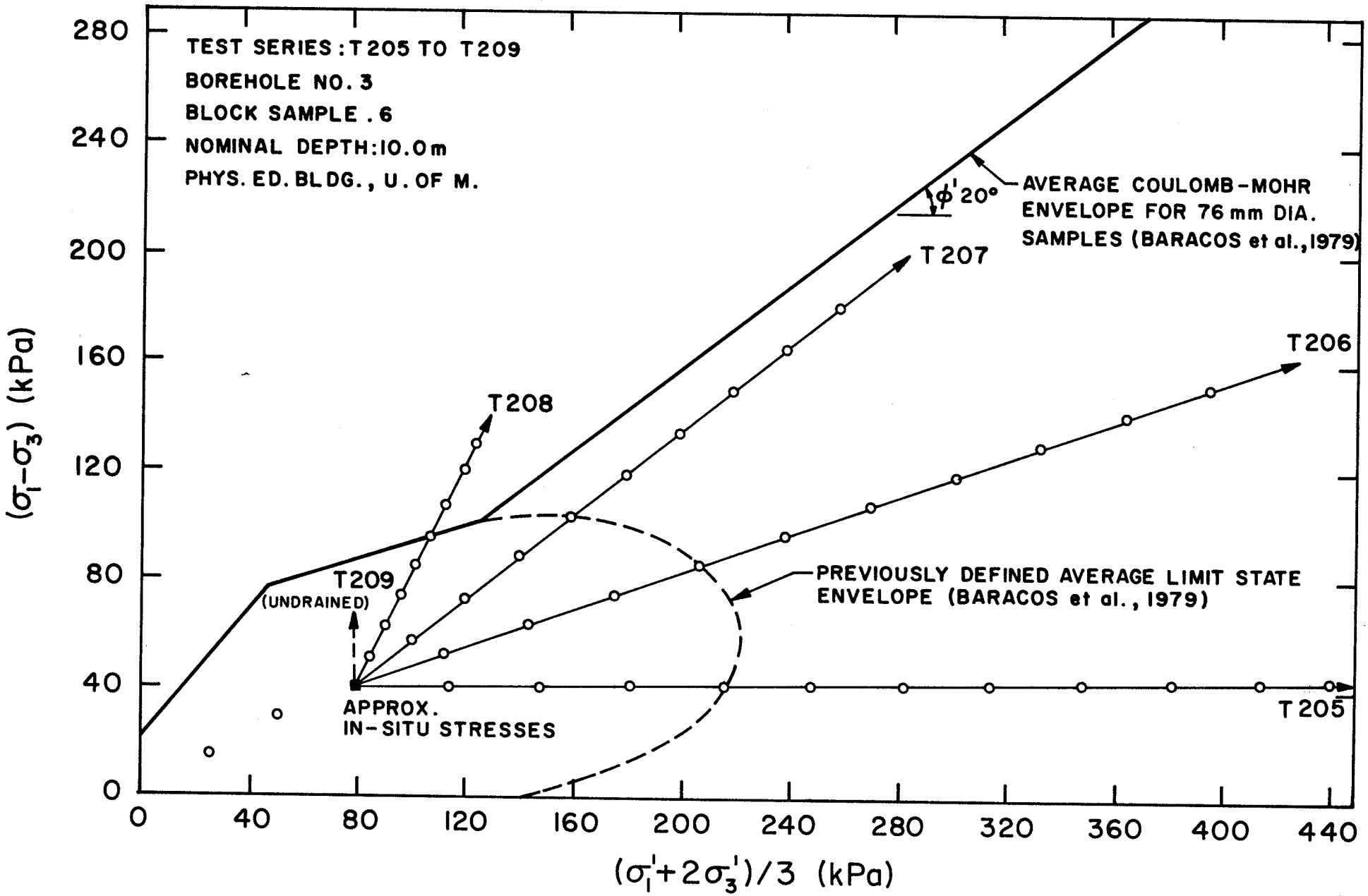

Fig. 3.3. Proposed Effective Stress Paths–Test Series: T205 TO T209

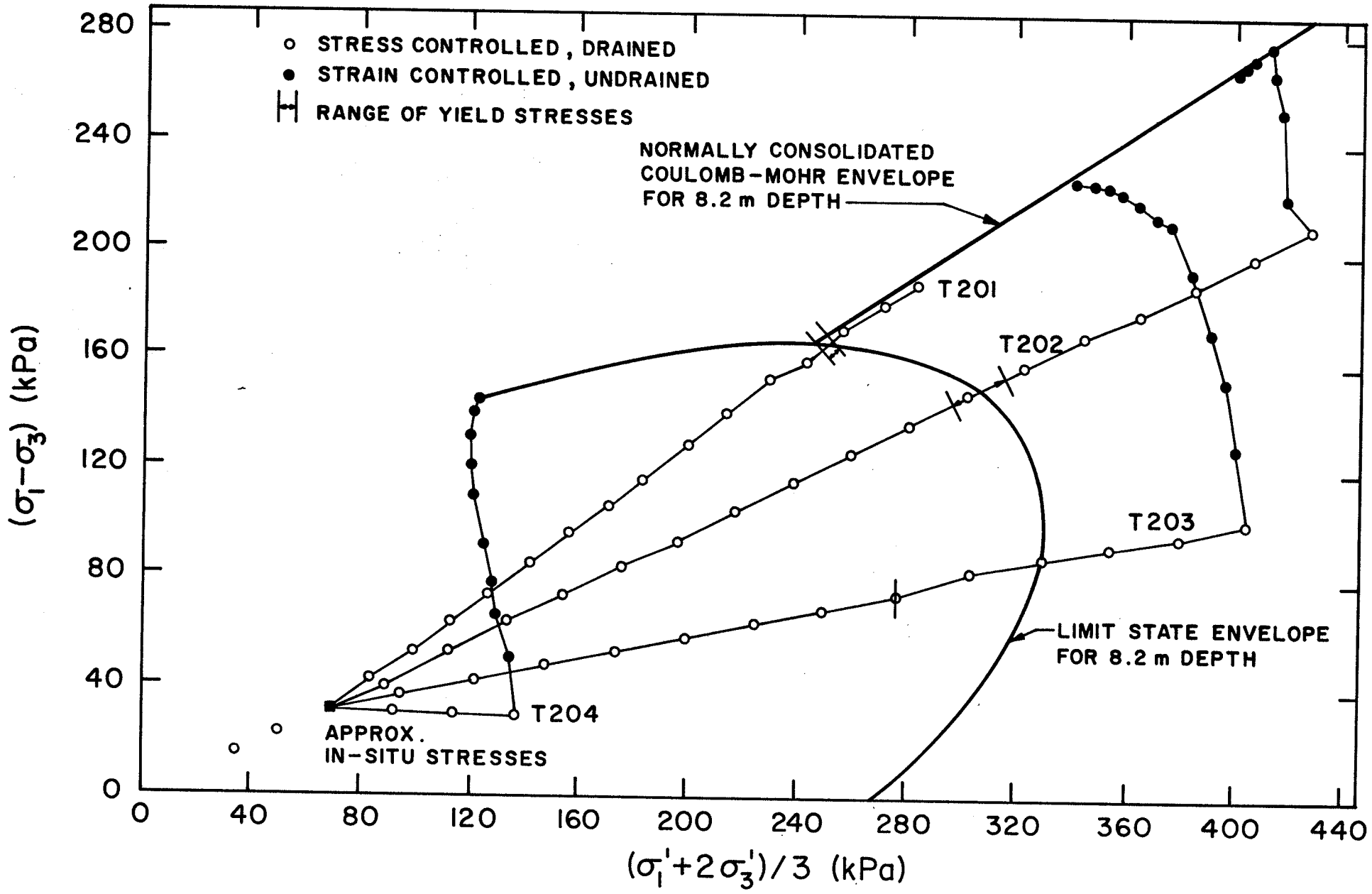

Fig. 3.4. Effective Stress Paths–Test Series : T201 TO T204

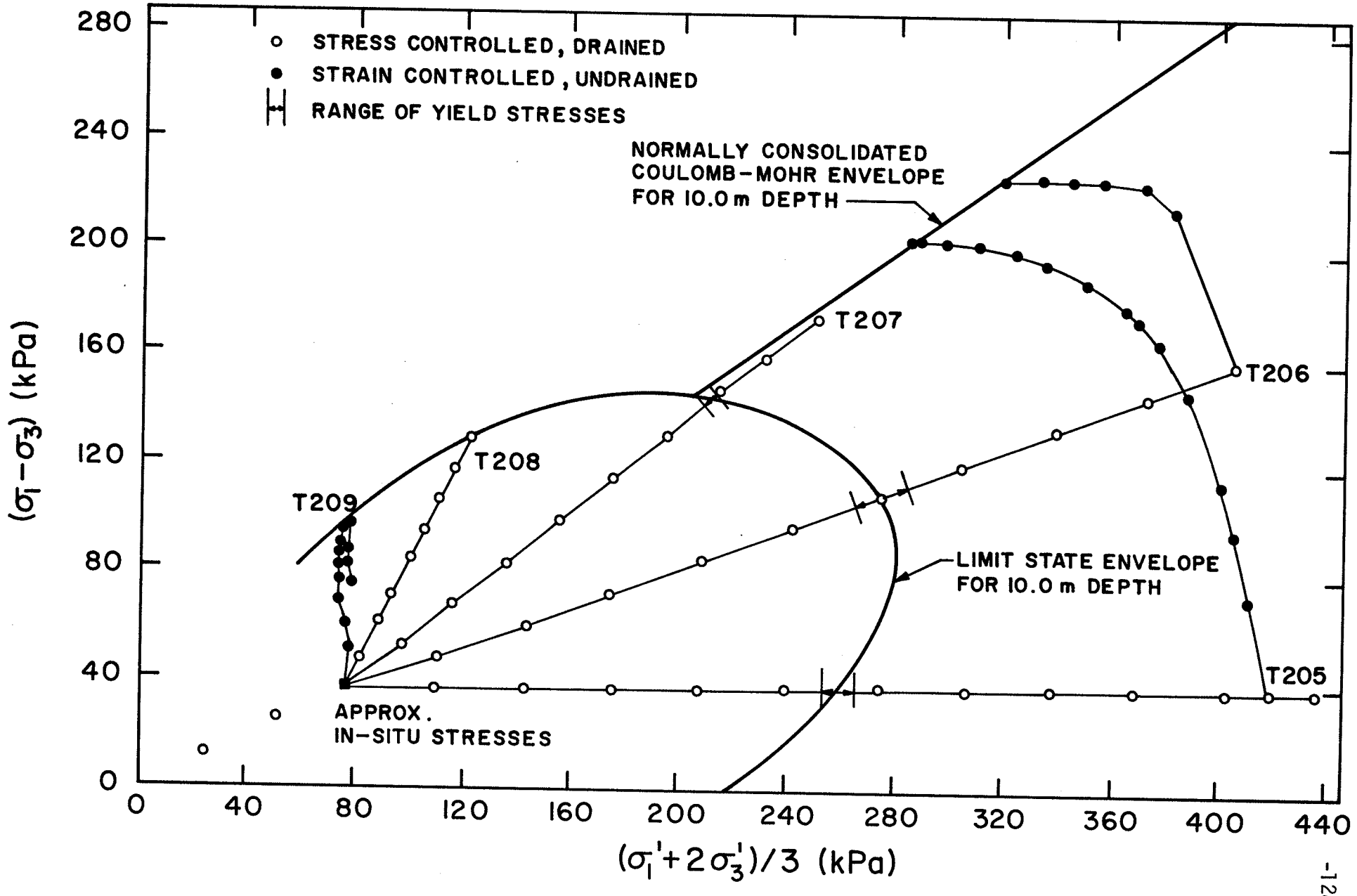

Fig. 3.5. Effective Stress Paths - Test Series : T205 TO T209

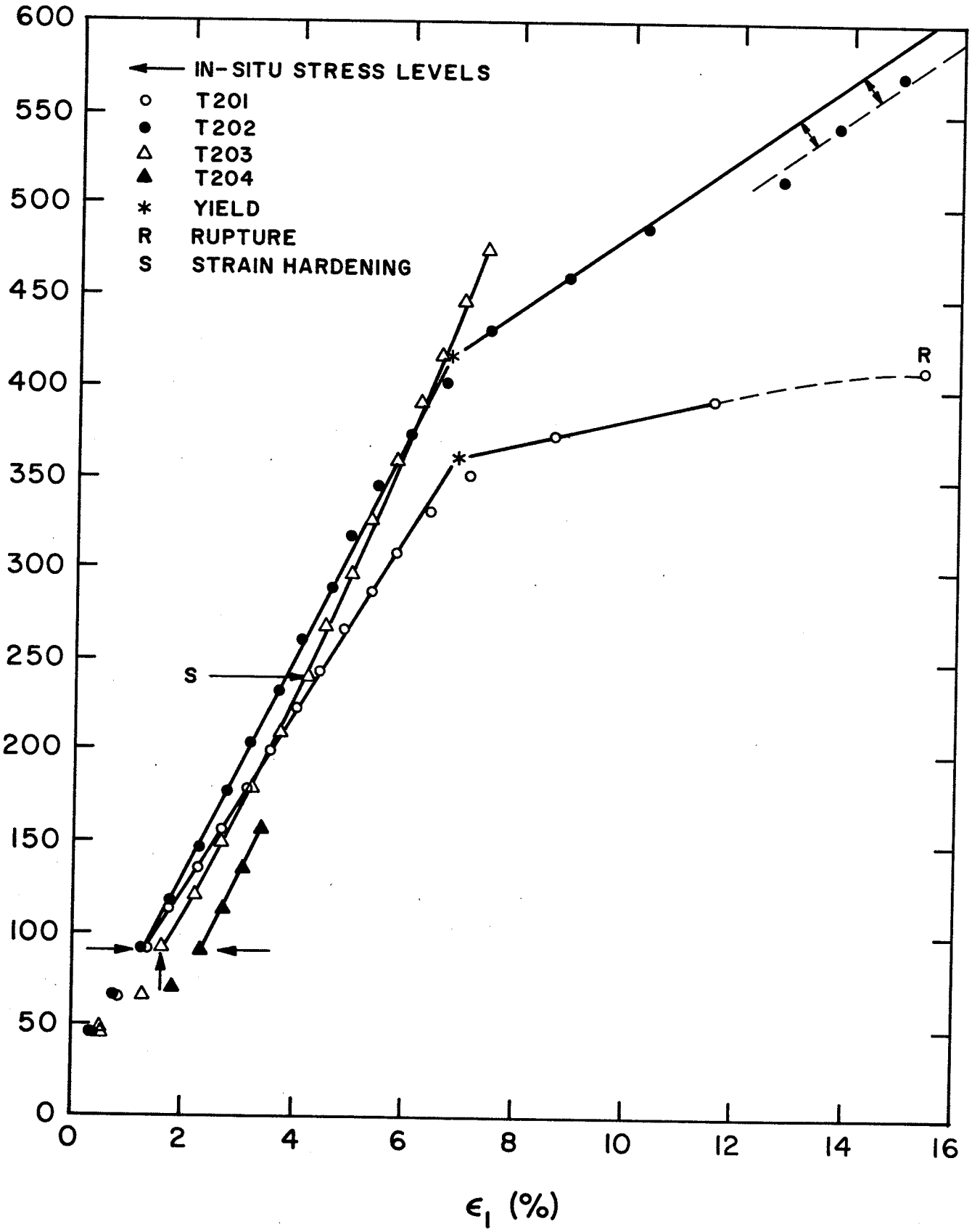

Fig. 3.6. The Relationship Between Effective Axial Stress and Axial Strain for Test Series: T201 TO T204

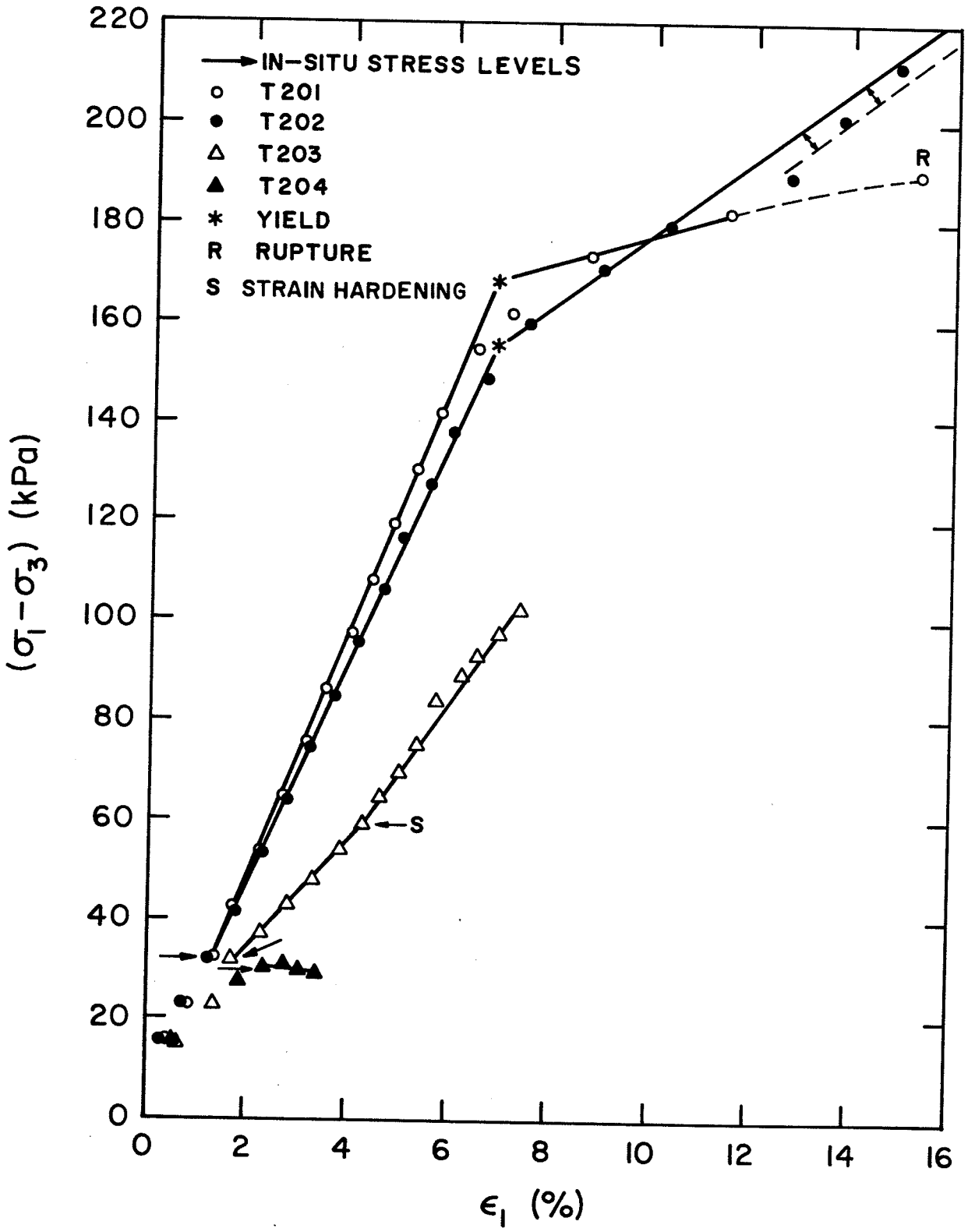

Fig. 3.7. The Relationship Between Principal Stress Difference and Axial Strain for Test Series : T201 TO T204

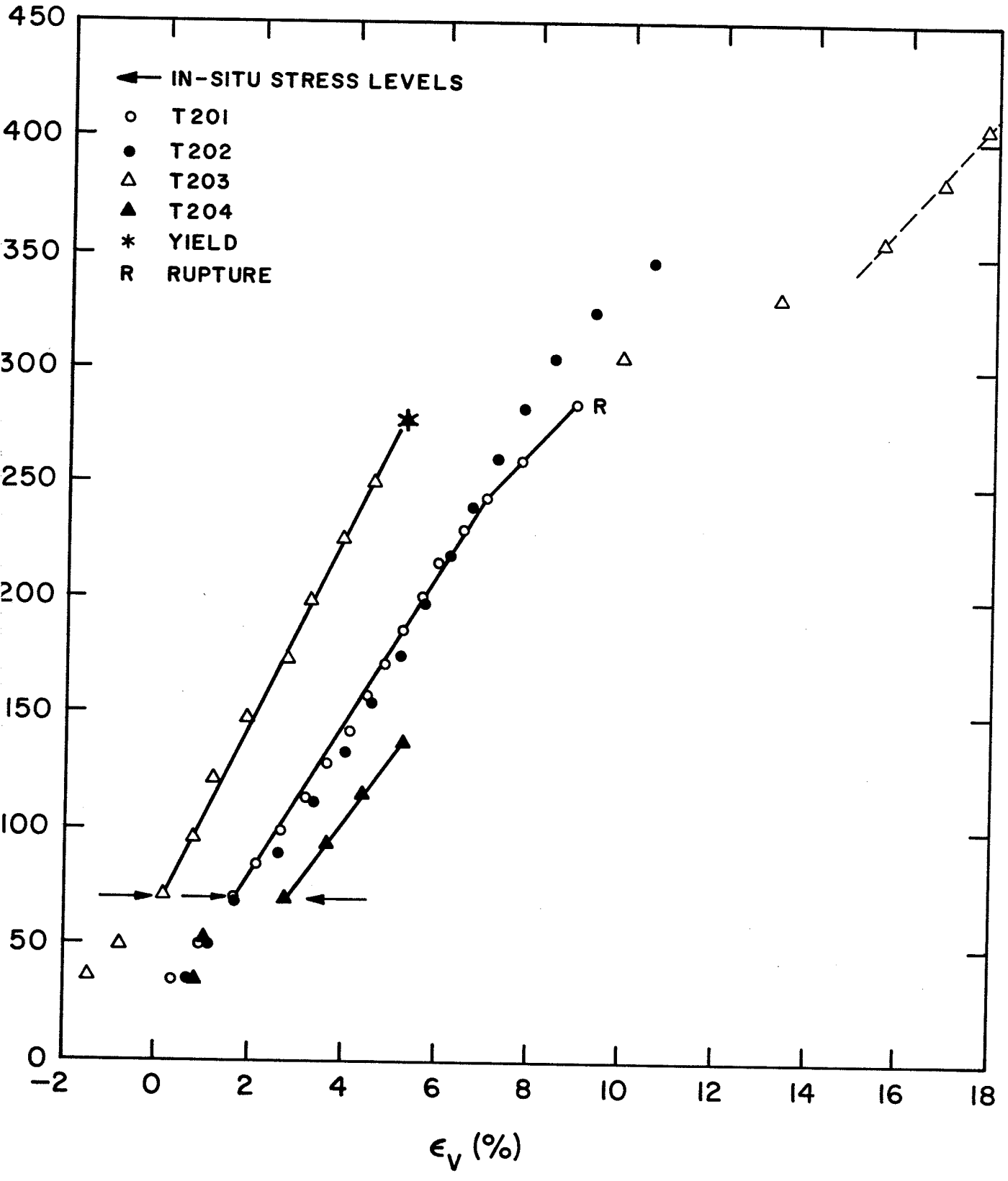

Fig. 3.8. The Relationship Between Effective Octahedral Normal Stress and Volumetic Strain for Test Series: T201 TO T204

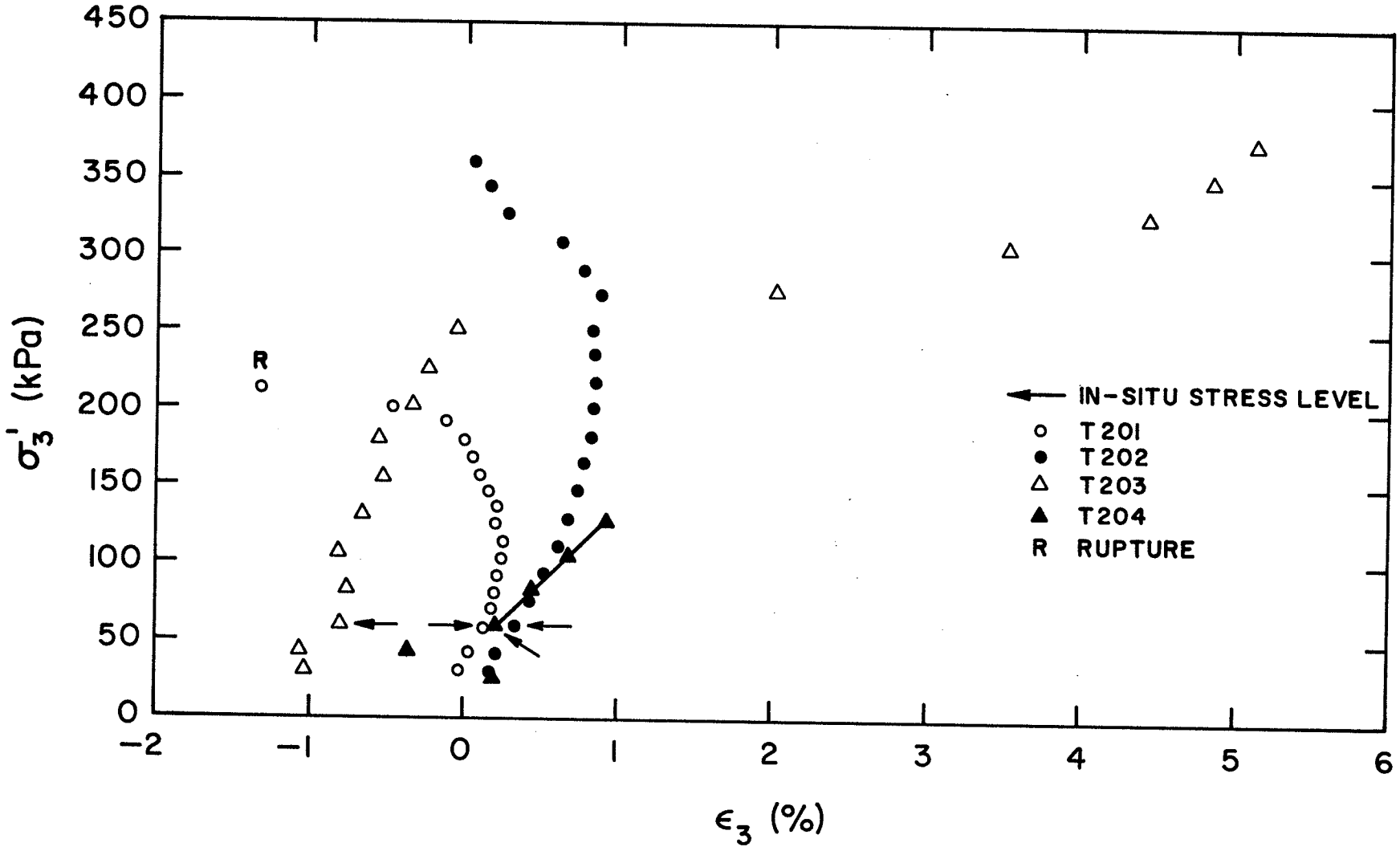

Fig. 3.9. The Relationship Between Effective Radial Stress and Radial Strain for Test Series : T201 TO T204

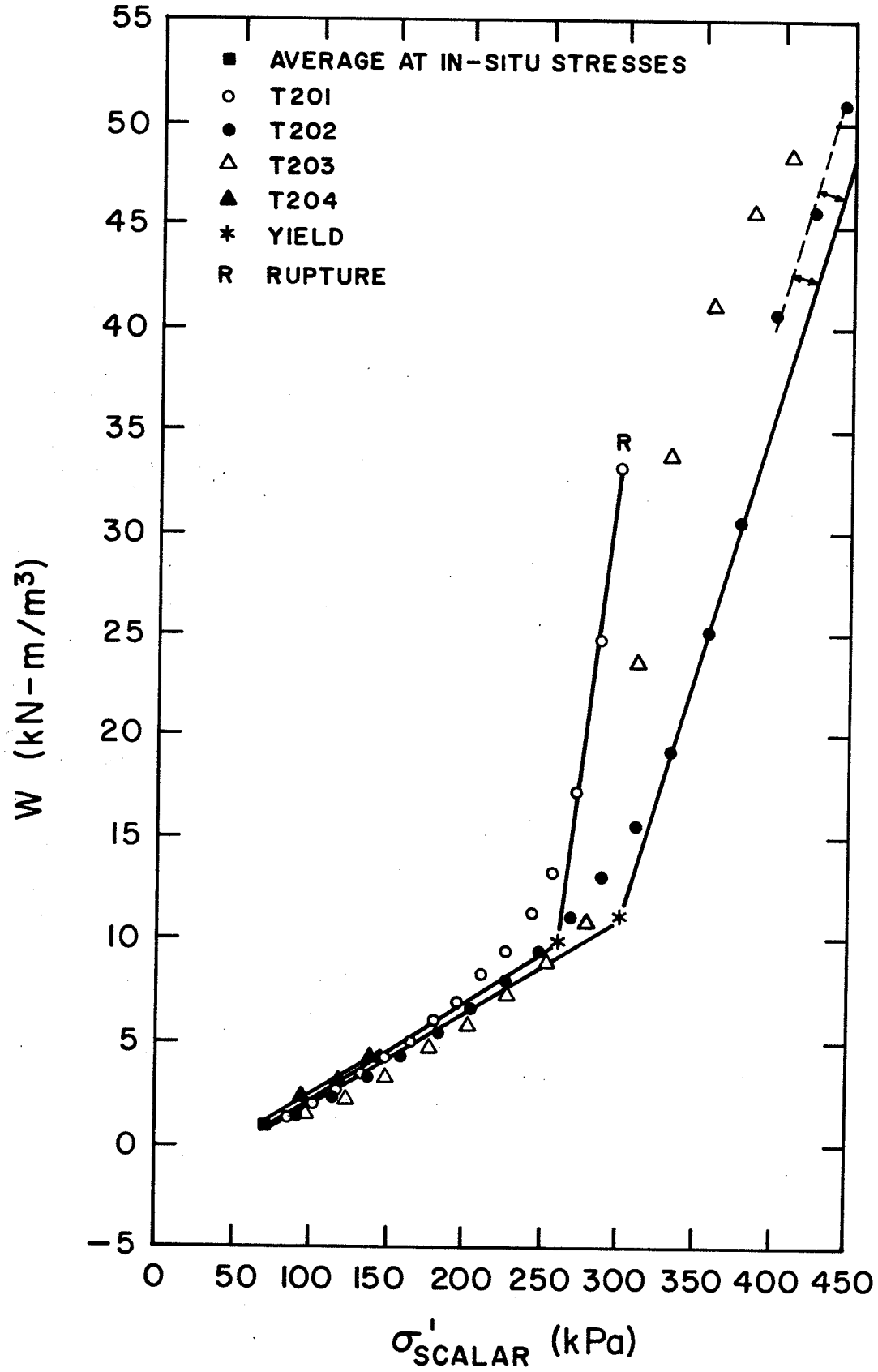

Fig. 3.10. The Relationship Between Strain Energy Absorbed Per Unit Volume and the Effective Scalar Stress for Test Series : T201 TO T204

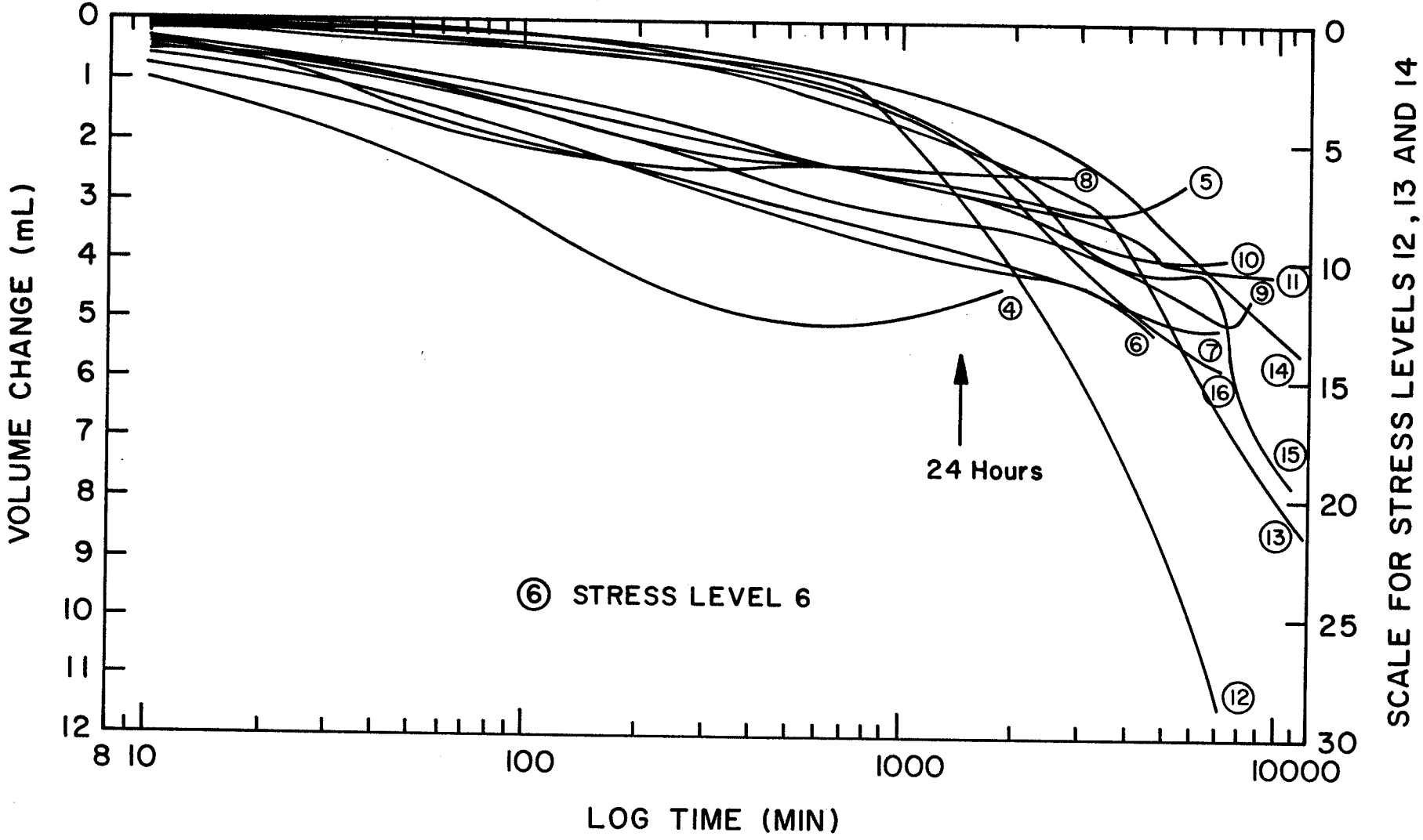

Fig. 3.11. The Relationship Between Volume Change and Log Time for Different Stress Levels in Test T203

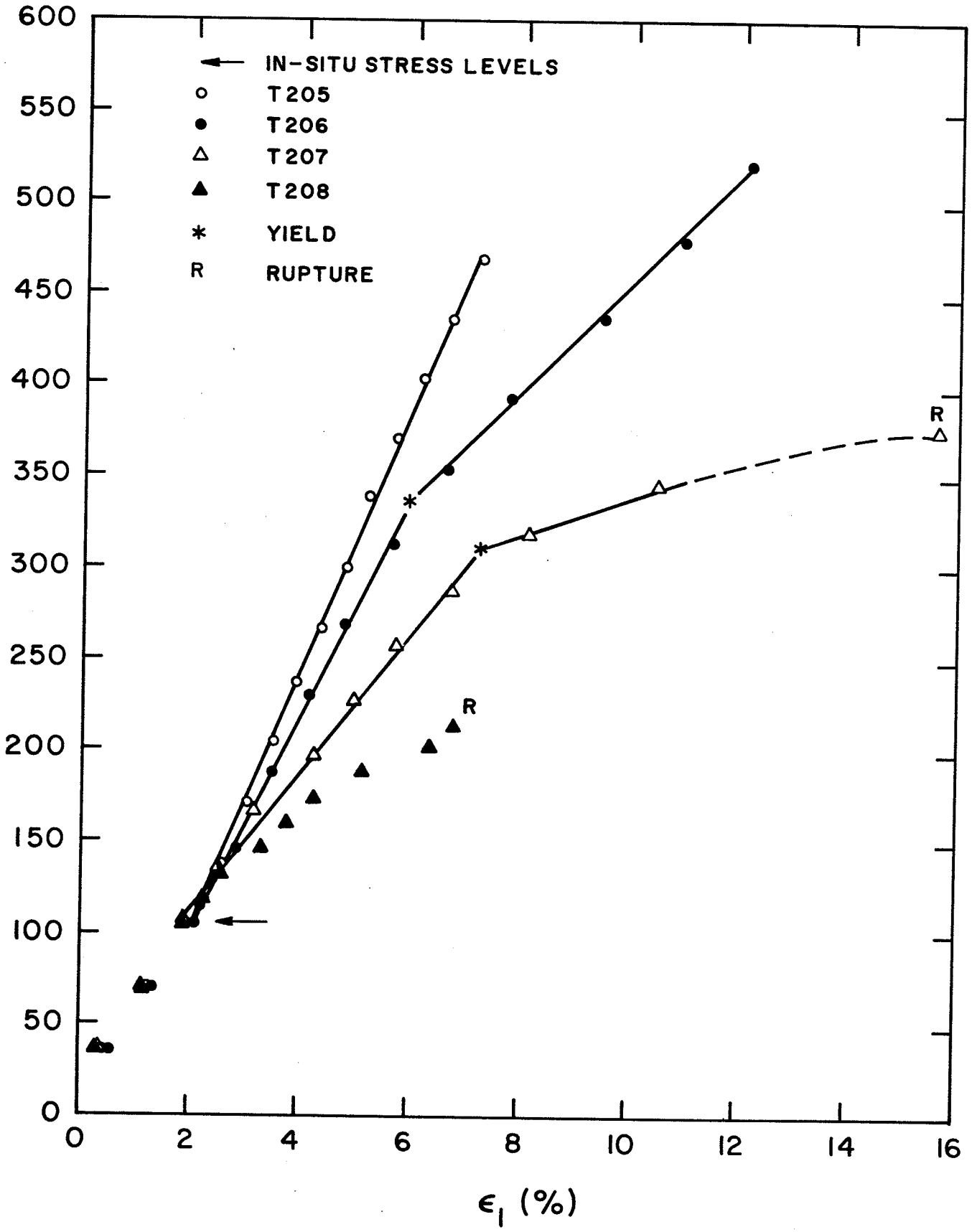

Fig.3.12. The Relationship Between Effective Axial Stress and Axial Strain for Test Series: T205 TO T209

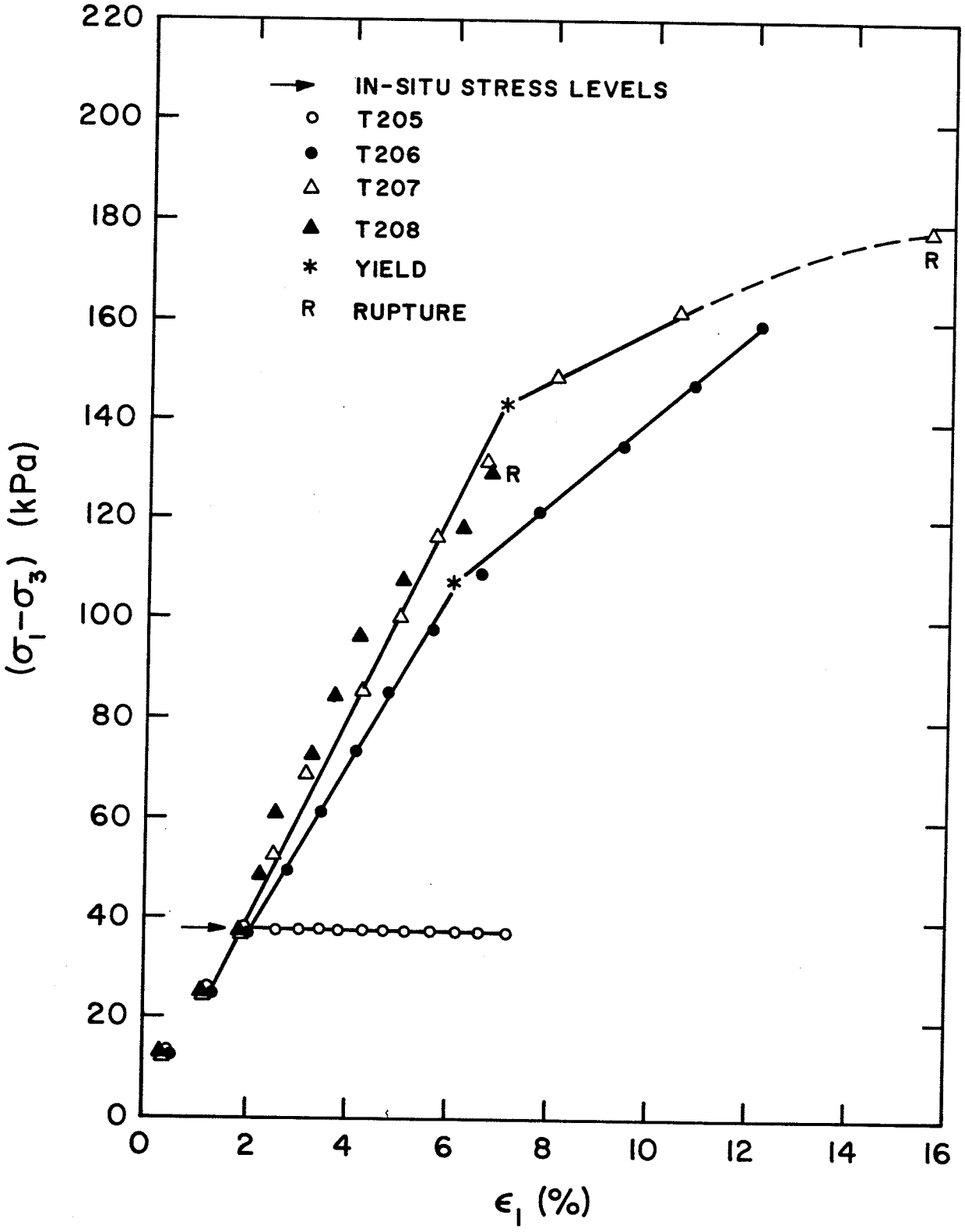

Fig. 3.13. The Relationship Between Principal Stress Difference and Axial Strain for Test Series: T205 TO T209

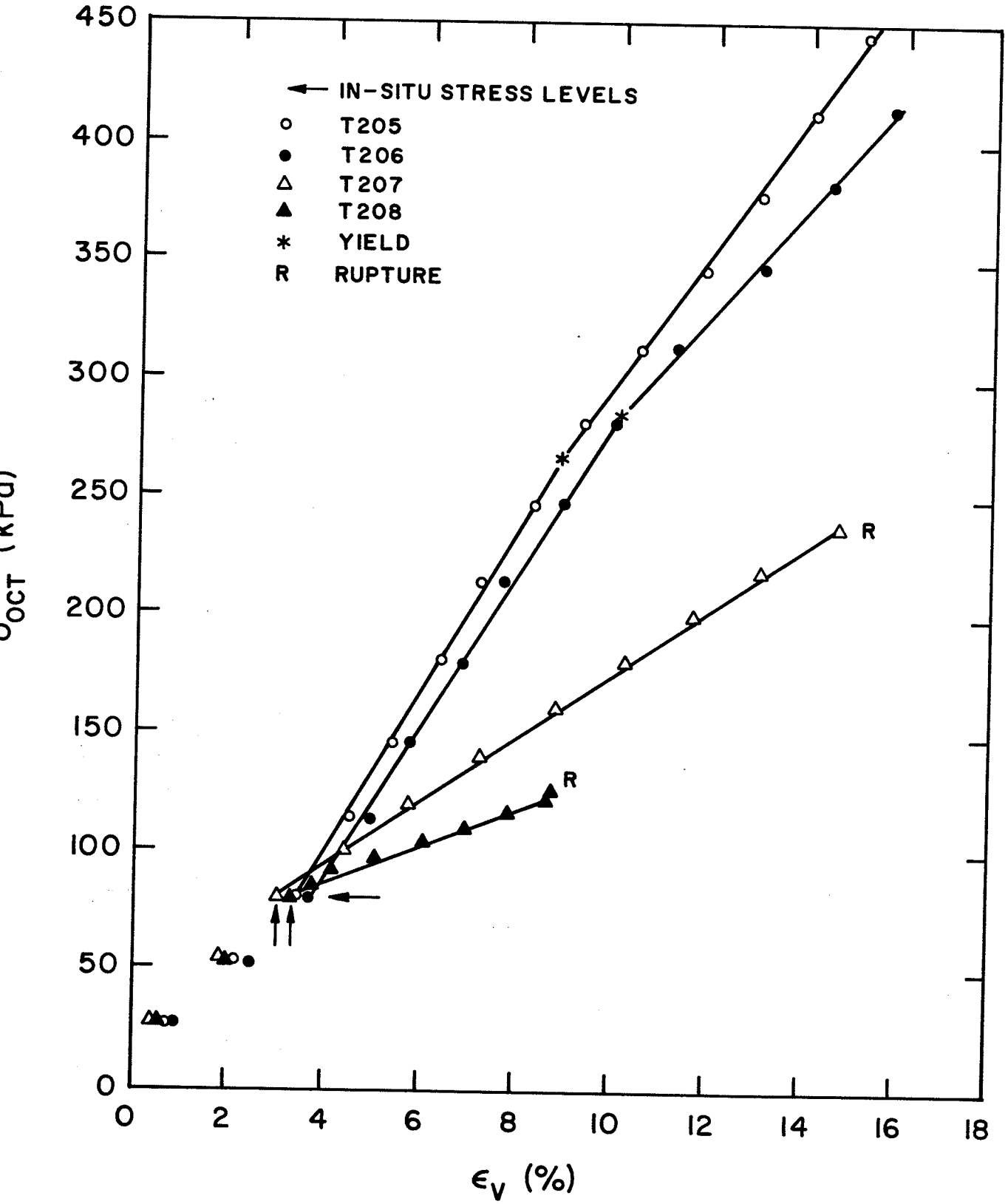

Fig. 3.14. The Relationship Between Effective Octahedral Normal Stress and Volumetric Strain for Test Series: T205 TO T209

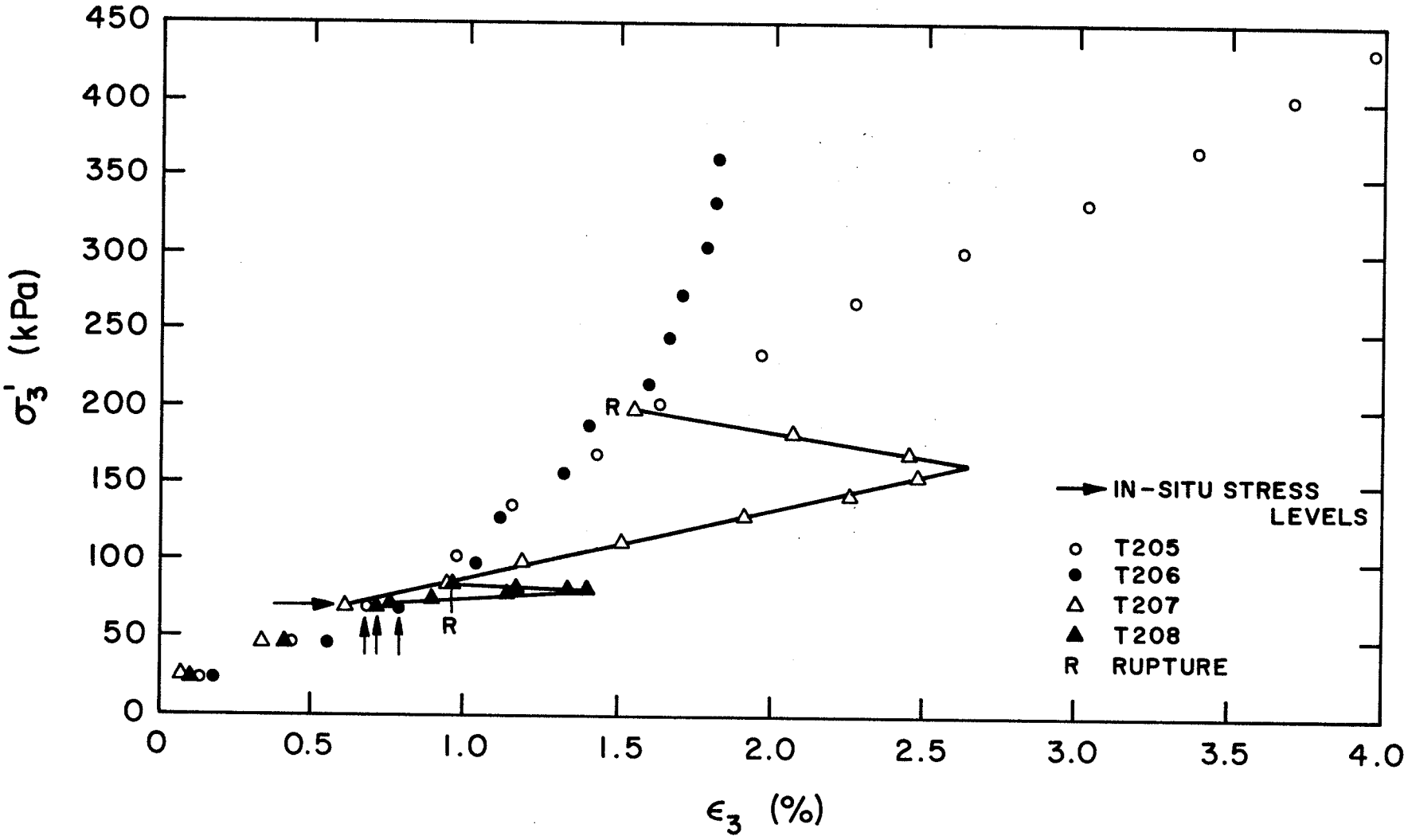

Fig. 3.15. The Relationship Between Effective Radial Stress and Radial Strain for Test Series: T205 TO T209

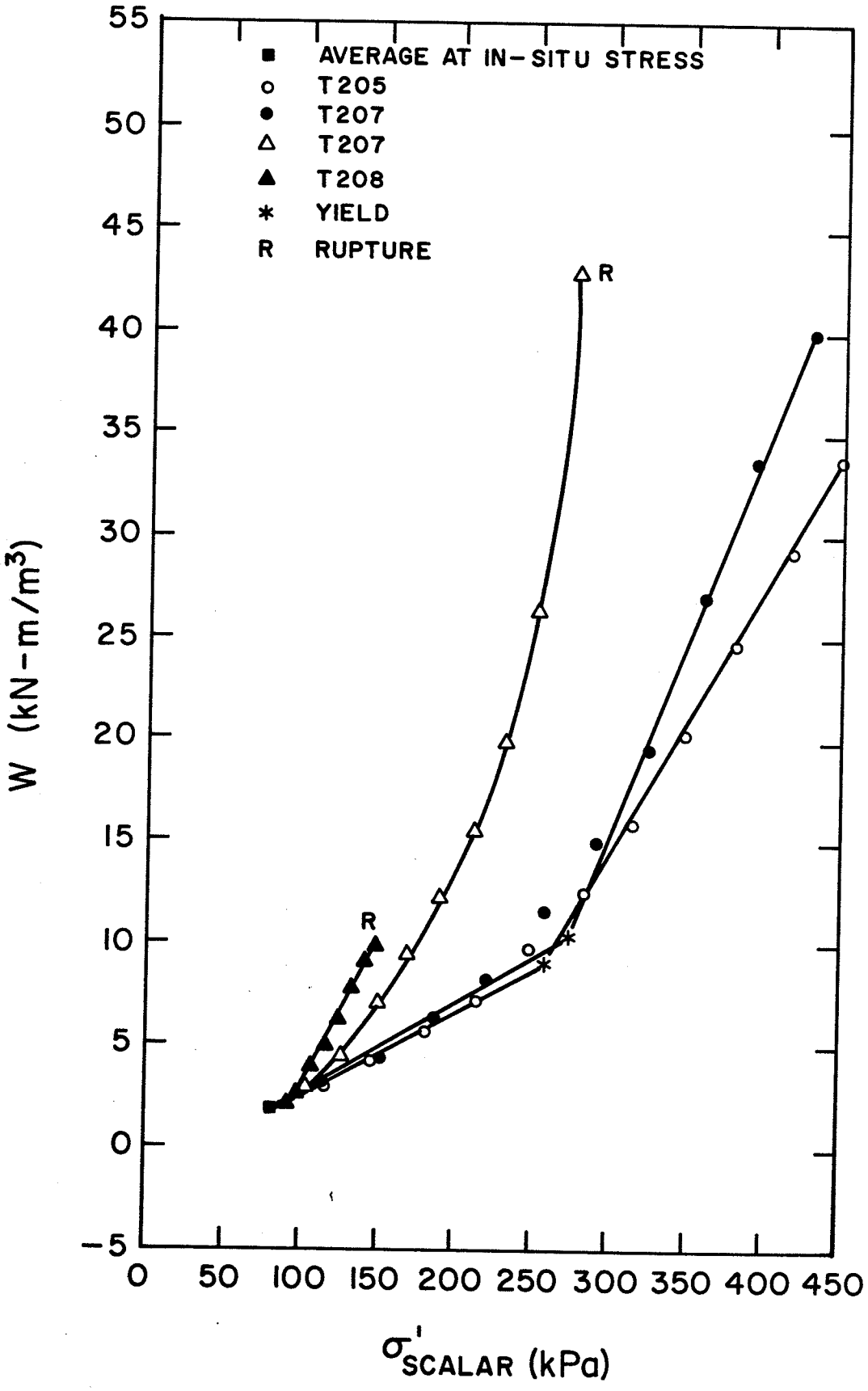

Fig. 3.16. The Relationship Between Strain Energy Absorbed Per Unit Volume and Effective Scalar Stress for Test Series : T205 TO T209

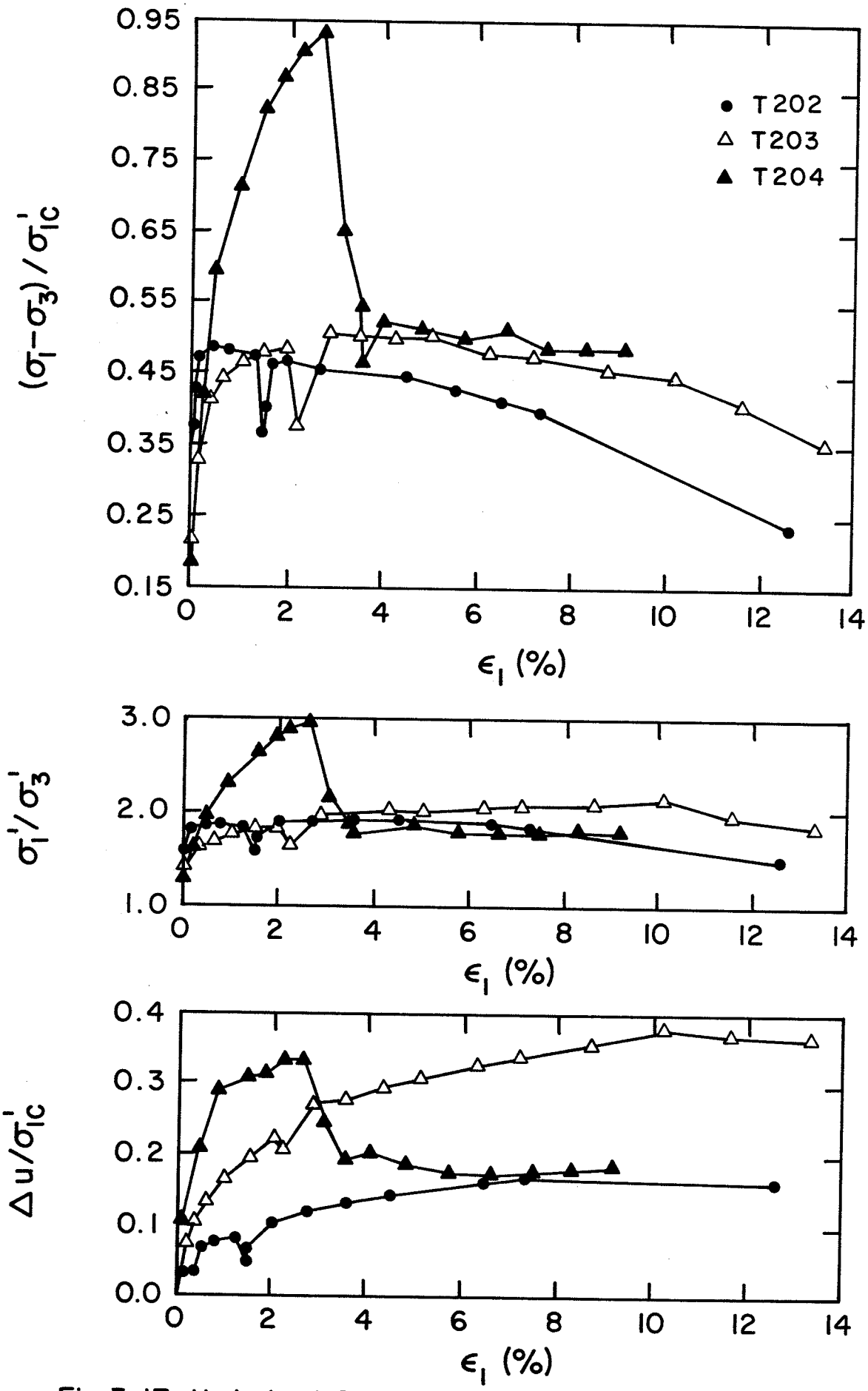

Fig. 3.17. Undrained Stress-Strain Results for Test Series: T201 TO T204

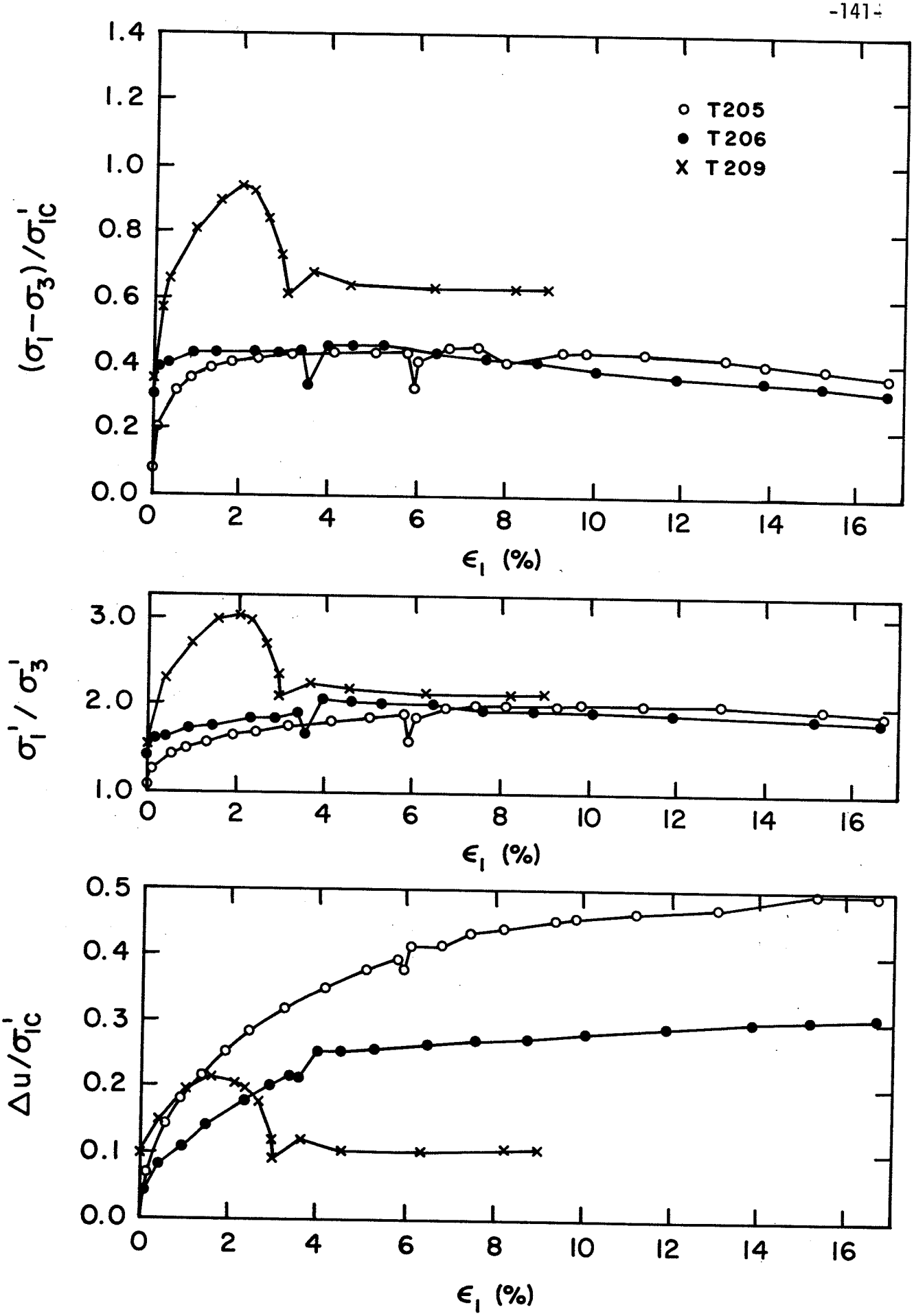

Fig. 3.18. Undrained Stress-Strain Results for Test Series: T205 TO T209

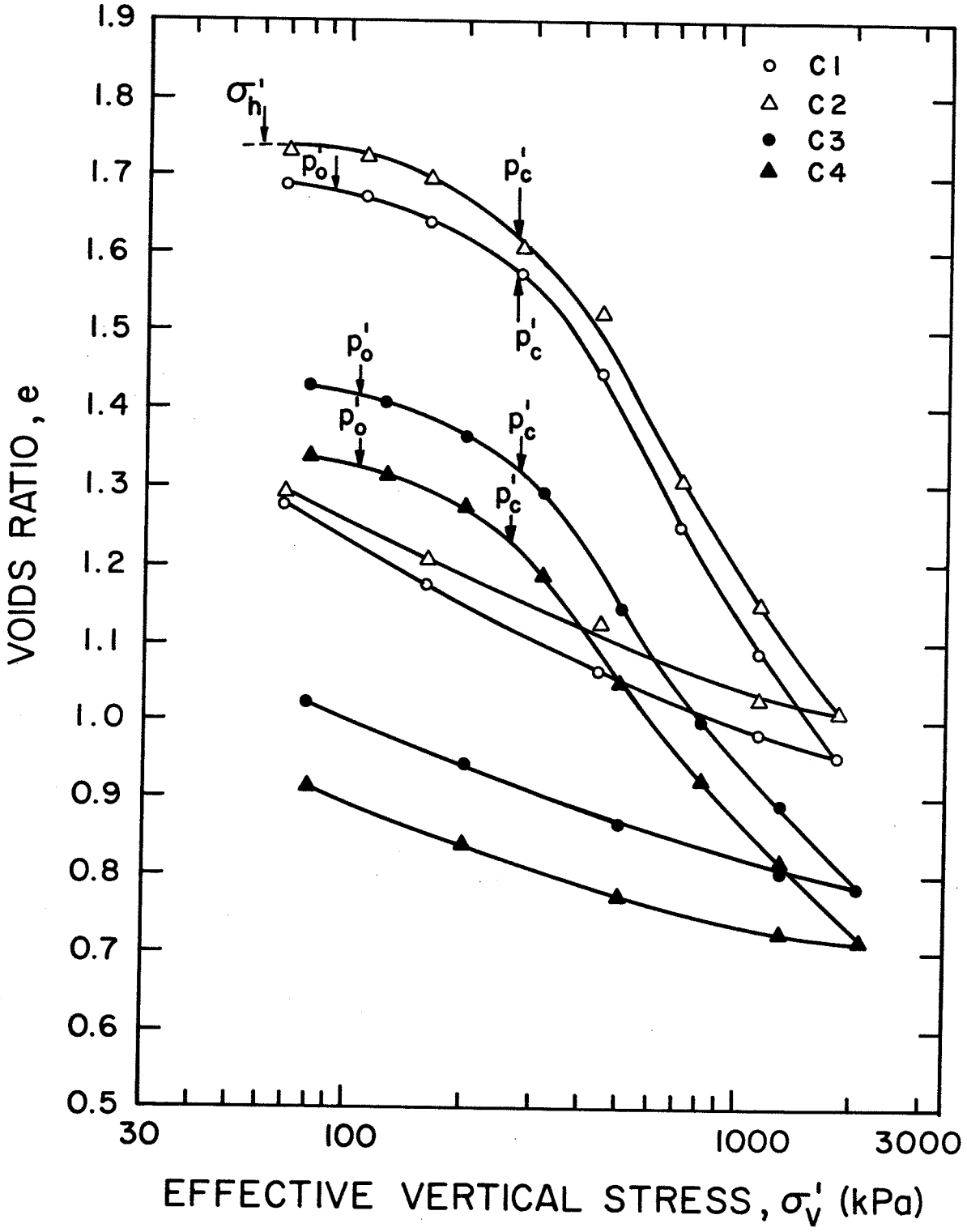

Fig. 3.19. One-Dimensional Consolidation Test Results

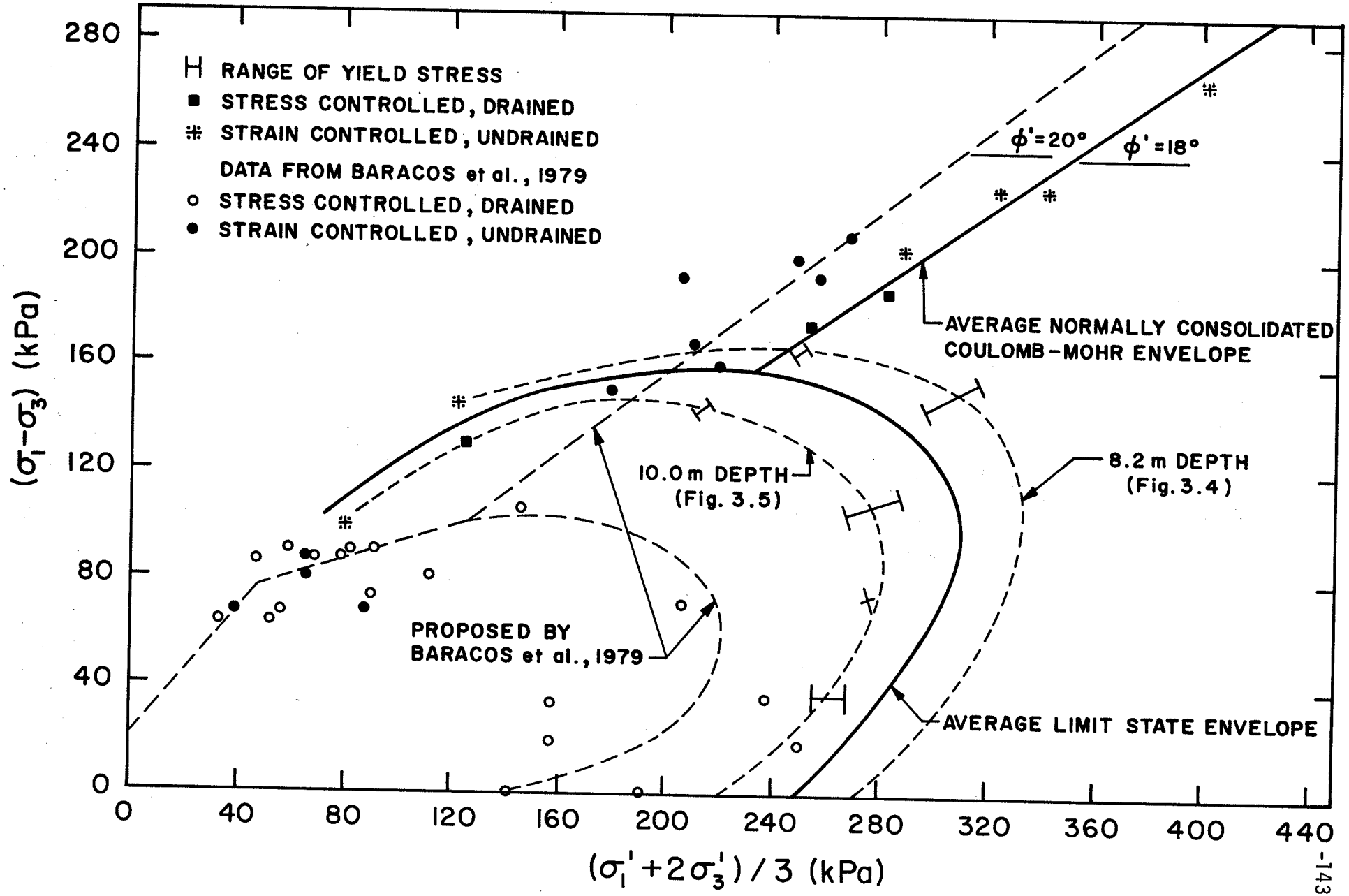

Fig. 3.20. Average Limit State and Coulomb-Mohr Envelopes for Samples from 8.2 m and 10.0 m

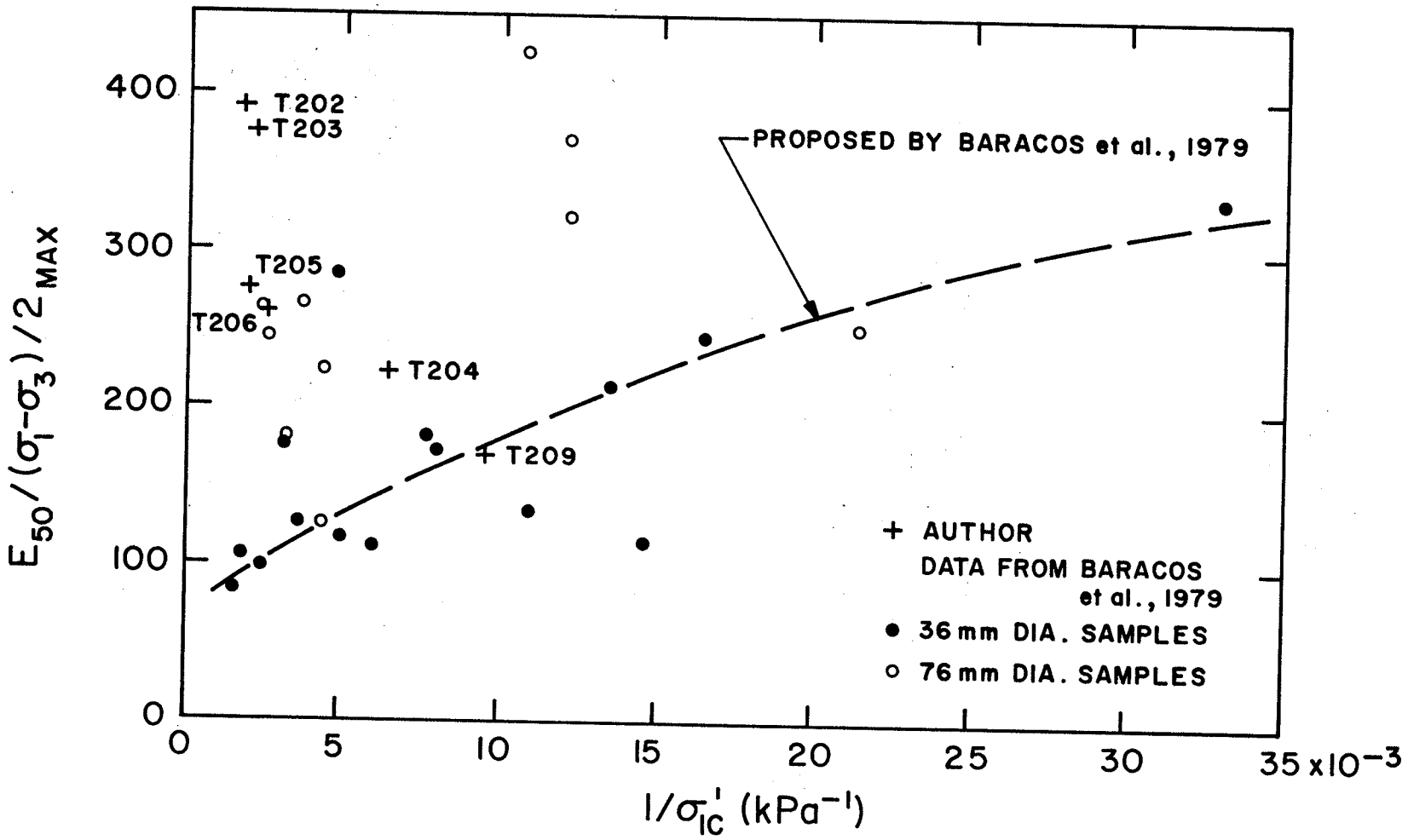

Fig.3.21. Elastic Moduli Results for Undrained Tests

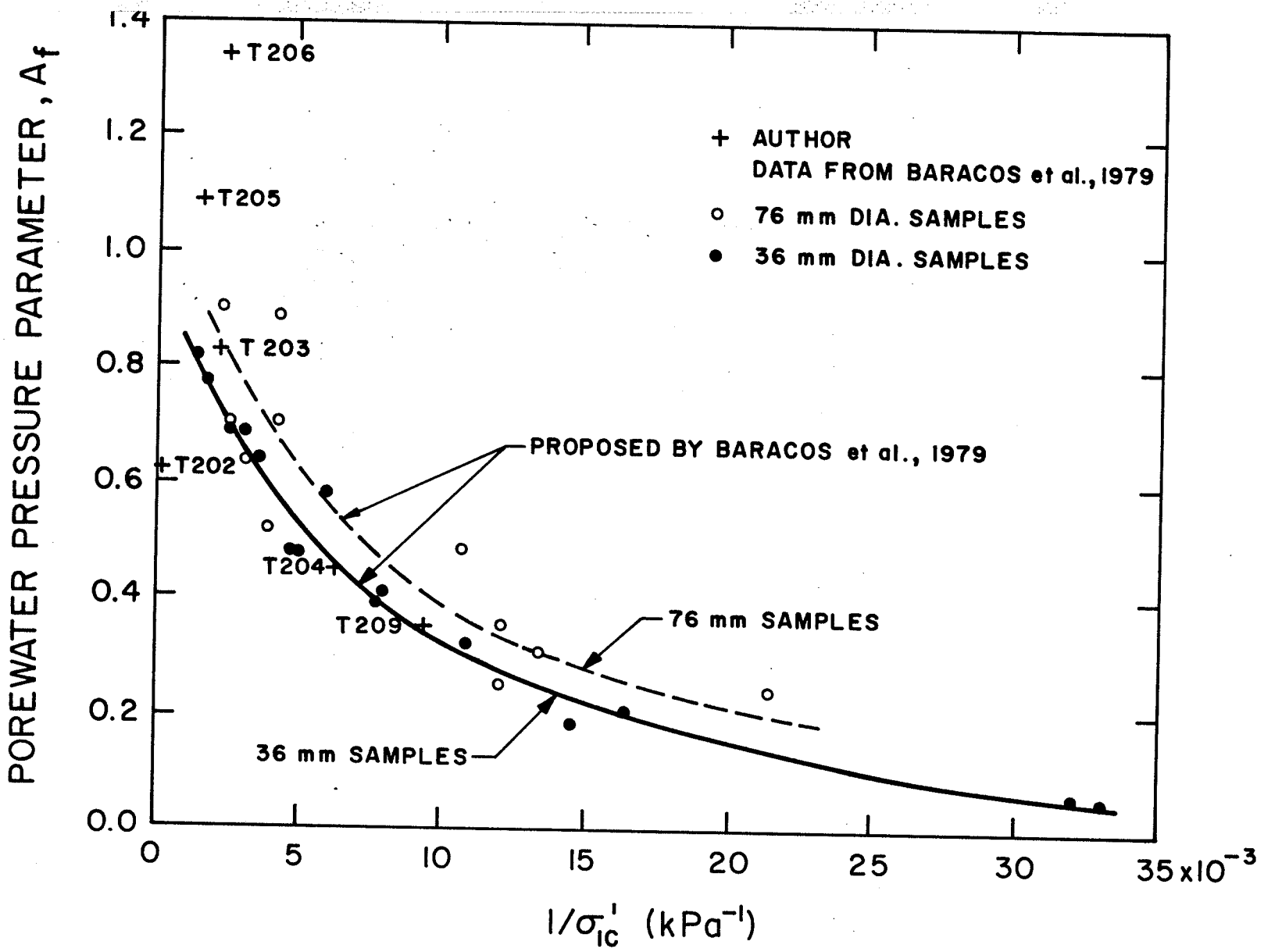

Fig. 3.22. The Relationship Between Porewater Pressure Parameter and Consolidation Pressure

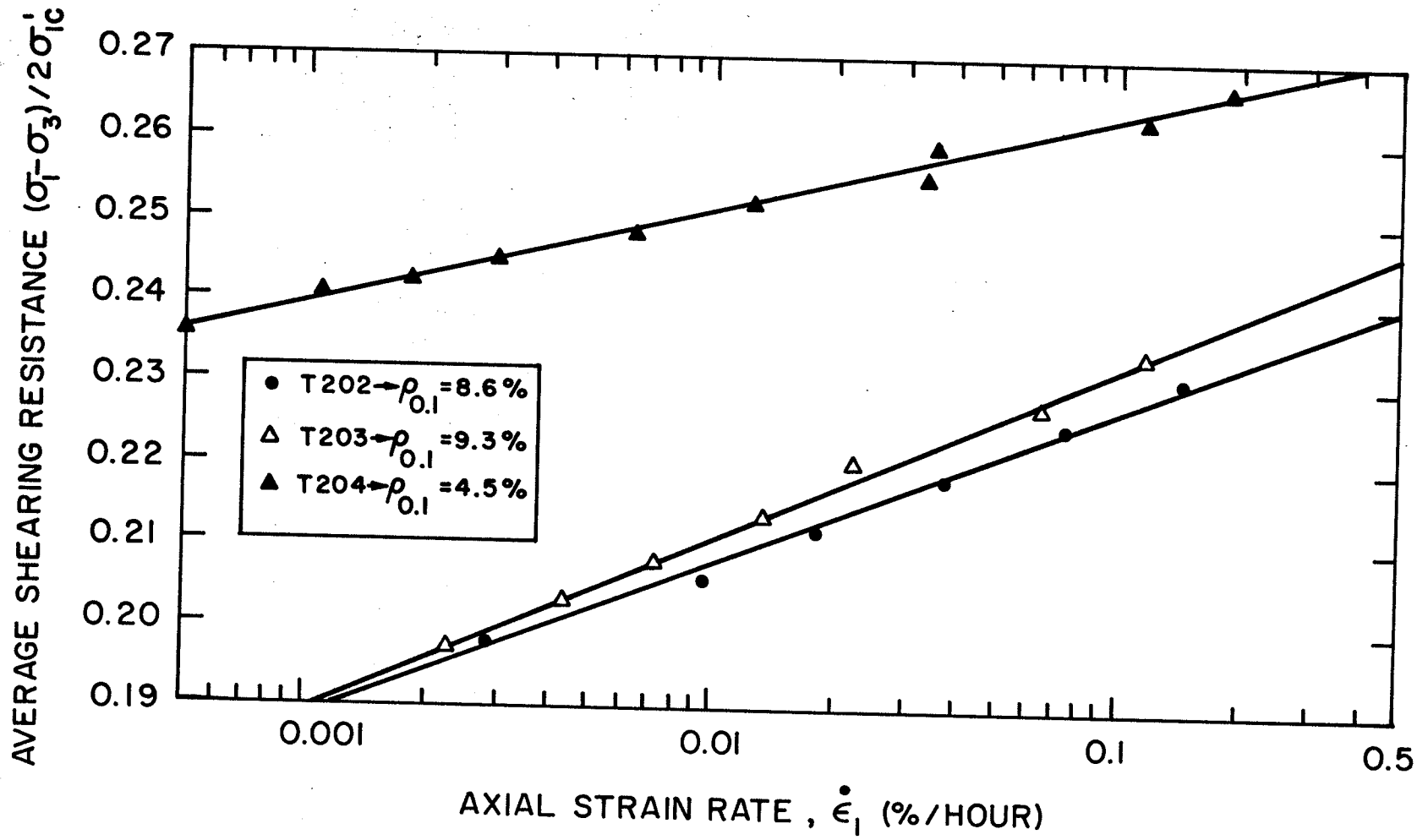

Fig. 3.23. Average Strain Rate Effect from Relaxation Tests for Test Series : T 201 TO T 204

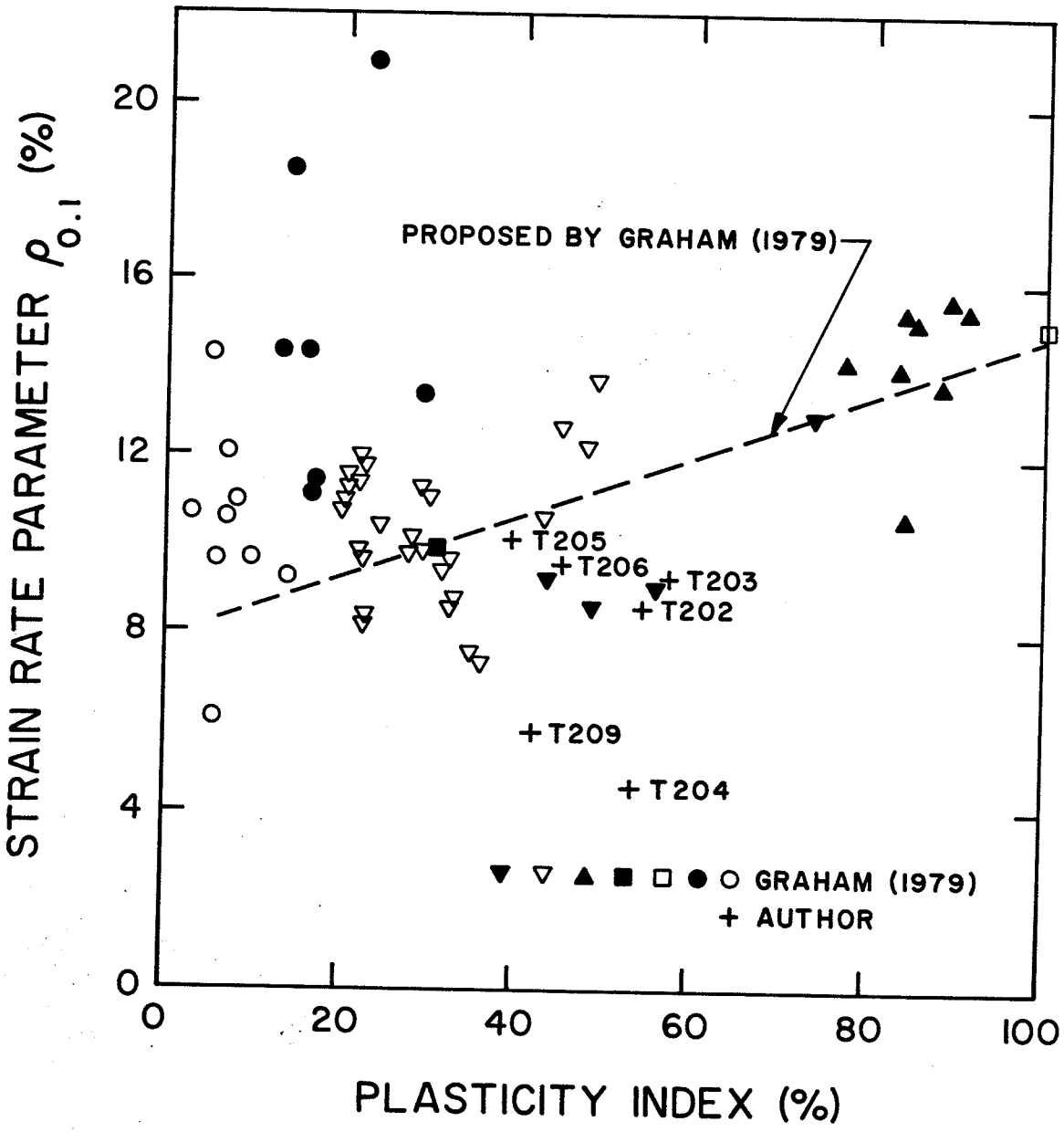

Fig. 3.24. The Relationship Between Strain Rate and Plasticity Index

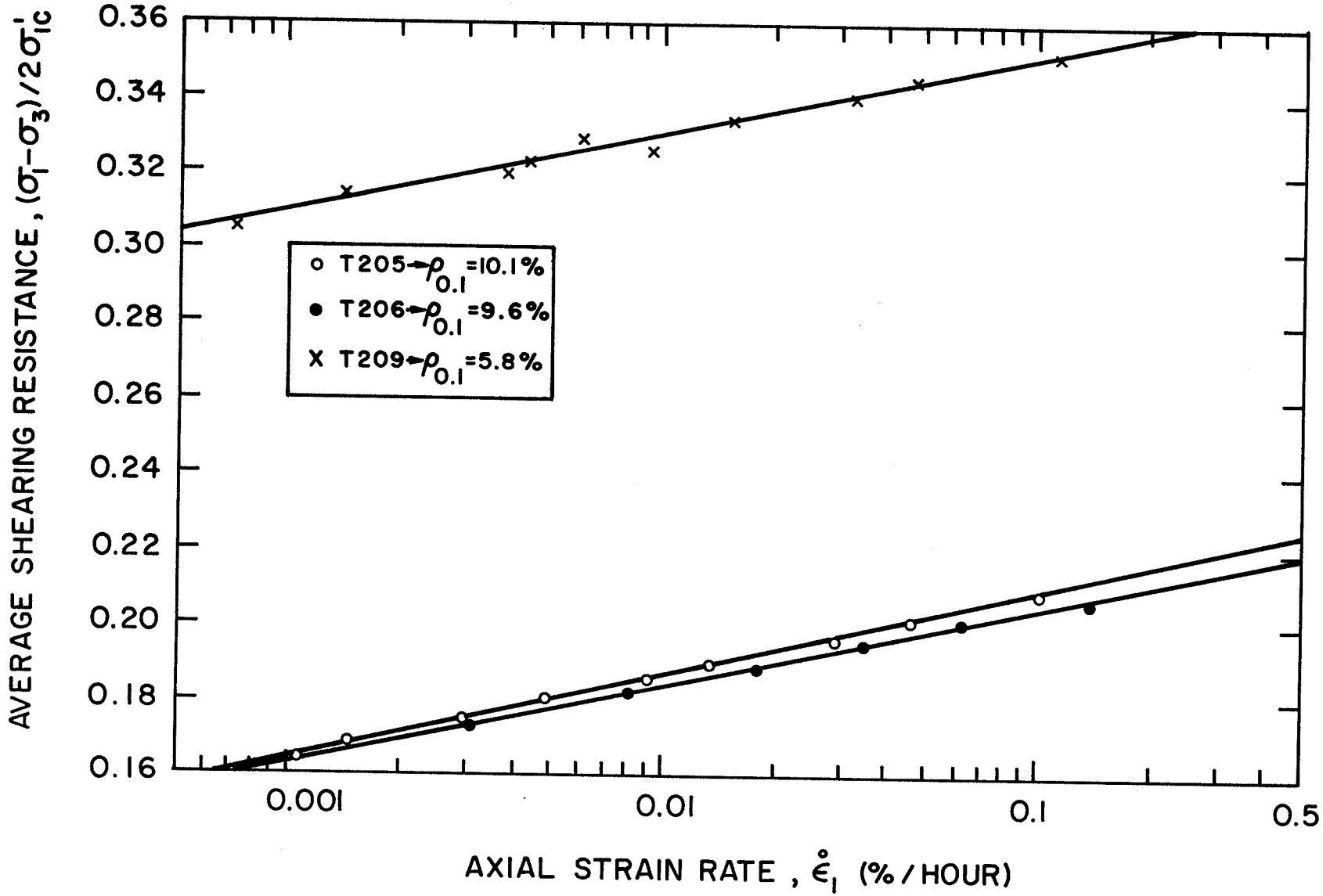

Fig. 3.25. Average Strain Rate Effect from Relaxation Tests for Test Series : T205 TO 209

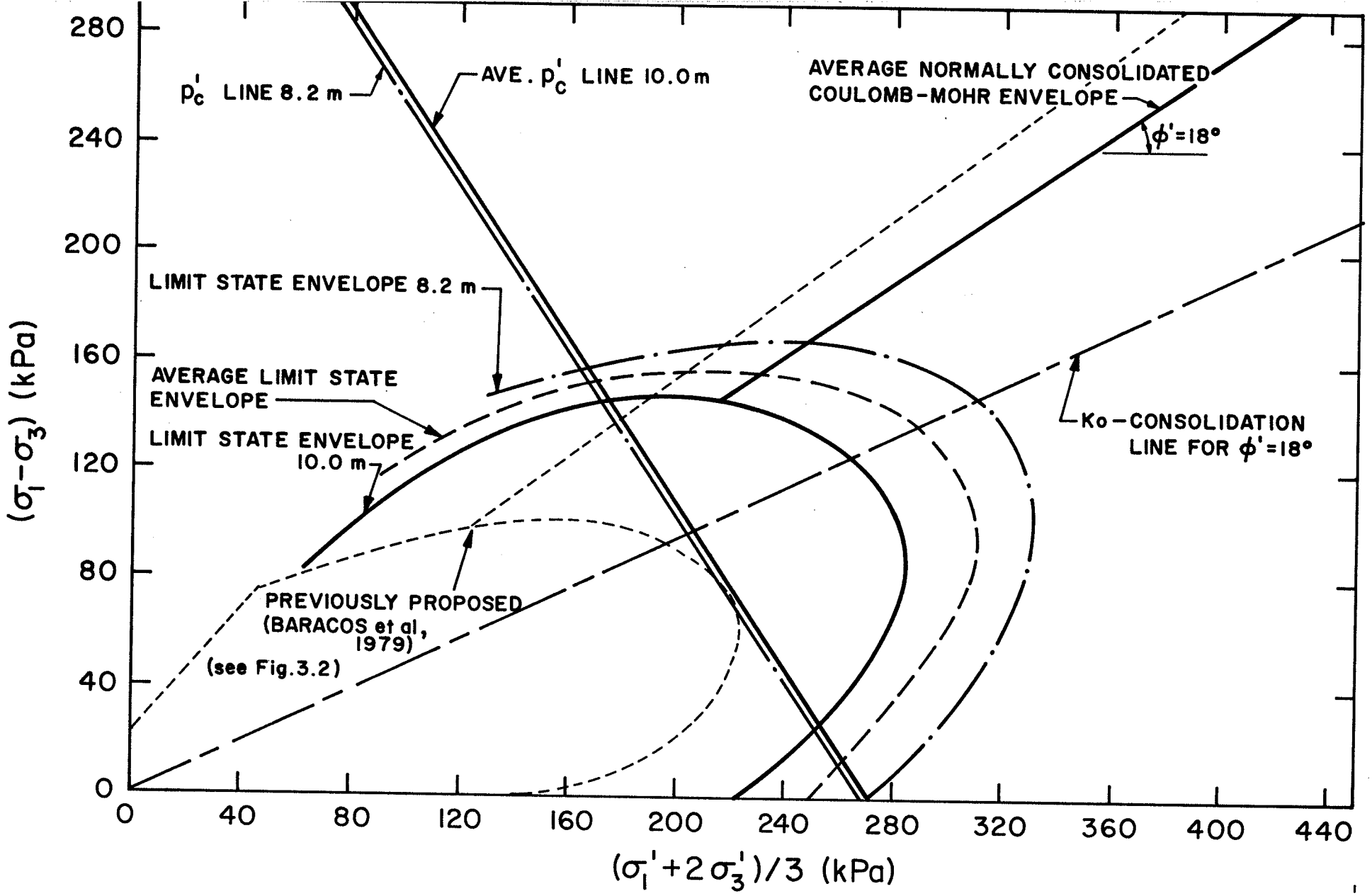

Fig. 4.1. Summary of Limit State and Oedometer Data

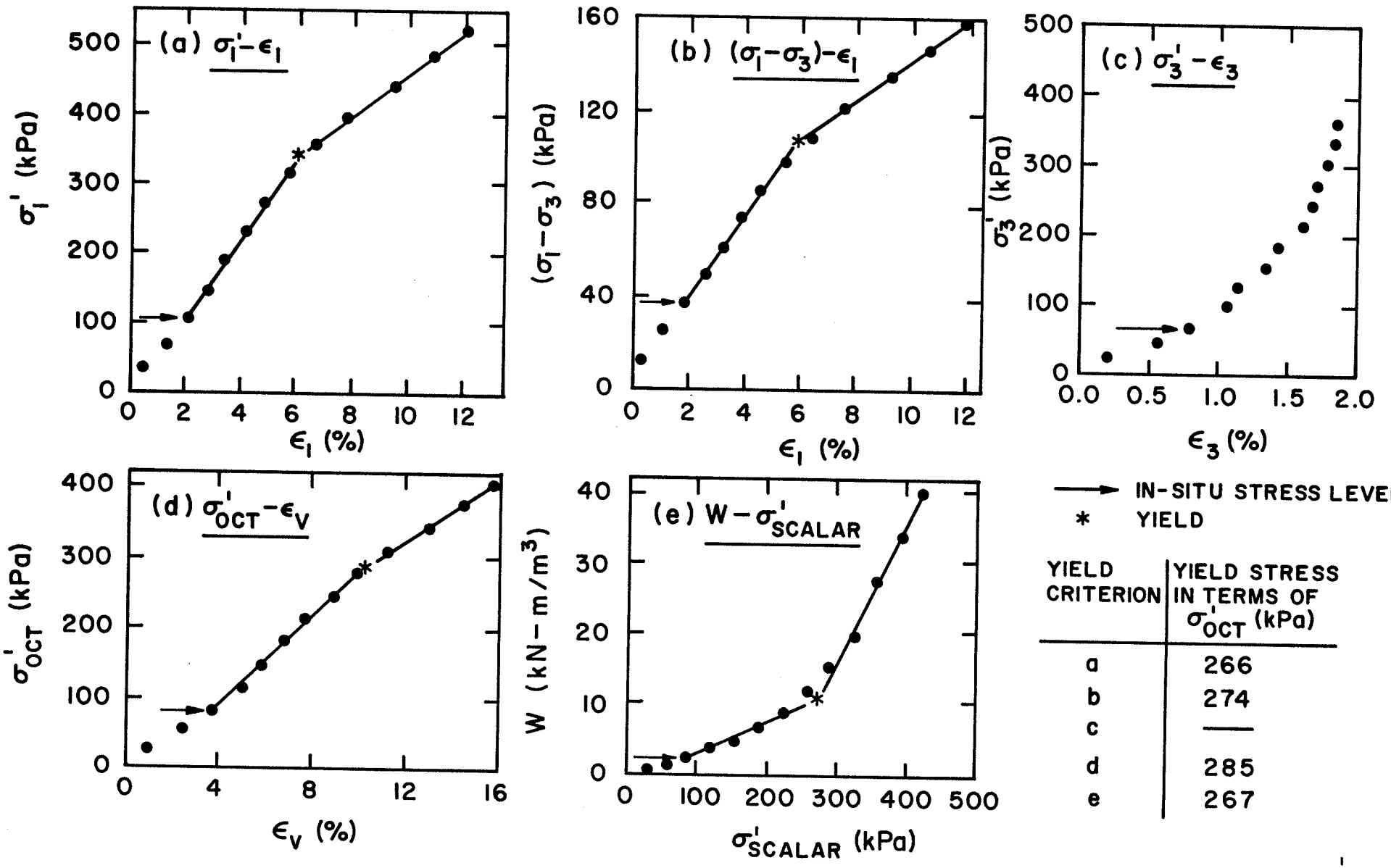

YIELD CRITERION	YIELD STRESS IN TERMS OF σ_{OCT}' (kPa)
a	266
b	274
c	—
d	285
e	267

Fig. 4.2. Yield Stresses by Different Yield Criteria – T206

BIBLIOGRAPHY

The following bibliography contains publications which are not referred to directly in the text. They are included since they contain background information which the author found useful in the present study.

Atkinson, J.H., and P.L. Bransby. The Mechanics of Soils - An Introduction to Critical State Soil Mechanics. Maidenhead (England): McGraw-Hill Book Co. (UK) Limited, 1978.

Balasubramaniam, A.S., R.P. Brenner, Z. Hasan, and R. Chotivittayathanian. "The Stress-Strain Behavior of Stiff Bangkok Clay". Proceedings, 9th International Conference on Soil Mechanics and Foundation Engineering, Tokyo, Japan, Vol. 1, pp. 31-38.

Baracos, A., J. Graham, and L. Domaschuk. 1979. "Yielding and Rupture in a Lacustrine Clay". Proceedings, 32nd Canadian Geotechnical Conference, Quebec City, Canada, pp. 2.188-2.211.

Bishop, A.W., and D.J. Henkel. The Measurement of Soil Properties in the Triaxial Test. London: Edward Arnold Publishers Ltd., 1962.

Bjerrum, L. 1967. "Engineering Geology of Norwegian Normally Consolidated Marine Clays as Related to Settlements of Buildings". Geotechnique, Vol. 17(2), pp. 83-119.

Bjerrum, L. 1973. "Problems of Soil Mechanics and Construction on Soft Clays and Structurally Unstable Soils (Collapsible, Expansive, and Others)". State-of-the-Art Report, Session 4, Proceedings, 8th International Conference on Soil Mechanics and Foundation Engineering, Moscow, Vol. 3, pp. 111-160.

Bjerrum, L., and T.C. Kenney. 1967. "Effect of Structure on the Shear Behavior of Normally Consolidated Quick Clays". Proceedings, Geotechnical Conference, Oslo, Norway, Vol. 2, pp. 19-27.

Bolton, M. A Guide to Soil Mechanics. London: The MacMillan Press Ltd., 1979.

Bowles, J.F. Engineering Properties of Soils and Their Measurement. Toronto: McGraw-Hill Book Company, 1978.

Brooker, E.W., and H.O. Ireland. 1965. "Earth Pressures at Rest Related to Stress History". Canadian Geotechnical Journal, Vol. 11, No. 1.

Brown, J.D. 1969. "Consolidation and Shear Behavior of Soft Bangkok Clay - Bangkok Siracha Highway". Internal Report F332.2, Norwegian Geotechnical Institute, Oslo, Norway.

Burland, J.B. 1967. "Deformation of Soft Clay". Ph.D. Thesis, Cambridge University, England.

Burland, J.B. 1971. "A Method for Estimating the Pore Pressures and Displacements Beneath Embankments on Soft, Natural Deposits". Proceedings, Roscoe Memorial Symposium on Stress-Strain Behavior of Soils. Ed. R.H.G. Parry. England: Foulis, pp. 505-536.

Campanella, R.G., and Y.P. Vaid. 1974. "Triaxial and Plane Strain Creep Rupture of an Undisturbed Clay". Canadian Geotechnical Journal, Vol. 11, pp. 1-10.

Chen, W.F. Limit Analysis and Soil Plasticity. New York: Elsevier Publishing Co., 1975.

Crawford, C.B. 1964. "Interpretation of the Consolidation Test". ASCE Journal of Soil Mechanics and Foundation Engineering Div., Vol. 90, No. SM5, pp. 87-102.

Crooks, J.H.A. 1973. "Laboratory Studies of Belfast Estuarine Deposits". Ph.D. Thesis, Queen's University of Belfast, Northern Ireland.

Crooks, J.H.A., and J. Graham. 1976. "Geotechnical Properties of the Belfast Estuarine Deposits". Geotechnique, Vol. 26(2), pp. 293-315.

Domaschuk, L. 1977. "Soil Block Sampler". Canadian Geotechnical Journal, Vol. 14, pp. 262-265.

Graham, J. 1969. "Laboratory Results from Mastemyr Quick Clay After Reconsolidation to In-Situ Stresses". Internal Report F372-5, Norwegian Geotechnical Institute, Oslo, Norway.

Graham, J. 1974. "Laboratory Testing of Sensitive Clay from Lyndhurst, Ontario". Civil Engineering Research Report CE 74-2, Royal Military College, Kingston, Ontario.

Graham, J. 1979. "Embankment Stability on Anisotropic Soft Clays". Canadian Geotechnical Journal, Vol. 16, pp. 295-308.

Kenney, T.C. 1966. "Shearing Resistance of Natural Quick Clays". Ph.D. Thesis, University of London.

Kenney, T.C., and D.J. Folkes. 1979. "Mechanical Properties of Soft Soils". State-of-the-Art Report, Session 2, Proceedings, 32nd Canadian Geotechnical Conference, Quebec City, Canada, pp. 1-51.

Ladd, C.C., R. Foott, K. Ishihara, F. Schlosser, and H.G. Poulos. 1977. "Stress-Deformation and Strength Characteristics". State-of-the-Art Report, Session 1, Proceedings, 9th International Conference on S.M.F.E., Tokyo, Vol. 2, pp. 421-494.

Landva, A. 1964. "Equipment for Cutting and Mounting Undisturbed Specimens of Clay in Testing Devices". Norwegian Geotechnical Institute Publications No. 56, Oslo, Norway.

Leonards, G.A., and A.G. Altschaeffl. 1964. "Compressibility of Clay". ASCE Journal of the S.M.F.E. Division, Vol. 90, SM5, pp. 133-155.

Leroueil, S., and F. Tavenas. 1977. "Discussion of "Geotechnical Properties of Belfast Estuarine Deposits"".Geotechnique, Vol. 27(3), pp. 441-446.

Leroueil, S., F. Tavenas, F. Brucy, P. LaRochelle and M. Roy. 1979. "Behavior of Destructured Natural Clays". ASCE Journal of the S.M.F.E. Division, Vol. 105, GT6, pp. 759-778.

Lo, K.Y. 1961. "Secondary Compression of Clays". ASCE Journal of the S.M.F.E. Division, Vol. 87, SM4, pp. 61-87.

McRostie, G.C., K.N. Burn, and R.J. Mitchell. 1972. "The Performance of Tied-Back Sheet Piling in Clay". Canadian Geotechnical Journal, Vol. 9(2), pp. 206-218.

Mitchell, J.K. Fundamentals of Soil Behavior. New York: John Wiley & Sons, Inc., 1976.

Mitchell, R.J. 1970. "On the Yielding and Mechanical Strength of Leda Clays". Canadian Geotechnical Journal, Vol. 7, pp. 297-312.

Ohta, H., and S. Hata. 1971. "On the State Surface of Anisotropically Consolidated Clays". Proceedings, Japan Society of Civil Eng., No. 196, pp. 117-124.

Parry, R.H.G., and S.F. Amerasinghe. 1973. "Components of Deformation in Clays". Proceedings, Symposium on Plasticity and Soil Mechanics. ed. A.C. Palmer. Cambridge, England.

Parry, R.H.G., and V. Nadarajah. 1973. "A Volumetric Yield Locus for Lightly Overconsolidated Clay". Geotechnique, Vol. 23(4), pp. 451-453.

Pietrzak, A.P. 1979. "Geotechnical Properties of Winnipeg Clay". Master of Engineering Project, University of Manitoba, Winnipeg, Manitoba.

Poulos, H.G., and E.H. Davis. Elastic Solutions for Soil and Rock Mechanics. New York: John Wiley & Sons, Inc., 1974.

Render, F.W. 1970. "Geohydrology of the Metropolitan Winnipeg Area As Related to Groundwater Supply and Construction". Canadian Geotechnical Journal, Vol. 7, pp. 243-274.

Roscoe, K.H. 1970. "The Tenth Rankine Lecture: The Influence of Strains in Soil Mechanics". Geotechnique, Vol. 20, pp. 129-170.

Roscoe, K.H., A.N. Schofield, and C.P. Wroth. 1958. "On the Yielding of Soils". Geotechnique, Vol. 8(1), pp. 22-53.

Roscoe, K.H., and J.B. Burland. 1968. "On the Generalized Stress-Strain Behavior of Wet Clay". Engineering Plasticity, ed. J. Weyman and F.A. Leckic. Cambridge University Press, pp. 535-609.

Salah, A.M., and R.J. Krizek. 1976. "At Rest Lateral Earth Pressure of a Consolidating Clay". ASCE Journal of the S.M.F.E. Division, Vol. 102(GT7), pp. 721-738.

Sangrey, D.A. 1972. "Naturally Cemented Sensitive Soils". Geotechnique, Vol. 22(1), pp. 139-152.

Schofield, A.N., and C.P. Wroth. Critical State Soil Mechanics. Maidenhead (England): McGraw-Hill Book Co. (UK) Limited, 1968.

Scott, R.F., Principles of Soil Mechanics. Reading (Mass.): Addison-Wesley Publishing Co., 1963.

Skempton, A.W. 1964. "Long Term Stability of Clay Slopes". Geotechnique. Vol. 14, pp. 77-101.

Tavenas, F. 1979. "The Behavior of Embankments on Clay Foundations". State-of-the-Art Report, Session 3, Proceedings, 32nd Canadian Geotechnical Conference, Quebec City, Canada.

Tavenas, F., and S. Leroueil. 1977. "The Effects of Stresses and Time on Yielding of Clays". Proceedings, 9th International Conference on S.M.F.E., Tokyo, Japan, Vol. 1, pp. 319-326.

Tavenas, F., J-P. Desrosiers, S. Leroueil, P. LaRochelle, and M. Roy. 1978a. "The Use of Strain Energy as a Yield and Creep Criterion for Soft Clays". Geotechnique, Vol. 29, pp. 285-303.

Tavenas, F., S. Leroueil, P. LaRochelle, and M. Roy. 1978b. "Creep Behavior of an Undisturbed Lightly Overconsolidated Clay". Canadian Geotechnical Journal, Vol. 15(3), pp. 402-423.

Trainor, P. 1980. Private Communication.

Vaid, Y.P., and R.G. Campanella. 1974. "Triaxial and Plane Strain Creep Rupture of an Undisturbed Clay". ASCE Journal of the Geotechnical Engineering Division, Vol. 103, GT7, pp. 693-709.

A P P E N D I X A

LABORATORY TECHNIQUES FOR TRIAXIAL TESTING OF UNDISTURBED COHESIVE SOILS

LABORATORY TECHNIQUES FOR TRIAXIAL TESTING OF UNDISTURBED COHESIVE SOILS

INTRODUCTION

The importance of good quality sampling and testing techniques has been emphasized by several investigators (Crooks, 1973; Graham, 1974; Crooks and Graham, 1976; Leroueil and Tavenas, 1977). This is especially true when investigating the concept of a limit state envelope because it is essentially a by-product of the in-situ grain structure of the soil. Any significant disturbance during sampling and testing tends to alter the in-situ structure of the soil and thus its in-situ properties. High quality triaxial testing of undisturbed clay samples requires considerable care during sample preparation and tightly controlled laboratory procedures during reconsolidation and shear.

The procedures and equipment outlined in this appendix are similar to those used by Crooks (1973), but have been modified to conform with the equipment currently available in the University of Manitoba. An important feature of this equipment is that the soil sample is supported at all stages of trimming and building-in. A detailed description of the test equipment and procedures is presented in the following section under the sub-divisions:

A. Equipment Preparation;

B. Sample Trimming and Building-in;

C. Drained Consolidation-Load Increment Procedures;

D. Back-pressuring and Preparation for Undrained Shear;

E. Undrained Shear;

F. Building-out.

A. EQUIPMENT PREPARATION

As in any laboratory testing it is important to have all of the testing apparatus and sample preparation equipment prepared in advance of their being required. This section presents the preliminary preparations prior to trimming and building-in the sample.

1. Collect the sample preparation equipment. This includes:

   a) Trimming and building-in apparatus (see Fig. A.1)

base plate	top loading cap
trimming platform	filter stone holder
cutting cylinder	three-holed clamp
top cap holder	split clamp
membrane stretcher	

   b) Associated equipment

glass plate	silicone oil
wire saw	stopcock
sharp knife	3" diameter rubber o-rings
filter stone	3" diameter rubber membranes
filter paper	

2. All the trimming equipment should be checked for smooth action and lightly oiled with silicone oil. The leading edge and inside surface of the cutting cylinder should be lightly greased also.

3. Check that there are adequate supplies of deaired distilled water. A pressure tank full of deaired, distilled water is required for filling the cell; the tank should be put under vacuum for at least 24 hours to ensure it is adequately deaired. In addition, about 2 litres of deaired, distilled water is required for the drainage leads, the burettes, and flushing purposes.

4. Deair the porous stone the day before the building-in the sample.

5. Prepare the triaxial cell and accompanying equipment. This includes:

   3" rotating bush, triaxial cell: cell base and top;

   3 burettes and a burette stand;

   pressure control equipment and measuring gauges;

   supply of engine oil and small mechanical pump;

   loading hanger and ball bearing;

   dead weights;

   dial gauge;

   piston clamp.

   Note that during most of the testing, cell pressure and back-pressures is supplied by an air line and reducing valve system. This system provides constant pressures up to about 400 kPa. Pressures above this were supplied by a self-compensating mercury pot system. Pressure gauges reading to ± 1.0 psi allow the cell pressure and back-pressure to be applied approximately. Precise control of the pressures is monitored by pressure transducers and a calibrated LED voltmeter. Pressure transducers are attached to one of the cell drainage leads and one of the pedestal drainage leads. These transducers, coupled with the LED voltmeter (i.e. electrical signal conditioner), provide readings of cell pressure and pore pressure to within ± 0.1 kPa.

6. Sometime before beginning each test the pressure transducers and the LED voltmeter are calibrated. The procedure for this calibration is:

a) fill the triaxial cell with deaired water to a level equal to the mid-height of the sample; this becomes the reference point for pressures;

b) open the drainage connection to the cell pressure transducer and pore pressure transducer and turn on the signal conditioner;

c) an air pressure line (from a reducing valve) is attached through a y-connection to both the top of the triaxial cell and a single limb mercury manometer; this enables a known pressure to be applied to the top of the water in the cell (and thus the pressure transducers);

d) a pressure of 39 psi (the maximum capacity of the existing manometer) is applied to the transducer (as measured by the mercury manometer); the span adjustments for both channels of the signal conditioner are then manipulated so that they read this pressure;

e) the air pressure is then reduced to atmospheric pressure (ensure this by opening the relief valve on top of the cell); the signal conditioner reading on both channels are adjusted to read zero by using the separate zero adjustment for each channel;

f) steps (d) and (e) are repeated until the correct pressure readings are found for both channels without further span or zero adjustments; this usually takes two or three repetitions of steps (d) and (e).

The pressure transducers and signal conditioner are now calibrated Daily rezeroing to account for changes in atmospheric pressure during testing is discussed in section C. The signal conditioner should now be left on continuously for the duration of the test.

7. The weight of equipment used in calculating axial stresses due to dead load is determined. These items include: the loading hanger, the loading piston, the ball bearing, the dial gauge, the top loading cap, and the rubber membranes. In addition, the weight and inner diameter of the cutting cylinder are needed.

8. Two moisture content tins are prepared and a large tare is used to hold sample trimmings. These trimmings are used to perform the standard classification tests such as Atterberg limits, specific gravity, and hydrometer grain size analysis.

B. SAMPLE TRIMMING AND BUILDING-IN

This phase begins after all of the preparatory work is completed. The triaxial cell top is off and the trimming equipment is not in place. A roughly cut sample should be ready. The use of the trimming equipment is shown in Fig. A.2. The trimming equipment itself is shown in Fig. A.1.

1. The cell pedestal is deaired by flushing water through the pedestal by means of burettes attached to the pedestal drainage leads; the deairing process is continued until no air bubbles are detected in the water flushing through the pedestal; a suction line is used to suck up the excess water flowing from the top of the pedestal.

2. The base plate of the trimming equipment is placed loosely on the cell base with the sample cutting cylinder in position on the uprights (cutting edge uppermost). The cell plate is adjusted until the cutting cylinder is accurately centered over the pedestal base, and then tightened in place. It should be noted that satisfactory operation of the trimming equipment can only be achieved if this centering process is carried out accurately.

3. The trimming table is attached to the base plate. Prior to placing the roughly trimmed sample on the trimming table, the bottom end is squared off. The sample is then placed centrally on the trimming table so that it lies within the projection of the cutting cylinder for its full length.

4. The cutting cylinder (cutting edge down) is now forced slowly down into the clay to a depth of slightly less than the full length of the cutting edge. The excess clay outside the cutting edge is then removed using a piece of cutting wire (or a sharp knife). Particular attention must be paid to avoid undercutting the leading edge (see Fig. A.2(a)).

5. Using the technique described above, the cutting cylinder is gradually filled with clay as it is pushed in steps towards the trimming table. During this trimming process two moisture content samples (one from near the top and one near the bottom) are taken from the trimmings. The remainder of the trimmings are collected in a tare and are used afterward for standard classi-

fication tests (i.e. Atterberg limits, grain size analysis, and specific gravity).

6. The trimming process continues until approximately 1 cm of clay protrudes from the top of the cutting cylinder. The cutting cylinder is then removed from the uprights, taking care to support the soil in the cylinder, and placed (cutting edge down) on a glass plate. The clay is trimmed flush with the non-cutting edge of the cylinder and the top loading cap is placed on this end. The cylinder is inverted and the loading cap forced approximately 1 cm into the cylinder. The clay is then trimmed flush with the cutting edge of the cylinder.

7. The top loading cap is removed and the cutting cylinder filled with wet clay is weighed. Note that any excess clay on the cutting cylinder must be removed prior to weighing.

8. The cutting cylinder is placed, cutting edge down, on a glass plate. The saturated deaired filter stone is placed in the filter stone holder. The filter stone and its holder are then attached to the top of the cutting cylinder. Care should be taken to ensure that the filter stone remains saturated during this process. The cutting cylinder, full of clay, with the filter stone holder in place, is shown in Fig. A.2(b). A glass plate has been placed under the cutting cylinder.

9. The trimming platform is removed and a meniscus of water is formed on the pedestal. The two pieces of the split clamp are slid to the bottom of the uprights.

10. The cutting cylinder is inverted (filter stone and holder on bottom), placed on the uprights, and slid down the uprights to the pedestal. At this point the filter stone is unclamped from its holder.

11. The top loading cap and its holder are placed on the uprights. The clamp is secured in place on the uprights and the top loading cap is lowered until contact is made with the top of the sample. The top loading cap is secured in this position by tightening the center screw of the clamp.

12. The cutting cylinder and attached filter stone holder are carefully slid up the uprights until they are about 8 cm clear of the top loading cap. They are secured in this position. The split clamp is brought up from the bottom of the uprights and clamped in place just above the loading cap. The sample is then standing on the pedestal base with its top supported (Fig. A.2(c)). The cutting cylinder and the other clamp are removed from the uprights.

13. The height and the diameter of the sample are determined and recorded on data sheet 1 (Fig. A.4). The diameter is taken as the average of measurements taken at the top, middle, and bottom of the sample. Similarly three measurements of the height of the sample are made to compute an average height.

14. A thin coat of silicone stopcock grease is applied to the side of the pedestal and the loading cap.

15. Lateral drains are provided by applying filter strips, approximately 1 cm wide, longitudinally around the circumference of the sample. Care must be taken to ensure that the filter strips overlap the filter stone at the bottom of the sample (Fig. A.2(d)). Note that the filter strips are saturated before being applied to the sample.

16. One rubber membrane is put on the membrane stretcher along with one o-ring at the bottom. The membrane stretcher is then put on the uprights and locked in position above the split clamp. The other clamp is placed on the uprights and is used to lock the top cap in place. This allows the split clamp to be separated and lowered below the sample while the other clamp supports the top loading cap. The membrane stretcher is lowered and the first membrane put over the sample with one o-ring at the bottom. The membrane stretcher is then raised above the sample and locked in place. The split clamp is again slid above the sample and used to lock the top cap. The membrane stretcher and the other clamp are removed from the uprights. After the first membrane is on, water is allowed through the pedestal from one of the pedestal drainage burettes. This allows the region between the membrane and the sample to be saturated. Care should be taken to ensure that most of the air bubles between the sample and the first membrane are eliminated.

17. A layer of silicone oil is applied to the outside of the first membrane. Using the same procedure as in step 16 a second membrane is put over the sample. However, in this case a total of

four additional o-rings are put on the sample. Two are put on the pedestal and two on the loading cap. Care must be taken not to pinch the sample when rolling the sealing rings on to the pedestal and the loading cap. Fig. A.2(e) shows the sample, with the membrane stretcher surrounding it just prior to rolling on the second rubber membrane and the 4 rubber o-rings.

18. After placing the second membrane and its o-rings, the membrane stretcher is secured above the sample so that the split clamp can be brought above the sample and locked in place.

19. The top cap holder screws are removed, allowing the top cap holder, the membrane stretcher, the split clamp and the other clamp to be taken from the uprights. The base plate is then carefully removed, leaving the sample free-standing on the pedestal as shown by Fig. A.2(f).

20. The cell top is fitted on the cell base and screwed down. This is a most critical step because the sample is free-standing and easily disturbed. Care should be taken to ensure that the loading piston is clamped and out of way, and that the bushing drive lines up with the bushing.

21. The loading piston is lowered until contact is made up with the sample. The piston is then locked in place; thus providing support for the sample.

22. The cell is filled with deaired water to a level just above the top cap. At this point a layer of engine oil about 2 to 3 cm

is pumped into the cell through the connection in the top of the cell. After this, filling of the cell through the cell base is continued until some of the engine oil begins to come out the top connection. The cell is now full and a plug is put in this top connection. The pressure in the cell should be very low.

23. Air trapped in the pedestal and drainage leads is now removed by passing water between two burettes attached to the pedestal drainage leads. This is accomplished by establishing a gradient between the two burettes and alternately flushing in one direction or the other. The process is continued until flushing produces no more air bubbles and all air bubbles are removed from the drainage lines.

24. One of the drainage leads from the pedestal is sealed off. The other is left open and the water level in its drainage lead burette is set at midheight of the sample. Additionally, a drainage lead and burette is attached to the cell pressure transducer connection. The water level in this burette is also set at midheight of the sample.

25. The rotating bush drive coupling is attached. The thrust post, which takes any torque imparted to the loading piston by the rotating bush, and the torque arm are put in place. Care must be taken to ensure that torque arm and thrust post are in contact and that the direction of the rotation of the bushing has been accounted for.

26. The vertical dial gauge is put in place. Its placement should facilitate its reading during loading and must accommodate the loading hanger when in place.

27. The ball bearing and loading hanger are placed in position on top of the loading piston.

The sample is now ready for its first load increment. Prior to this it is advisable to clean the trimming equipment and set it aside. Fig. A.3 shows the triaxial set-up.

C. DRAINED CONSOLIDATION - LOAD INCREMENT PROCEDURES

1. In calculating the first load increment for the sample the dead load contribution, W_o, to the stress at the midheight of the sample is required. This calculation is completed on data sheet 1 (Fig. A.4).

2. The initial volume, V_o, of the sample, its initial height, H_o, and initial cross-sectional area, A_o, are established on the basis of the measurements taken while building-in the sample. These values, along with the dead load value W_o, are transferred to data sheet 2 (the standard data collection sheet for the drained portion of the test) shown in Fig. A.5.

3. The desired stresses for the first loading increment are transferred to the data sheet. The axial loading required to give the correct value of σ_1' from the selected σ_3' is calculated by the relationship:

$$\sigma_1' = \sigma_3'(1 - \frac{a}{A}) + \frac{W_o + P}{A}$$

where

a = piston area

A = instantaneous sample cross-sectional area = $\frac{V}{H}$

W_o = dead loading described above

P = extra loading on hanger.

4. Prior to applying the first loading increment the following items should be checked. Only one of the drainage leads from the pedestal should be open. The water level in the burette from this lead is set at the midheight of the sample and the burette reading is noted. The axial displacement gauge should be set and the initial reading recorded. Both of the pressure transducers should be reading approximately zero pressure. The loading piston is unclamped at this point and the rotating bushing turned on.

5. At a convenient time, the axial and cell pressures are applied. The cell pressure should be applied first, followed as quickly as possible by placement of the dead weights on the hanger. Dial gauge and burette readings are then taken with time to monitor the consolidation of the sample. The most complete set of readings are achieved if the standard 'doubling' of time intervals is used (i.e. 1 min, 2 min, 4 min, 8 min, 15 min, 30 min, 1 h, 2 h, 4 h, etc.). The readings are recorded on a data sheet similar to Fig. A.5 and may then be plotted against the log of time to monitor the axial and volumetric straining of the sample.

6. Subsequent load increments are usually applied at 24 hour intervals. The most convenient time is as early as possible in the morning because it allows a complete set of dial gauge and burette readings to be taken in a standard working day. The daily loading procedure is summarized in the following steps:

Daily Loading Procedures:

a) The time, burette reading, and dial gauge reading are recorded.

b) A known volume of water is flushed through the sample drainage system using the second burette attached to the other pedestal drainage lead. This enables the volume of any air in the cell base to be determined and noted. On this basis, volume changes due to the explusion of water from the sample, can be determined. This is particularly important when dealing with organic clays which can produce gas and thus misleading burette readings.

c) Having flushed the drainage system, the second drainage lead is again closed and the other, being used to measure volume change, is reset such that its water level is at midheight of the sample.

d) Due to changes in atmospheric pressure the pressure transducers should be rezeroed every day before applying a new load increment. This is accomplished by closing the drainage leads of the triaxial cell on the cell side of the two pressure transducers. A head of water equal to the midheight of the sample is then applied to the transducers using a burette.

The digital readings for the two channels of the signal conditioner are noted and then reset to zero using the zero adjustments. The drainage leads at the cell are again re-opened and the actual cell pressure is then recorded.

e) The final stresses for the loading increment are established. First the height and volume of the sample at the end of the increment are calculated on the basis of the change in dial gauge reading and the change in burette reading. The final cross-sectional area of the sample is found by dividing the sample volume by its height. Knowing the cell pressure, the final axial stress is calculated from the equation:

$$\sigma_1' = \sigma_3'(1 - \frac{a}{A}) + \frac{W_o + P}{A} \quad .$$

f) The next set of stresses along the desired stress path are determined. Using the equation above, the necessary additional dead load is calculated and the procedures listed in step 5 of this section are again followed.

7. These procedures are followed as the sample is consolidated along its predetermined stress path.

D. BACK-PRESSURING AND PREPARATION FOR UNDRAINED SHEAR

If the sample has not failed during the drained stress-controlled portion of the test, it is put into undrained shear. The following section describes the steps necessary to move the sample from the stress-controlled, triaxial consolidation set-up in Fig. A.3 to a

strain-controlled compression frame for undrained shearing. The back-pressuring procedure whereby the cell pressure and porewater pressure are simultaneously raised to dissolve any unwanted air in the porewater, is also described.

1. The daily loading procedures, outlined in section C6, are followed to the point of calculating the final stresses on the sample due to the previous day's load increment.

2. A strain-controlled compression frame with a suitable proving ring or load cell is readied and brought in close proximity to the stress-controlled set-up.

3. The axial load on the proving ring necessary to replace the dead load on the sample from the hanger and dead weights is calculated. This calculation is performed using the data sheet in Fig. A.6. In addition, the change in proving ring reading caused by a 6.9 kPa change in cell pressure acting on the loading piston area is calculated.

4. Preparations are made to transfer the triaxial cell from the set-up in Fig. A.3 to the strain-controlled compression frame. First, the compression frame is moved as close as possible to the stress-controlled set-up. The rotating bush motor is turned off and the bushing connection is uncoupled. The loading piston is clamped in place and the hanger and dead weights removed. All of the cell's drainage leads are closed. The final effective stresses on the sample are maintained by the clamped loading piston, and the cell and porewater pressures existing on the sample prior to closing the drainage leads. The time, axial dial gauge reading,

cell pressure, and pore pressure are all recorded at this stage (Fig. A.6).

5. All burettes are closed off and disconnected.

6. The cell is then transferred to the compression frame. This should be done with the cell pressure and porewater pressure transducers still connected to the signal conditioner. The necessity of turning off the signal conditioner is thus avoided.

7. Once the cell is transferred to the compression frame, the effective stresses which existed in the drained stress-controlled set-up are re-established. The cell pressure is reconnected and the correct pressure is reapplied using the cell pressure reducing valve. The burettes are reattached and the pedestal drainage is reopened. Care should be taken when reconnecting the burettes so that no air is introduced into the system. The level of the water in the burettes is reset to the midheight of the sample. The rotating bush drive is reattached to the bushing. The proving ring is then brought in contact with the loading piston using the strain-controlled compression machine's fine feed adjustment. The proving ring reading necessary to reintroduce the final axial stress (calculated in step 3) is slowly applied. The load piston is then unclamped and the bush motor is reactivated. At this point the following information is noted on Fig. A.6: time, axial dial gauge reading, proving ring reading, sample drainage burette, cell pressure, and pore pressure. The effective stresses on the sample have now been reestablished in the

strain-controlled set-up. No major axial or volume displacements should be observed at this stage.

8. Prior to proceeding with back-pressuring, the sample drainage system should be flushed to remove any air introduced by re-attaching the burettes. In addition, it is prudent to again rezero the pressure transducers.

9. The sample is ready for back-pressuring. The cover is placed on the back-pressure burette and air pressure supply is attached to the burette. Note that this may produce a small reading on the porewater pressure transducer. However, the transducer should not be rezeroed.

10. The back-pressure is usually from 20 to 30 psi (138 to 207 kPa) and is applied in four intervals to ensure that no sudden changes in effective stress occur. Initially the first quarter of the back-pressure is applied to the back-pressure burette. Simultaneously the cell pressure is increased by the same increment and the proving ring reading is increased by an amount equal to the upward force from the cell pressure increment. The cell pressure, pore pressure, proving ring, back-pressure burette, and axial dial gauge readings are all recorded. This process is continued in intervals until the full back-pressure has been applied.

11. The next step is to check that the sample is adequately saturated for undrained shearing. This is accomplished with a 'B' test. First the back-pressure burette is closed-off. The cell pressure

is increased by 5 psi (34.5 kPa) and a corresponding compensatory loading is applied to the proving ring. The pore pressure change accompanying the increase in cell pressure is monitored for a period of up to 30 minutes. The readings are recorded in Fig. A.6. The value is calculated from: $B = \Delta u/\Delta\sigma_3$.

12. If B is greater than 98 percent, the sample is ready for undrained shearing. For a B value less than this, the sample should be allowed to sit overnight under full back-pressure. Another B test is done in the morning. If this is still unsatisfactory, further flushing and back-pressuring may be necessary.

13. At the completion of the initial part of B test the cell pressure and proving ring readings should be reset to their values prior to the test. The porewater pressure during this phase is also monitored for a period of about 30 minutes. This reduction in cell pressure provides for the calculation of another B value.

14. After completing the B test and prior to starting undrained shear, the porewater pressure should be allowed to stabilize under full back-pressure for a period. If the porewater pressure reading changes significantly after closing the back-pressure burette, excess porewater pressures from the B test still exist in the sample. It should be allowed to sit until closing of the burette causes no such changes. The sample is then ready for undrained shear.

E. UNDRAINED SHEARING

1. Before shearing, the desired strain rate is set on the compression machine. A rate of approximately 1 percent per hour is acceptable for most tests. Care should be taken to ensure that the proper combination of gears have been chosen to produce the desired strain rate.

2. When ready to shear, the back-pressure burette is closed and the compression machine is turned on. Readings of axial dial gauge, proving ring, cell pressure, and pore pressure are taken with time. These are taken every 10 minutes for the first hour and at 20 minute intervals thereafter. The readings are recorded on the data sheet shown in Fig. A.7.

3. After reaching a peak proving ring reading, the sample is strained for another 2 to 3 percent of axial strain. The compression machine is then switched off to carry out a relaxation test to estimate strain rate effects. This consists of taking readings of proving ring and axial dial gauge with time. After switching off, the time interval for these readings is as follows: 15 s, 30 s, 1 min, 2 min, 4 min, 8 min, 15 min, 30 min, 1 hr, etc. The minimum switched-off period which gives a useful range of strain rates is about 1 hour. However it was often convenient to leave the motor off overnight. Note that pore-water pressures do not usually change significantly during this process. Dial gauge and proving ring readings should be interpolated to 0.1

4. If the test is left overnight, shearing is recommenced in the morning. At this point the sample is sheared to large strains (up to 20 percent) with readings taken at 1/2 hour intervals.

F. BUILDING-OUT

Although the test might now normally be considered finished, considerable care must still be exercised so that an accurate determination of the final moisture content of the sample can be made. This determination allows the compatibility of the initial moisture content, the drainage volume during consolidation, and the final moisture content to be checked.

1. The compression machine drive is switched-off and the proving ring reading is reduced to zero. The sample drainage connections should be closed at this point. The drainage fitting is put in the top of the cell.
2. The engine oil still in the cell is forced out of the top of the cell and collected for separation and reuse.
3. The cell is drained through the cell connection to the water tank.
4. The cell drainage leads are closed at the cell base and the burettes are detached. The electrical connections from the signal conditioner to the pressure transducers are uncoupled. The loading piston is clamped in place such that it supports the top of the sample.
5. The triaxial cell is then moved from the compression frame to a

more convenient location for cleaning and sample removal. The cell top is removed.

6. The lower sealing o-rings are rolled down the pedestal and the lower portion of the rubber membranes is pulled up to bring the pressure inside the sample to atmospheric. The top o-rings are removed from the loading cap.

7. The rubber membranes are slid to the bottom of the pedestal. This allows the removal of the sample from the pedestal with the loading cap and filter stone still in place.

8. The lateral drainage filter strips are removed. This is facilitated by using a hypodermic needle filled with water to saturate them prior to their removal.

9. The filter stone and top loading cap are removed from the sample.

10. A moisture content determination is made from the sample. Depending on its future use, the remainder of the sample is then stored in an appropriate manner.

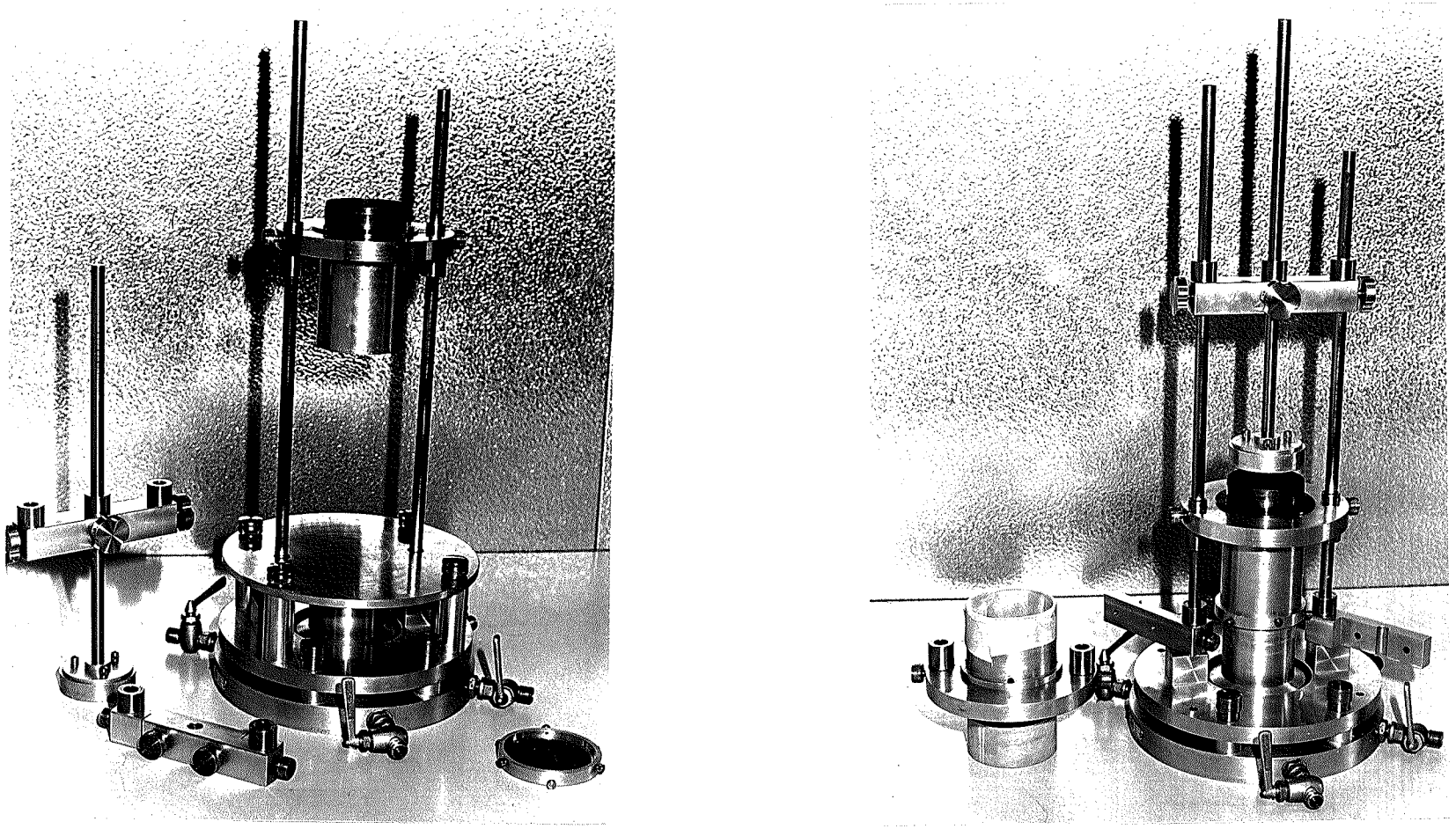

FIG. A.1 TRIMMING AND BUILDING-IN EQUIPMENT

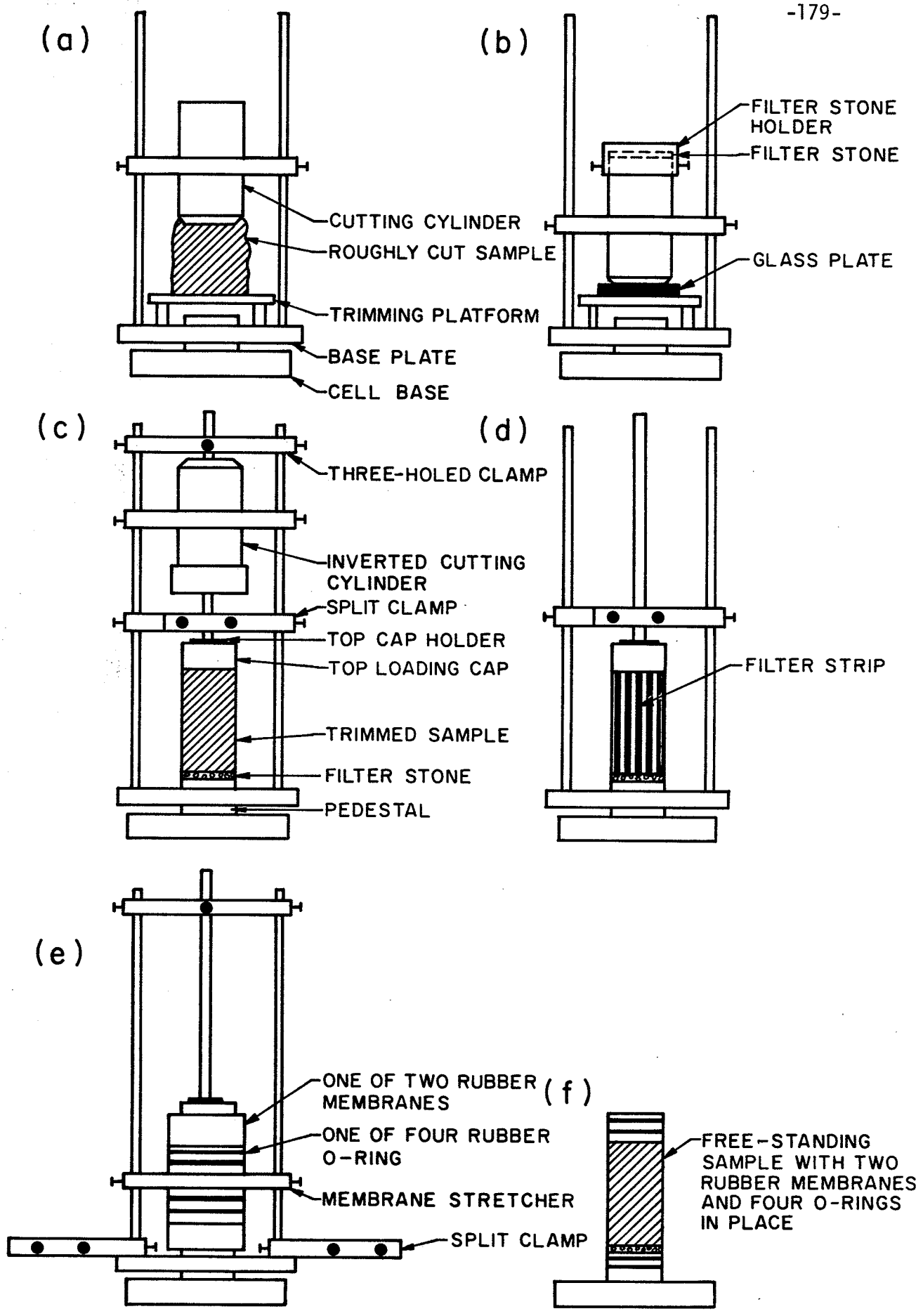

Fig. A.2. Use of Trimming Equipment

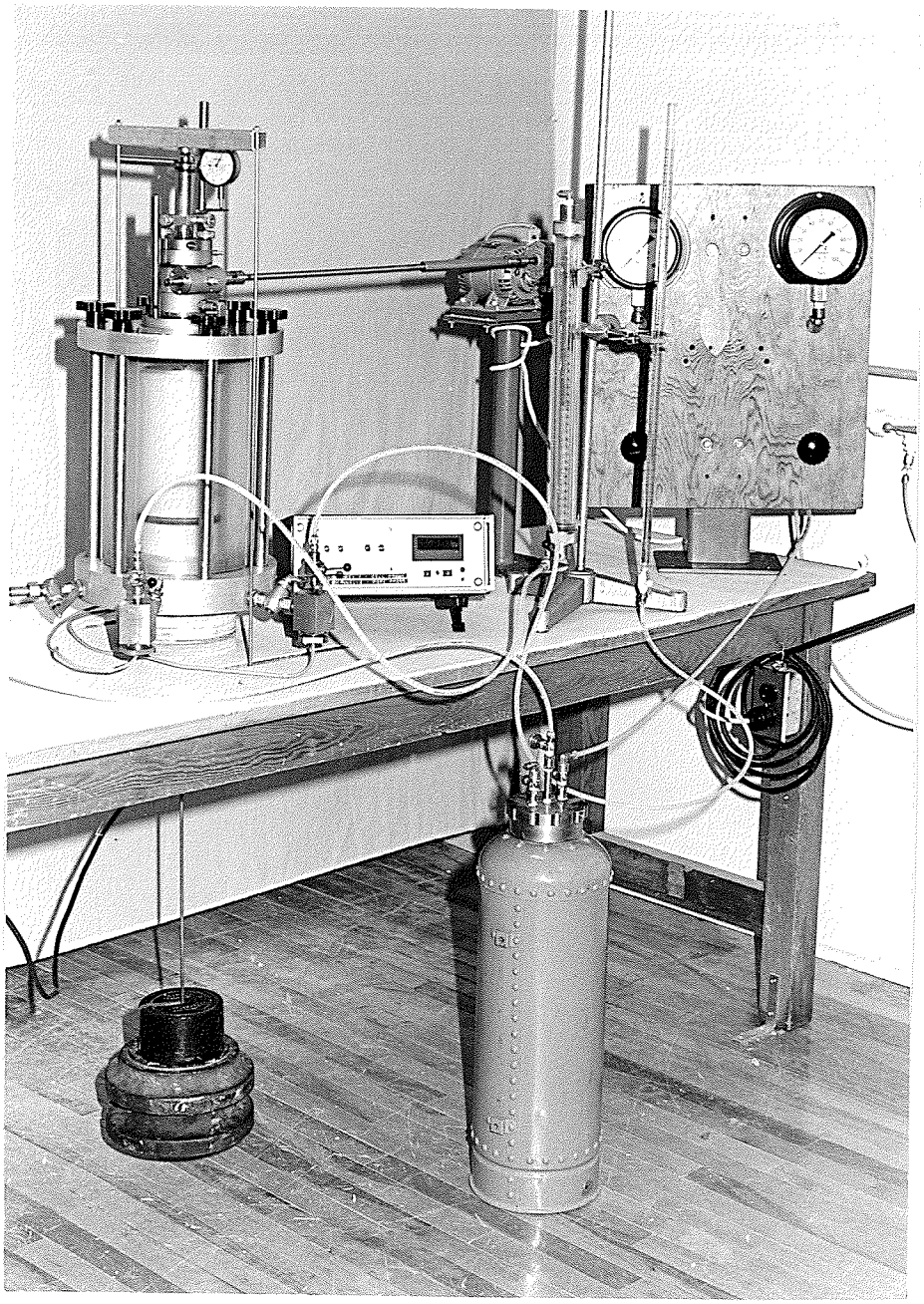

FIG. A.3 TRIAXIAL SET-UP DURING DRAINED STRESS CONTROLLED TESTING

Sheet 1

TRIAXIAL TEST

Test No:_____ Date:_____

Test Type:_____ Tested By:_____

Sample Identification: BH Sample No:____ Depth: _____ ft. M.

Sample Description:_____

_____

TEST SAMPLE DIMENSIONS AND UNIT WEIGHT DETERMINATION

Diameter of test sample,	D_o =	ins.	cms.
Height of test sample,	H_o =	ins.	cms.
Volume of test sample,	V_o =	in^3	cc.

Weight of test sample + cutting ring	=	gms.
Weight of cutting ring	=	gms.
Weight of test sample W_o	=	gms.
Wet Unit Weight $= W_o/V_o$	=	

DETERMINATION OF W_o

Downward Force, F_D		
Weight of hanger	=	gms.
Weight of piston	=	gms.
Weight of ball	=	gms.
Weight of dial gauge	=	gms.
Weight of top cap	=	gms.
Weight of ½ test sample	=	gms.
Weight of ½ membrane	=	gms.
TOTAL F_D	=	gms.

Upward Force, $F_U = A_o h_m^* \gamma_w = 0.7854 D_o^2 h_m^* \gamma_w$ = gms.

Net load at mid-height of test sample,
$W_o = F_D - F_v$ = gms.

Remarks: $^*h_m$ = Distance between the top of the sample and mid-height of sample.

FIG. A.4 - DATA SHEET FOR BUILDING-IN SAMPLE

TRIAXIAL CONSOLIDATION.

SAMPLE NO ..... TEST TYPE ..... SHEET NO.
LOCATION. .... CONST. LOAD .....
$1\,cm^3 = 0{,}061\,in^3$ $1\,LB/in^2 \equiv 5{,}61\,cm\,Hg$ ..... PISTON AREA .....

DATE	TIME	TOTAL AXIAL LOAD (INC W_b)	AXIAL G. READING ( )	Δh_c ( )	$(1-\%_A)$	$\sigma_3(1-\%_A)$	WEIGHT TERM P/A	HEIGHT = ($-\Delta h$)	VOLUME = ($-\Delta v$)	AREA = V/H	BURETTE (cm^3)	ΔV = VOL WATER EXPELLED		σ_3	σ_1	σ_3/σ_1

FIG. A.5 - DATA SHEET FOR RECORDING LOAD INCREMENT DATA

BACK PRESSURE APPLICATION

SAMPLE _____ TEST TYPE _____ SHEET NO ____

LOCATION _____ DATE _____

CHECK CONSOLIDATION WEIGHTS: CORRECT ☐ INCORRECT, WT= ☐

W_o DURING CONSOLIDATION _____
REMOVE HANGER WT. _____ P.RING FACTOR ☐
W_o DURING SHEAR _____ (LB/DIV; kg/DIV)

TOTAL AXIAL LOAD (END OF CONSOLIDATION) _____
AXIAL LOAD – SHEAR W_o (LB or kg) _____ ≡ P.RING DIV. ____

PISTON AREA _____ (IN^2) CELL PRESSURE INCREASE OF 1 psi PRODUCES LOAD ON RING = ____ LB ≡ ____ DIV.

WHEN MOVED TO COMP. FRAME,
ZERO TRANSDUCERS: CELL PRESSURE ____ → ____ : ____ → ____
PORE PRESSURE ____ → ____

DATE	TIME	ACTIVITY	AXIAL DIAL GAUGE	PROVING RING	BURET	CELL PRESSURE	PORE PRESSURE
____	___	END OF CONSOLIDATION	_____		____	____	____
	____	CLAMP PISTON	____				
		MOVE TO COMP. FRAME; SET					
	____	P.RING; UNCLAMP.	____	____	____	____	____
	____	PLUS 1/4 x BACK PRESS. 5-7.5 psi	____	____	____	____	____
	____	" 2/4 " "	____	____	____	____	____
	____	" 3/4 " "	____	____	____	____	____
	____	" 4/4 " " 20-30 psi	____	____	____	____	____

CHECK SATURATION CLOSE OFF BURET. INCREASE $\Delta\sigma_3$ ABOUT 5 psi AND INCREMENT P.RING APPROPRIATELY. READ Δu. $B = \Delta u/\Delta\sigma_3$

DATE	TIME	CELL PRESS	PORE PRESS	AXIAL D.G	P.RING	$B = \Delta u/\Delta\sigma_3$
____	____	_____	_____	____	____	____
____	____	_____	_____	____	____	____
____	____	_____	_____	____	____	____
____	____	_____	_____	____	____	____
____	____	_____	_____	____	____	____
____	____	_____	_____	_____	____	____

FIG. A.6 - DATA SHEET FOR TRANSFER OF SAMPLE TO STRAIN-CONTROLLED COMPRESSION FRAME, BACK-PRESSURING, AND B TEST

UNDRAINED SHEAR

SAMPLE _____ TEST TYPE ____ SHEET NO ____

LOCATION _____ DATE _____

PROVING RING NO. _____ PROVING RING FACTOR ____ LB/DIV
KG/DIV

TESTING RATE _____ IN/MIN MM/MIN %/HR
_____ GEAR BOX (LETTER, DRIVER/DRIVEN,
FOR EXAMPLE D, 54/36)

ZERO TRANSDUCERS: CELL PRESSURE ____ → ____ : ____ → ____
PORE PRESSURE ____ → ____

DATE	TIME	AXIAL DIAL GAUGE	PROVING RING	CELL PRESSURE	PORE PRESSURE	NOTES

FIG. A.7 - DATA SHEET FOR UNDRAINED SHEAR

A P P E N D I X B

STRESS CONTROLLED DRAINED TEST RESULTS

TABLE B.1 STRESS CONTROLLED DRAINED RESULTS - TEST T20I

Stress Level	Load Duration (h)	σ_1' (kPa)	σ_3' (kPa)	σ_{oct}' (kPa)	$(\sigma_1-\sigma_3)$ (kPa)	σ_3'/σ_1'	ε_1 (%)	ε_v (%)	ε_3† (%)	A (cm^2)	W ($kN-m/m^3$)
1	17	45.0	29.3	34.5	15.7	0.651	0.40	0.34	-0.03	45.01	0.08
2	28	64.7	42.1	49.6	22.6	0.651	0.84	0.91	0.04	45.16	0.37
3*	46	91.3	59.2	69.9	32.2	0.648	1.37	1.63	0.13	45.06	0.88
4	20	112.9	70.1	84.4	42.8	0.621	1.76	2.12	0.18	45.03	1.34
5	23	135.3	81.6	99.5	53.8	0.603	2.25	2.67	0.21	45.01	1.99
6	23	156.2	91.8	113.3	64.4	0.587	2.69	3.15	0.23	44.98	2.67
7	24	178.7	103.1	128.3	75.6	0.577	3.13	3.61	0.24	44.98	3.43
8	23	199.9	113.5	142.3	86.4	0.568	3.57	4.06	0.25	44.97	4.27
9	25	222.4	124.8	157.3	97.6	0.561	4.01	4.42	0.21	45.01	5.12
10	25	243.5	135.3	171.3	108.2	0.555	4.41	4.83	0.21	45.00	6.05
11	22	265.8	146.2	186.1	119.6	0.550	4.82	5.16	0.17	45.04	6.98
12	23	287.8	157.2	200.7	130.6	0.546	5.35	5.57	0.11	45.07	8.26
13	24	309.3	167.7	214.9	141.6	0.542	5.80	5.92	0.06	45.14	9.44
14	24	331.3	178.7	229.6	154.4	0.539	6.41	6.43	0.01	45.19	11.23
15	22	350.8	189.5	243.3	161.2	0.540	7.13	6.92	-0.11	45.31	13.24
16	24	374.1	200.8	258.5	173.4	0.537	8.63	7.73	-0.45	45.65	17.35
17	26	393.8	211.5	272.3	182.3	0.537	11.49	8.86	-1.32	46.55	24.74
18***	8	411.9	221.7	285.1	190.2	0.538	15.35	9.83	-2.76	48.17	33.18

* Approximate in-situ stresses

*** Sample failed in drained shear during this increment; results shown are calculated from the last set of readings and are assumed to represent the failure condition

† Calculated from: $\varepsilon_3 = (\varepsilon_v-\varepsilon_1)/2$

TABLE B.2 STRESS CONTROLLED DRAINED RESULTS - TEST T202

Stress Level	Load Duration (h)	σ_1' (kPa)	σ_3' (kPa)	σ'_{oct} (kPa)	$(\sigma_1'-\sigma_3')$ (kPa)	σ_3/σ_1	ε_1 (%)	ε_v (%)	ε_3 † (%)	A (cm^2)	W ($kN-m/m^3$)
1	21	44.9	29.2	34.4	15.8	0.650	0.34	0.68	0.17	44.88	0.13
2	23	65.0	42.3	49.9	22.8	0.650	0.74	1.13	0.20	44.79	0.37
3*	23	91.0	59.2	69.8	31.8	0.650	1.25	1.91	0.33	44.66	0.90
4	20	116.8	75.8	89.5	41.0	0.649	1.74	2.60	0.43	44.57	1.54
5	23	147.2	94.2	111.9	53.0	0.640	2.30	3.35	0.52	44.48	2.43
6	24	176.3	112.2	133.6	64.2	0.636	2.76	3.99	0.62	44.40	3.38
7	23	204.0	129.8	154.5	74.2	0.636	3.22	4.56	0.67	44.34	4.38
8	23	232.3	147.4	175.7	85.0	0.635	3.68	5.16	0.74	44.27	5.57
9	25	260.7	165.3	197.1	95.4	0.634	4.08	5.62	0.77	44.24	6.66
10	24	288.9	182.9	218.2	106.0	0.633	4.56	6.17	0.81	44.20	8.12
11	22	316.9	200.3	239.2	116.6	0.632	4.98	6.61	0.82	44.19	9.43
12	23	345.5	218.3	260.7	127.2	0.632	5.48	7.16	0.84	44.17	11.17
13	24	374.2	236.5	282.4	137.8	0.632	6.01	7.68	0.84	44.17	13.07
14	24	402.3	253.9	303.4	148.4	0.631	6.65	8.31	0.83	44.17	15.51
15	22	430.5	271.4	324.4	159.2	0.630	7.47	9.22	0.88	44.12	19.19
16	24	459.8	289.0	345.9	170.8	0.628	8.89	10.41	0.76	43.82	25.06
17	26	486.3	306.9	366.7	179.4	0.631	10.22	11.44	0.61	43.95	30.47
18	117	514.0	325.1	388.0	189.0	0.632	12.70	13.20	0.25	44.29	40.60
19	145	543.7	342.6	409.6	201.1	0.630	13.78	14.05	0.14	44.40	45.54
20**	264	571.9	360.2	430.8	211.6	0.630	14.88	14.94	0.03	44.50	50.94

* Approximate in-situ stresses

** Sample put into undrained shear after this stress level

† Calculated from: $\varepsilon_3 = (\varepsilon_v - \varepsilon_1)/2$

TABLE B.3 STRESS CONTROLLED DRAINED RESULTS - TEST T203

Stress Level	Load Duration (h)	σ_1' (kPa)	σ_3' (kPa)	σ_{oct}' (kPa)	$(\sigma_1-\sigma_3)$ (kPa)	σ_3'/σ_1'	ε_1 (%)	ε_v (%)	ε_3 † (%)	A (cm^2)	W ($kN-m/m^3$)
1≠	42	44.0	29.5	34.3	14.5	0.671	0.54	-1.50	-1.02	45.77	-0.18
2	51	65.2	42.3	49.9	22.8	0.650	1.30	-0.80	-1.05	45.69	0.21
3*	46	90.9	59.7	70.1	31.2	0.657	1.64	0.08	-0.78	45.56	0.81
4	48	120.3	83.4	95.7	36.9	0.693	2.21	0.69	-0.76	45.55	1.44
5	95	149.8	107.3	121.5	42.5	0.717	2.73	1.13	-0.80	45.59	2.06
6	72	179.6	131.6	147.6	48.0	0.733	3.25	1.93	-0.66	45.46	3.25
7	120	209.3	156.0	173.8	53.3	0.745	3.77	2.74	-0.52	45.32	4.67
8	48	238.9	180.1	199.7	58.7	0.754	4.23	3.15	-0.54	45.28	5.72
9	144	268.2	204.3	225.5	64.1	0.761	4.54	3.89	-0.33	45.15	7.33
10	121	296.1	226.5	249.7	69.6	0.775	4.93	4.52	-0.21	45.04	8.95
11	167	326.8	252.0	276.9	74.9	0.771	5.35	5.20	-0.08	44.92	10.88
12	120	359.9	276.0	304.0	83.8	0.767	5.79	9.83	2.02	42.92	23.45
13	194	389.4	300.7	330.2	88.7	0.772	6.20	13.27	3.54	41.39	33.73
14	191	416.9	324.1	355.0	92.8	0.777	6.57	15.48	4.46	40.49	40.99
15	192	446.1	348.7	381.2	97.4	0.782	6.97	16.73	4.88	40.07	45.55
16**	123	474.4	372.3	406.3	102.1	0.785	7.37	17.66	5.15	39.79	48.34

* Approximate in-situ stresses

** Sample put into undrained shear after this stress level

† Calculated from : $\varepsilon_3 = (\varepsilon_v - \varepsilon_1)/2$

≠ A volume increase was recorded during the first load increment

TABLE B.4 STRESS CONTROLLED DRAINED RESULTS - TEST T204

Stress Level	Load Duration (h)	σ'_1 (kPa)	σ'_3 (kPa)	σ'_{oct} (kPa)	$(\sigma_1-\sigma_3)$ (kPa)	σ'_3/σ'_1	ε_1 (%)	ε_v (%)	ε_3 † (%)	A (cm^2)	W ($kN-m/m^3$)
1	39	46.1	30.5	35.7	15.7	0.661	0.53	0.84	0.16	44.82	0.17
2 ≠	113	69.6	42.4	51.5	27.2	0.609	1.81	1.05	-0.38	45.32	1.07
3 *	286	89.5	59.1	69.2	30.4	0.660	2.33	2.72	0.20	44.79	1.63
4	191	113.1	82.0	92.4	31.0	0.726	2.74	3.61	0.44	44.57	2.38
5	193	134.9	104.9	114.9	29.9	0.778	3.07	4.39	0.66	44.35	3.21
6 **	216	156.9	127.8	137.5	29.1	0.815	3.40	5.26	0.93	44.10	4.32

* Approximate in-situ stresses

** Sample put into undrained shear after this stress level

† Calculated from: $\varepsilon_3 = (\varepsilon_v-\varepsilon_1)/2$

≠ Suspected leakage required replacement of original rubber membranes during this increment; strains are estimated

TABLE B.5 STRESS CONTROLLED DRAINED RESULTS - TEST T205

Stress Level	Load Duration (h)	σ'_1 (kPa)	σ'_3 (kPa)	σ'_{oct} (kPa)	$(\sigma_1-\sigma_3)$ (kPa)	σ'_3/σ'_1	ε_1 (%)	ε_v (%)	ε_3 † (%)	A (cm^2)	W ($kN-m/m^3$)
1	36	35.5	23.0	27.2	12.5	0.649	0.43	0.72	0.14	44.85	0.11
2	23	70.9	45.2	53.7	25.9	0.637	1.26	2.13	0.44	44.59	0.75
3 *	23	106.0	68.3	80.9	37.6	0.645	2.03	3.38	0.68	44.36	1.71
4	22	139.6	102.2	114.7	37.4	0.732	2.58	4.54	0.98	44.08	2.89
5	27	172.8	135.3	147.8	37.5	0.783	3.02	5.31	1.15	43.92	3.99
6	25	206.3	168.9	181.4	37.4	0.819	3.48	6.34	1.43	43.65	5.71
7	21	239.1	201.7	214.1	37.4	0.844	3.87	7.14	1.64	43.45	7.21
8	24	272.2	234.9	247.3	37.4	0.863	4.32	8.26	1.97	43.13	9.80
9	24	306.7	268.7	281.3	37.9	0.876	4.73	9.28	2.27	42.84	12.50
10	24	339.2	301.3	314.0	37.8	0.888	5.18	10.41	2.62	42.50	15.95
11	24	371.9	334.3	346.8	37.5	0.899	5.67	11.73	3.03	42.09	20.29
12	24	404.9	367.4	378.4	37.5	0.907	6.17	12.94	3.39	41.73	24.76
13	24	438.0	400.8	413.2	37.3	0.915	6.67	14.07	3.70	41.42	29.25
14 **	24	471.2	433.6	446.2	37.5	0.920	7.20	15.13	3.97	41.13	33.82

* Approximate in-situ stresses

** Sample put into undrained shear after this increment

† Calculated from: $\varepsilon_3 = (\varepsilon_v-\varepsilon_1)/2$

TABLE B.6 STRESS CONTROLLED DRAINED RESULTS - TEST T206

Stress Level	Load Duration (h)	σ_1' (kPa)	σ_3' (kPa)	σ'_{oct} (kPa)	$(\sigma_1-\sigma_3)$ (kPa)	σ_3'/σ_1'	ε_1 (%)	ε_v (%)	ε_3 † (%)	A (cm^2)	W ($kN-m/m^3$)
1	17	36.1	23.7	27.9	12.4	0.657	0.49	0.86	0.19	44.82	0.13
2	23	70.0	45.0	53.3	25.1	0.642	1.33	2.45	0.56	44.48	0.83
3 *	23	106.1	68.5	81.1	37.6	0.646	2.09	3.68	0.79	44.25	1.76
4	22	147.7	98.1	114.6	49.6	0.664	2.83	4.92	1.04	44.02	3.12
5	27	189.2	127.8	148.3	61.4	0.675	3.47	5.71	1.12	43.93	4.38
6	25	230.0	156.3	180.9	73.7	0.680	4.15	6.80	1.33	43.74	6.40
7	21	272.1	186.5	215.0	85.6	0.685	4.81	7.64	1.41	43.64	8.33
8	24	313.5	215.5	248.2	98.0	0.688	5.66	8.86	1.60	43.45	11.58
9	24	355.2	245.5	282.1	109.7	0.691	6.60	9.95	1.67	43.37	15.05
10	24	395.2	273.3	313.9	121.9	0.692	7.76	11.17	1.70	43.32	19.56
11	24	438.8	303.6	348.7	135.2	0.692	9.44	13.00	1.78	43.21	27.02
12	24	480.5	333.2	382.3	147.3	0.693	10.85	14.48	1.81	43.15	33.70
13 **	25	522.2	362.8	415.9	159.5	0.695	12.09	15.73	1.82	43.12	39.98

* Approximate in-situ stresses

** Sample put into undrained shear after this increment

† Calculated from: $\varepsilon_3 = (\varepsilon_v-\varepsilon_1)/2$

TABLE B.7 STRESS CONTROLLED DRAINED RESULTS - TEST T207

Stress Level	Load Duration (h)	σ_1' (kPa)	σ_3' (kPa)	σ'_{oct} (kPa)	$(\sigma_1-\sigma_3)$ (kPa)	σ_3'/σ_1'	ε_1 (%)	ε_v (%)	ε_3 † (%)	A (cm^2)	W ($kN-m/m^3$)
1	14	36.3	23.9	28.0	12.3	0.660	0.35	0.42	0.07	44.95	0.07
2	22	70.9	46.1	54.3	24.8	0.650	1.15	1.84	0.35	44.67	0.69
3 *	26	106.6	69.2	81.7	37.4	0.649	1.86	3.08	0.61	44.42	1.62
4	24	136.6	83.5	101.2	53.1	0.611	2.52	4.43	0.95	44.10	2.94
5 ≠	24	166.6	97.6	120.6	69.0	0.586	3.18	5.53	1.18	43.89	4.36
6	23	197.6	112.4	140.8	85.2	0.569	4.26	7.28	1.51	43.57	7.01
7	23	227.7	127.0	160.6	100.7	0.558	4.95	8.79	1.92	43.16	9.46
8	23	258.1	141.7	180.5	116.4	0.549	5.72	10.23	2.26	42.83	12.25
9	23	288.0	155.9	200.0	132.0	0.542	6.72	11.67	2.48	42.59	15.63
10	22	318.5	170.3	219.7	148.2	0.535	8.10	13.03	2.46	42.57	19.75
11	25	345.7	183.9	237.8	161.7	0.532	10.50	14.64	2.07	42.90	26.34
12 ***	26	375.9	199.0	258.0	178.9	0.529	15.63	18.76	1.56	43.31	42.90

* Approximate in-situ stresses

*** Sample failed in drained shear during this increment; results shown are calculated from the last set of readings and are assumed to represent the failure condition

† Calculated from: $\varepsilon_3 = (\varepsilon_v-\varepsilon_1)/2$

≠ Loss of cell pressure near the end of increment; final strains were extrapolated from earlier readings

TABLE B.8 STRESS CONTROLLED DRAINED RESULTS - TEST T208

Stress Level	Load Duration (h)	σ_1' (kPa)	σ_3' (kPa)	σ'_{oct} (kPa)	$(\sigma_1-\sigma_3)$ (kPa)	σ_3'/σ_1'	ε_1 (%)	ε_v (%)	ε_3 † (%)	A (cm^2)	W ($kN-m/m^3$)
1	10	36.0	23.6	27.7	12.4	0.655	0.28	0.50	0.11	44.88	0.08
2	22	70.5	45.4	53.8	25.0	0.645	1.14	1.98	0.42	44.59	0.75
3 *	26	106.7	69.2	81.7	37.6	0.648	1.88	3.30	0.71	44.33	1.74
4	24	119.5	70.6	86.9	48.9	0.591	2.21	3.73	0.76	44.28	2.18
5 †	24	133.4	72.6	92.9	60.8	0.544	2.55	4.13	0.79	44.25	2.67
6	23	147.0	74.4	98.6	72.6	0.506	3.28	5.09	0.90	44.14	3.85
7	23	161.4	76.7	104.9	84.7	0.475	3.77	6.05	1.14	43.91	4.97
8	24	174.4	78.0	110.1	96.4	0.447	4.29	6.98	1.35	43.71	6.17
9	24	188.1	80.0	116.1	108.0	0.426	5.07	7.87	1.40	43.65	7.66
10	21	201.7	82.0	121.9	118.8	0.406	6.27	8.62	1.17	43.85	9.17
11 ***	1	214.0	83.4	126.9	130.6	0.390	6.80	8.69	0.95	44.06	9.91

* Approximate in-situ stresses

*** Sample failed in drained shear during this increment; results shown are calculated from the last set of readings and are assumed to represent the failure condition

† Calculated from: $\varepsilon_3 = (\varepsilon_v-\varepsilon_1)/2$

≠ Loss of cell pressure near end of increment; final strains extrapolated from earlier readings

TABLE B.9 STRESS CONTROLLED DRAINED RESULTS - TEST T209

Stress Level	Load Duration (h)	σ_1' (kPa)	σ_3' (kPa)	σ'_{oct} (kPa)	$(\sigma_1-\sigma_3)$ (kPa)	σ_3'/σ_1''	ε_1 (%)	ε_v (%)	ε_3 † (%)	A (cm^2)
1	19	35.6	23.0	27.2	12.5	0.647	0.64	1.21	0.28	44.73
2	23	70.9	45.9	54.3	25.0	0.647	1.44	2.65	0.61	44.43
3 *	27	106.1	68.7	81.2	37.4	0.645	2.04	3.82	0.89	44.17

* Approximate in-situ stresses sample put into undrained shear after this increment

† Calculated from: $\varepsilon_3 = (\varepsilon_v-\varepsilon_1)/2$